PERFORMANCE OF DIGITAL DISTANCE RELAY ALGORITHMS FOR PROTECTING TRANSFORMER TERMINATED LINES

A Thesis

Submitted to the College of Graduate Studies and Research

in Partial Fulfilment of the Requirements

for the Degree of

Master of Science

in the

Department of Electrical Engineering

University of Saskatchewan

by

MAXWELL MUCHAYI

Saskatoon, Saskatchewan

November 1993

COPYRIGHT

ACKNOWLEDGEMENTS

The author wishes to express his thanks to Dr. T.S. Sidhu for the supervision of this project. His advice and assistance in preparation of this thesis is highly appreciated.

The author extends his deepest gratitude to his wife Shelly, brother Ernest and other family members for their encouragement and moral support. Thanks are due to all friends who helped in many different ways in bringing this project to a successful conclusion.

Special thanks are due to the Canadian Commonwealth Scholarship and Fellowship Committee for providing financial assistance in form of a scholarship and equally important, the Government of the Republic of Zimbabwe for granting a study leave.

UNIVERSITY OF SASKATCHEWAN

Electrical Engineering Abstract 93A387

PERFORMANCE OF DIGITAL DISTANCE RELAY ALGORITHMS FOR PROTECTING TRANSFORMER TERMINATED LINES

Student: Maxwell Muchayi Supervisor: Dr. T.S. Sidhu

M. Sc. Thesis Submitted to the
College of Graduate Studies and Research
November 1993

ABSTRACT

Recent advances in microelectronics has enabled the use of micro-processors in distance protection of transmission lines. This area has drawn much attention of power system researchers. Different algorithms for use in digital distance relays are reported in the literature. The performance of these algorithms can be evaluated off-line before actual implementation in power systems. Frequency response and effects of decaying d.c. which is normally present in transient currents are among some of the characteristics of the algorithms that can be examined. Their performance can also be examined using fault data or data of transients like inrush currents which occur during switching-on of transformers.

This thesis is concerned with the simulation of inrush current and the assessment of the performance of digital algorithms for distance protection during the presence of inrush current. Initially, the modelling of transformers is examined so as to simulate and analyze inrush current. Some of the simulation studies of inrush current are reported in the thesis. The ability of each algorithm for detecting faults in the presence of inrush current is checked by using simulated data. The faults on transformer terminated lines are simulated using an electromagnetic transients program, EMTDC. Development and assessment of a fault direction discriminating algorithm for protection of transformer terminated lines is also presented. Results reported in the thesis demonstrate that this algorithm performs satisfactorily.

Table of Contents

COPYRIGHT i
ACKNOWLEDGEMENTS ii
ABSTRACT iii
TABLE OF CONTENTS iv
LIST OF FIGURES vi
LIST OF TABLES xii
1. INTRODUCTION 1
1.1. Background 1
1.2. Tools for Transient Studies 1
1.2.1. Transient Network Analysers 2
1.2.2. Digital Computers 2
1.3. Power System Protection 3
1.3.1. Zones of Protection 3
1.3.2. Changing Trends in Power System Protection 5
1.3.3. Effects of Transients on Protective Relays 6
1.4. Objectives of the Thesis 8
1.5. Thesis Outline 8
2. TRANSMISSION LINE PROTECTION 10
2.1. Introduction 10
2.2. Types of Faults on Transmission Lines 10
2.3. Protection of Transmission Lines 11
2.3.1. Distance and Directional Relay Comparators. 13
2.3.2. Distance Protection 16
2.4. Transformer Terminated Lines 21
2.5. Summary 21
3. DIGITAL RELAYS 23
3.1. Introduction 23
3.2. Fundamental Functional Blocks of a Digital Relay 23
3.3. Benefits of Digital Relaying 25
3.4. Digital Relay Algorithms 26
3.4.1. Trigonometric Algorithms 27
3.4.2. Least Error Squares Algorithm 29
3.4.3. Correlation Algorithms 31
3.5. Digital Distance Relay Algorithms 35

3.5.1. Impedance Calculation 35
3.5.2. Differential Equation Algorithm 36
3.6. Summary 37
4. DIGITAL SIMULATION OF MAGNETIZING INRUSH CURRENT 39
4.1. Introduction 39
4.2. Magnetizing Inrush Current Phenomenon 40
4.3. Factors Which Determine the Magnitude of Inrush Current 42
4.4. Modelling of Single-Phase Transformers 46
4.5. Modelling Saturation in Single-Phase Transformers 49
4.6. Extension of Single-Phase to Three-Phase Transformer Modelling 51
4.7. Simulation Results 53
4.8. Some Measures to Reduce Inrush Current 56
4.9. Summary 64
5. EVALUATION OF DIGITAL DISTANCE RELAY ALGORITHMS FOR PROTECTING A TRANSFORMER TERMINATED LINE 66
5.1. Introduction 66
5.2. Model of the Power System Selected for the Studies 66
5.2.1. Design of a Low Pass Filter 69
5.2.2. Processing of Sampled Data 72
5.2.3. The Design and Frequency Response of the Digital Algorithms 73
5.3. Dynamic Response of the Digital Distance Relay Algorithms 80
5.3.1. Inrush Current Only 81
5.3.2. Inrush Current with a Single Phase to Ground Fault 90
5.3.3. Inrush Current with a Phase to Phase Fault 90
5.4. Summary 99
6. FAULT DIRECTION DISCRIMINATING ALGORITHM 100
6.1. Introduction 100
6.2. Development of the Algorithm 100
6.2.1. Forward Fault 105
6.2.2. Reverse Fault 106
6.2.3. Direction Discrimination 108
6.3. Assessment of the Algorithm 110
6.4. Summary 114
7. SUMMARY AND CONCLUSIONS 115
REFERENCES 119
Appendix A. EMTDC Program 123
A.1. Scope of Simulation Studies 123
A.1.1. Limitations 124
Appendix B. Results on Dynamic Response of the Digital Relay 125
B.1. Inrush Current with a Single-Phase to Ground Fault 125
B.2. Inrush Current with a Phase to Phase Fault 125

List of Figures

Figure 1.1:	One line diagram of a power system illustrating primary relaying.	4
Figure 2.1:	Types of transmission line faults.	12
Figure 2.2:	Block representation of comparators.	14
Figure 2.3:	A block diagram of a typical amplitude comparator.	15
Figure 2.4:	A block diagram of a typical phase comparator.	15
Figure 2.5:	Time-distance characteristic of a typical three-zone distance protection scheme.	17
Figure 2.6:	Representation of distance relay characteristics in the impedance plane.	17
Figure 2.7:	Distance relay characteristics: (a) Impedance, (b) Admittance, (c) Reactance and (d) Blinder relays.	20
Figure 3.1:	Functional block diagram of a typical digital relay.	24
Figure 3.2:	The correlation of voltage samples with sine and cosine waves [37].	34
Figure 4.1:	Magnetizing characteristics of a typical single-phase power transformer.	41
Figure 4.2:	Residual flux density and inrush current phenomenon.	42
Figure 4.3:	Two mutually coupled windings.	47
Figure 4.4:	Single phase transformer saturation modelling with a current source across the winding.	49
Figure 4.5:	Saturation characteristic of a transformer	50
Figure 4.6:	The transformer model constructed.	53
Figure 4.7:	Inrush current during switching in of the transformer at 0.0167 seconds showing inrush current at least in two of the phases	57
Figure 4.8:	Inrush current in the delta winding during the switching in of transformer at 0.0167 seconds	58
Figure 4.9:	The corresponding flux when there is no residual magnetism during switching in of the transformer at 0.0167 seconds.	59
Figure 4.10:	Inrush current during switching in of the transformer at 0.010 seconds, showing different shapes.	60
Figure 4.11:	Increasing the external resistance reduces the inrush current; switching in of the transformer at 0.0167 seconds	61

Figure 4.12:	The flux in the transformer showing the residual flux before the transformer is switched in; switching in at 0.00835 seconds	62
Figure 4.13:	The presence of residual flux makes the inrush current somewhat greater or less than if there was no residual flux. In this case it is greater; switching in at 0.00835 seconds	63
Figure 5.1:	The schematic diagram of the test system.	68
Figure 5.2:	The frequency response of the fourth order filter.	71
Figure 5.3:	Voltage before filtering at relay location during inrush current.	72
Figure 5.4:	Inrush current before filtering at relay location.	73
Figure 5.5:	Voltage after filtering at relay location during inrush current.	74
Figure 5.6:	Inrush current after filtering at relay location.	75
Figure 5.7:	Frequency response of the Sine filter of the Fourier algorithm.	76
Figure 5.8:	Frequency response of the Cosine filter of the Fourier algorithm.	77
Figure 5.9:	Frequency response of the Sine filter of the Least Error Squares algorithm.	78
Figure 5.10:	Frequency response of the Cosine filter of the Least Error Squares algorithm.	78
Figure 5.11:	Frequency response of the Sine filter of the Mann and Morrison short window algorithm.	79
Figure 5.12:	Frequency response of the Cosine filter of the Mann and Morrison short window algorithm.	80
Figure 5.13:	Trajectory of the impedance estimates of the ground elements during inrush current using the Least Error Squares algorithm.	82
Figure 5.14:	Trajectory of the impedance estimates of the ground elements during inrush current using the Fourier algorithm.	82
Figure 5.15:	Trajectory of the impedance estimates of the ground elements during inrush current using the R-L algorithm.	83
Figure 5.16:	Trajectory of the impedance estimates of the ground elements during inrush current using the Mann and Morrison short window algorithm.	83
Figure 5.17:	Trajectory of the impedance estimates of the phase elements during inrush current using the Least Error Squares algorithm.	84
Figure 5.18:	Trajectory of the impedance estimates of the phase elements during inrush current using the Fourier algorithm.	84

Figure 5.19:	Trajectory of the impedance estimates of the phase elements during inrush current using the R-L algorithm.	85
Figure 5.20:	Trajectory of the impedance estimates of the phase elements during inrush current using the Mann and Morrison short window algorithm.	85
Figure 5.21:	Trajectory of the impedance estimates of the ground elements during inrush current using the Least Error Squares algorithm with source impedance increased.	86
Figure 5.22:	Trajectory of the impedance estimates of the ground elements during inrush current using the Fourier algorithm with source impedance increased.	86
Figure 5.23:	Trajectory of the impedance estimates of the ground elements during inrush current using the R-L algorithm with source impedance increased.	87
Figure 5.24:	Trajectory of the impedance estimates of the ground elements during inrush current using the Mann and Morrison short window algorithm with source impedance increased.	87
Figure 5.25:	Trajectory of the impedance estimates of the phase elements during inrush current using the Least Error Squares algorithm with source impedance increased.	88
Figure 5.26:	Trajectory of the impedance estimates of the phase elements during inrush current using the Fourier algorithm with source impedance increased.	88
Figure 5.27:	Trajectory of the impedance estimates of the phase elements during inrush current using the R-L algorithm with source impedance increased.	89
Figure 5.28:	Trajectory of the impedance estimates of the phase elements during inrush current using the Mann and Morrison short window algorithm with source impedance increased.	89
Figure 5.29:	Trajectory of the impedance estimates of the ground elements for a single-phase to ground fault using the Least Error Squares algorithm.	91
Figure 5.30:	Trajectory of the impedance estimates of the ground elements for a single-phase to ground fault using the Fourier algorithm.	91
Figure 5.31:	Trajectory of the impedance estimates of the ground elements for a single-phase to ground fault using the R-L algorithm.	92
Figure 5.32:	Trajectory of the impedance estimates of the ground elements for a single-phase to ground fault using the Mann and Morrison short window algorithm.	92

Figure 5.33:	Trajectory of the impedance estimates of the phase elements for a single-phase to ground fault using the Least Error Squares algorithm.	93
Figure 5.34:	Trajectory of the impedance estimates of the phase elements for a single-phase to ground fault using the Fourier algorithm.	93
Figure 5.35:	Trajectory of the impedance estimates of the phase elements for a single-phase to ground fault using the R-L algorithm.	94
Figure 5.36:	Trajectory of the impedance estimates of the phase elements for a single-phase to ground fault using the Mann and Morrison short window algorithm.	94
Figure 5.37:	Trajectory of the impedance estimates of the ground elements for a phase-phase fault using the Least Error Squares algorithm.	95
Figure 5.38:	Trajectory of the impedance estimates of the ground elements for a phase-phase fault using the Fourier algorithm.	95
Figure 5.39:	Trajectory of the impedance estimates of the ground elements for a phase-phase fault using the R-L algorithm.	96
Figure 5.40:	Trajectory of the impedance estimates of the ground elements for a phase-phase fault using the Mann and Morrison short window algorithm.	96
Figure 5.41:	Trajectory of the impedance estimates of the phase elements for a phase-phase fault using the Least Error Squares algorithm.	97
Figure 5.42:	Trajectory of the impedance estimates of the phase elements for a phase-phase fault using the Fourier algorithm.	97
Figure 5.43:	Trajectory of the impedance estimates of the phase elements for a phase-phase fault using the R-L algorithm.	98
Figure 5.44:	Trajectory of the impedance estimates of the phase elements for a phase-phase fault using the Mann and Morrison short window algorithm.	98
Figure 6.1:	Pre-fault positive-sequence network of the transformer terminated line for a forward fault.	101
Figure 6.2:	Post-fault positive-sequence network of the transformer terminated line for a forward fault.	101
Figure 6.3:	Pre-fault negative-sequence network of the transformer terminated line for a forward fault.	102
Figure 6.4:	Post-fault negative-sequence network of the transformer terminated line for a forward fault.	102
Figure 6.5:	Pre-fault positive-sequence network of the transformer terminated line for a reverse fault.	103

Figure 6.6: Post-fault positive-sequence network of the transformer terminated line for a reverse fault. 103
Figure 6.7: Pre-fault negative-sequence network of the transformer terminated line for a reverse fault. 104
Figure 6.8: Post-fault negative-sequence network of the transformer terminated line for a reverse fault. 104
Figure 6.9: Thevenin's equivalent circuit for the postive-sequence network as seen from Bus *Y* in the transformer terminated line for a forward fault. 107
Figure 6.10: Thevenin's equivalent circuit for the negative-sequence network as seen from Bus *Y* in the transformer terminated line for a forward fault. 108
Figure 6.11: Thevenin's equivalent circuit for the postive-sequence network as seen from Bus *Y* in the transformer terminated line for a reverse fault. 109
Figure 6.12: Thevenin's equivalent circuit for the negative-sequence network as seen from Bus *Y* in the transformer terminated line for a reverse fault. 109
Figure 6.13: Trajectory of the positive- and negative- sequence impedances for a single phase fault in front of the relay location. 111
Figure 6.14: Trajectory of the positive- and negative- sequence impedances for a phase-phase fault in front of the relay location. 111
Figure 6.15: Trajectory of the positive- and negative- sequence impedances for a single phase fault behind the relay location. 112
Figure 6.16: Trajectory of the positive- and negative- sequence impedances for a phase- phase fault behind the relay location. 112
Figure 6.17: Trajectory of the positive-sequence impedance for a three-phase to ground fault in front of the relay location. 113
Figure 6.18: Trajectory of the positive-sequence impedance for a three-phase to ground fault behind the relay location. 113
Figure B.1: Trajectory of the impedance estimates of the ground elements for a single-phase to ground fault at the mid-point of the line using the Least Error Squares algorithm. 126
Figure B.2: Trajectory of the impedance estimates of the ground elements for a single-phase to ground fault at the mid-point of the line using the Fourier algorithm. 126
Figure B.3: Trajectory of the impedance estimates of the phase elements for a single-phase to ground fault at the mid-point of the line using the Least Error Squares algorithm. 127

Figure B.4: Trajectory of the impedance estimates of the phase elements for a single-phase to ground fault at the mid-point of the line using the Fourier algorithm. 127

Figure B.5: Trajectory of the impedance estimates of the ground elements for a phase-phase fault at the mid-point of the line using the Least Error Squares algorithm. 128

Figure B.6: Trajectory of the impedance estimates of the ground elements for a phase-phase fault at the mid-point of the line using the Fourier algorithm. 128

Figure B.7: Trajectory of the impedance estimates of the phase elements for a phase-phase fault at the mid-point of the line using the Least Error Squares algorithm. 129

Figure B.8: Trajectory of the impedance estimates of the phase elements for a phase-phase fault at the mid-point of the line using the Fourier algorithm. 129

List of Tables

Table 2.1: Inputs to the Distance Relay. 19
Table 4.1: Transformer data. 54
Table 5.1: Thevenin Equivalent Source and Transmission line data. 68
Table 5.2: Data for the transformer and load. 69

1. INTRODUCTION

1.1. Background

The primary objective of a power system is to generate, transmit and distribute electric power. A power system operates in the steady state for most of the time but experiences various kinds of disturbances occasionally. A power system is designed to withstand most operating conditions which may cause excessive electrical and mechanical stresses. These conditions develop in a power system during transient states. Some of the equipment specifications, such as, insulation levels and breaker interrupting capability are established from considerations of power system transients [1]. It is, therefore, important to study transients that can occur in a power system.

Transients manifest themselves in a power system as overvoltages and/or overcurrents. They are experienced either due to switching of lines, atmospheric disturbances or due to the system being subjected to a fault. Transients can be simulated very efficiently using time domain methods [2, 3, 4, 5]. Such studies require very detailed modelling of the system under consideration. Modelling of the entire system in detail may be prohibitive in terms of available computing resources and time. However, the use of proper equivalents can reduce the system model complexity which, in turn will reduce the overall study time [4, 6, 7].

1.2. Tools for Transient Studies

Two distinct approaches are presently used for studying transients in power systems. One is using Transient Network Analysers (TNAs) and the second approach uses digital computers. Both approaches use mathematical models of the power system components.

1.2.1. Transient Network Analysers

These are physical miniaturised models representing components of a power system and are interconnected to represent a power system. In these models, power system components are scaled down so that low voltage (about 100 volts or less) and low current (a few milliamperes) devices can be used. Using TNAs leads to simulation in real time which is sometimes desirable. However, they are relatively inflexible and it takes considerable time to set up a TNA for a system study [8].

Another technical problem with using TNAs is that power losses in miniature inductor models are disproportionately high. The line models are also not very accurate because a finite number of Tee/Pi sections have to be used. In spite of these disadvantages, TNAs have been used for transient studies for several years and will continue to be used for many years to come.

1.2.2. Digital Computers

Another approach to transient studies is to use a mathematical model of the system to be studied and solve the model using a computer program. Using computers, offers some advantages over the TNAs. These are speed, flexibility and cost. The results obtained from computer studies are usually accurate and are obtained at a relatively lower cost [8].

However, there are difficulties in the calculation of transients. Simulation needs preparation of sufficiently accurate and extensive system data. This is important, since the accuracy of any calculation cannot be better than the data on which it is based. For the most accurate results, full knowledge of the variation of the circuit elements with frequency is necessary, and this may not always be available. Comparisons of the results from TNAs and digital computers tend to show a good overall correlation but with differences in the fine details of the transient waveforms [9].

1.3. Power System Protection

Power systems occasionally experience faults and abnormal operating conditions. The occurrence of a fault may result in damage to the equipment that is in the vicinity of the fault, due to high currents, unbalanced currents or severe low voltages produced by the fault. It can also result in loss of synchronism of the system and substantial loss of revenue due to interruption of service. A faulted element of a power system must, therefore, be disconnected without unnecessary delay. For this purpose, protective relays are used in the power systems to detect faults and isolate faulted elements with minimum time delay by opening circuit breakers.

1.3.1. Zones of Protection

The present philosophy in protecting power systems is to divide the system into protective zones and to protect each zone by a set of relays [10, 11, 12]. A protective zone normally includes one major electrical component and a set of circuit breakers to disconnect it from adjacent components. If a fault occurs in a zone, relays open the appropriate set of circuit breakers to isolate the faulted zone to limit the damage to the system. Primary relays are the first line of defence and are set to operate with minimum time delay. If the primary relays fail to isolate a fault, either the local back-up or remote back-up relays should operate to isolate the fault. It is also essential that different zones of protection overlap so that the entire system is protected.

Figure 1.1 illustrates the primary relaying zones of a power system. It can be observed that a separate zone of protection is established around one or more system elements. It is also evident that, for failures within the region where two adjacent protection zones overlap, more breakers will be tripped than the minimum necessary to disconnect the faulty element. But, if there were no overlap, a failure in a region between zones would not lie in either zone, and as a result no breakers will be tripped. The adjacent protection zones overlap around a circuit breaker. This is the general practice so that a minimum number of circuit breakers need to be tripped with the exception for failures in the overlap region. However, at times it becomes desirable for economic or space-saving reasons to connect a transformer directly to a transmission line without the

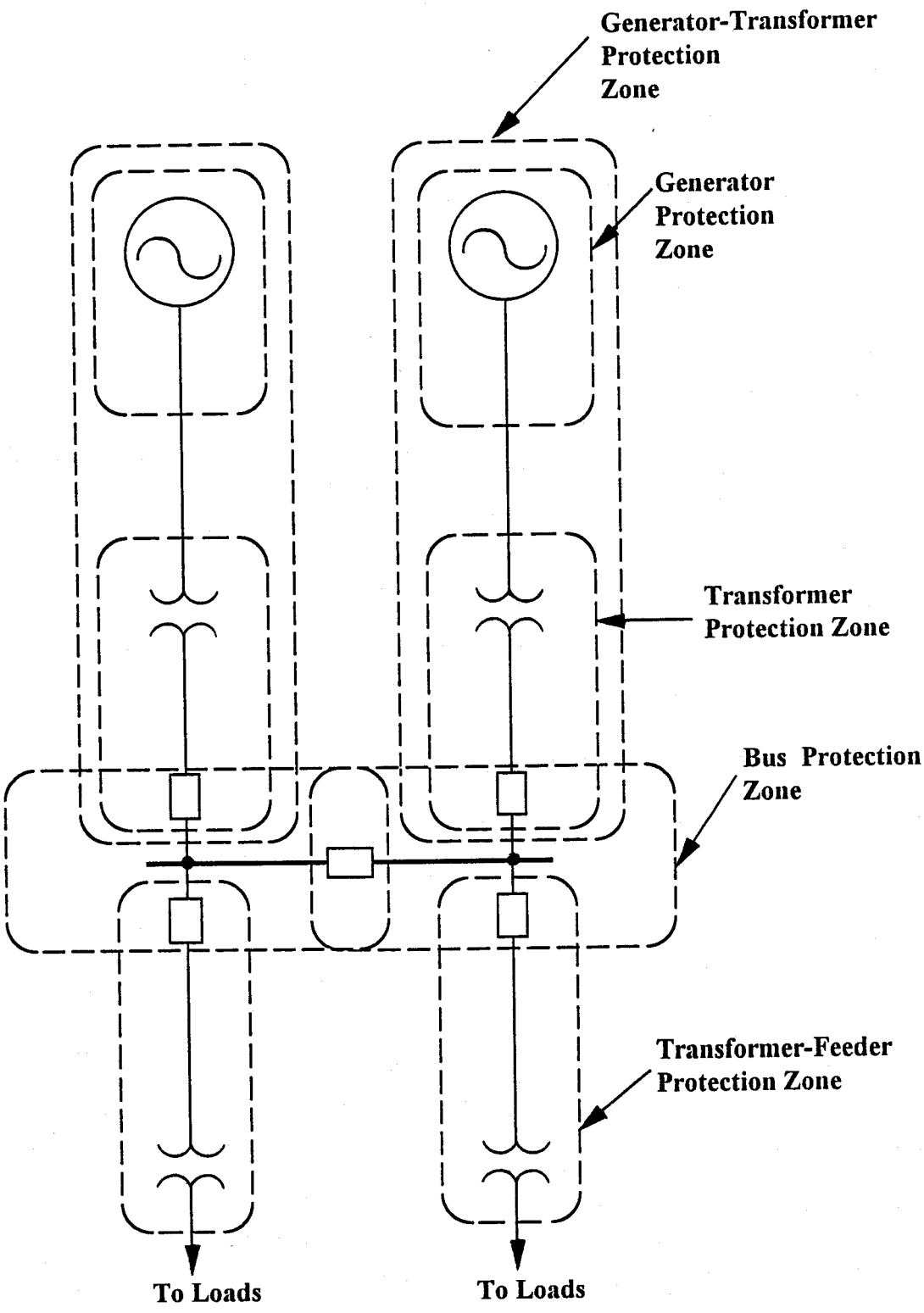

Figure 1.1: One line diagram of a power system illustrating primary relaying.

intervention of switchgear [9, 13] and this constitutes a transformer-feeder as shown in the figure. In such cases, the transformer-feeder is protected as a single zone.

1.3.2. Changing Trends in Power System Protection

Fuses were the first devices to be used to isolate faulted equipment as quickly as possible. They are effective but have the disadvantage of requiring replacement immediately after the interruption of the fault current. This inconvenience was reduced by the use of automatic circuit breakers and later electromechanical relays whose contacts controlled the trip coils of the circuit breakers. In order to meet the requirements of the increasingly complex power systems, protective devices with greater sensitivity and selectivity were developed.

Research into the development of solid state electronic relays started in the 1950's. These relays were not generally accepted in the early stages due to the high failure rates of the electronic components and inappropriate designs. For example, these designs were based on the assumption that the power system voltages and currents during transients contain only fundamental frequency components. Later, semiconductor technology and improved designs were used. There are now several kinds of solid state relays being used in power systems [14].

With the advent of digital technology, the development of microprocessor based relays has received considerable attention [15, 16, 17]. The accuracy and speed with which a processor can perform computations aroused the interest of relay engineers in this technology. F. H. Last and A. Stalewsky [17] were the first to propose the use of real time computations for power system protection in 1966. In a pioneering paper in 1969, Rockfeller [18] proposed an overall philosophy for using a digital computer in protecting a substation and the transmission lines emanating from it.

Digital relay research has reached a level that some digital relays are now commercially available. The speed and accuracy of these relays depend mainly on the software and the hardware used. The accuracy of computed results is influenced by the word size of the analog to digital converter, the digital processor, the relay software or algorithm, the relay characteristic and the operating environment.

1.3.3. Effects of Transients on Protective Relays

Influence of System Transients:

As already mentioned, relays detect disturbances in power systems. The relays are subjected to the adverse effects of uncontrollable variables such as transients in current signals during faults. The major components of a fault current in a power system are:
a. An exponentially decaying a.c. component.

b. An exponentially decaying d.c. component.
A simplified expression for short-circuit current neglecting a.c. decrement is:

$$i_f = i_{a.c.} + i_{d.c}$$

$$i_f = I_m \sin(\omega t + \psi - \phi) + I_m \sin(\phi - \psi) e^{-t/\tau} \qquad (1.1)$$

where:

i_f is the fault current,
ω is the nominal angular frequency,
ψ is the fault inception angle,
ϕ is the phase angle,
τ is the system time constant and
I_m is the peak value of current.

The d.c. component in the fault current is dependent upon the instant in the voltage cycle at which the fault occurs (i.e. upon the angle ψ) [19]. If $(\psi - \phi)$ is zero, the d.c. component is zero and the fault current signal is a pure sine wave. If $(\psi - \phi) = \pi/2$, the d.c. component is a maximum and the fault current signal is initially a fully offset cosine wave. The typical value of time constant, τ, for a 230kV line is 30ms. The d.c. component is an important source of error for relays. For example, it tends to reduce the impedance seen by a distance relay used for transmission line protection and causes it to overreach.

Nonlinear-impedance elements in the system like loads that utilize power electronics may produce a number of harmonic components [20]. Semiconductors are used for example in adjustable-speed drives for a.c. and d.c. motors. As power

semiconductors are suddenly switched on and off at any point on the voltage waveform, high frequency oscillatory transients with decaying amplitude are generated [21]. If the switching occurs at the same point on each cycle, the transient becomes periodic; however, it is non-stationary. Its frequency is not an integer multiple of $60Hz$ [20]. The harmonic distortion and high-frequency transient may cause multiple zero crossings. Therefore, control devices based on zero crossing detection may malfunction. The zero-crossing detection is used, for example, in many applications in control and power systems, such as solid-state overcurrent relays and solid-state relays (SSR's). The effect of harmonics and random high-frequency distortion is to delay the opening or closing of the SSR's [20].

In the presence of transients like magnetizing inrush current, which occurs while energizing a transformer, the differential relays for the transformers do include a restraint feature to avoid tripping. However, these relays are known to operate at times during some magnetizing inrush current conditions. Other algorithms for digital differential protection for transformers reported in the literature [22, 23] use the second harmonic components to restrain relay operation.

Influence of Transducer Transients:

The measuring element of a relay receives its signals from the secondaries of current and voltage transformers. These transformers, therefore, influence the dynamic performance of a protection scheme [19].

Current transformers are connected with their primaries in series with the protected circuit. When a current change occurs in the primary a.c. system, one or more of the three-phase currents will have some d.c. offset. The performance of a current transformer (CT) is affected by the d.c. component. It can saturate the CT core so that the secondary reproduction of the primary current can be severely limited and distorted. As a generality, CT performance is most critical at the relay decision point. For example, if saturation occurs in CTs before transmission line protection relays can operate, generally a delay in operation occurs until the CTs recover [11].

Capacitor voltage transformers are widely used for voltage measurements at 100kV and above. However, when a sudden change takes place in the primary voltage, the energy stored in the capacitor voltage transformer circuit results in distorted voltage output. This has a marked effect on relay operating time. The transient errors in the capacitor voltage transformer output result in slower zone 1 operating time for distance relays in transmission line protection [19].

This thesis examines a transient phenomenon known as magnetizing inrush current and assesses the performance of digital distance relays protecting transformer terminated lines in the presence of inrush current. Also presented is the development and assessment of a fault direction discriminating algorithm using the positive- and negative- sequence impedances.

1.4. Objectives of the Thesis

The work reported in this thesis is aimed to fulfil the following objectives:

1. To model transformers, compute and study one of the transients; namely, magnetizing inrush current which occurs during switching-on of transformers.
2. Apply the transformer model in a transformer terminated line and assess the performance of digital distance relays protecting the line.
3. Develop and assess a fault direction discriminating algorithm using the positive- and negative- sequence impedances.

1.5. Thesis Outline

This thesis is organized into seven chapters. Chapter 1 provides an introduction to the subject of transient studies, protection and changing trends in power system protection. The organization of the thesis and the work covered are also outlined.

The types of transmission line faults experienced in power systems are described in Chapter 2. An introduction to the types of transmission line protection is given. The use of distance relays in the zonal protection of transmission lines is presented together with some of the basic characteristics of distance relays. Protection of transformer terminated line is briefly discussed as well.

Chapter 3 describes the functional blocks of a typical digital relay and an outlines the advantages of using digital relays for power system protection. Some of the digital relaying algorithms, including their mathematical background are presented.

Chapter 4 introduces modelling of transformers and saturation in transformers. Inrush current phenomenon experienced during switching-on of transformers and some of the simulation results on inrush current are also presented.

The power system selected for the tests conducted is described in Chapter 5. Also presented is the evaluation of the suitability of digital distance relay algorithms for transmission line protection in the presence of inrush current only and inrush current in the presence of a fault. The ability of the relay to accurately detect faults that are in the operating zone of the relay is examined using fault data from the Electromagnetic Transients DC Analysis Program (EMTDC) simulations.

The development and assessment of a fault direction discriminating algorithm is examined in Chapter 6. Chapter 7 gives the summary and the conclusions deduced from the work reported in this thesis. A list of references used in this project is given after Chapter 7 which is followed by two appendices.

2. TRANSMISSION LINE PROTECTION

2.1. Introduction

Power system protection has been briefly presented in Chapter 1. This chapter describes a variety of faults which are likely to be experienced by transmission lines. These faults can cause damage to equipment and severe drop in voltage as already discussed in the previous chapter. It is, therefore, necessary to establish the location of the fault in order to trip circuit-breakers at each end of the faulted line section, and thus isolate that section from the power system. Some of the different types of relays used for transmission line protection are presented in this chapter. This is followed by a discussion about the protection of transformer terminated lines.

2.2. Types of Faults on Transmission Lines

Faults on transmission lines are generally caused by mechanical damage and insulation failure. These faults can be divided into two main categories; shunt faults and open circuits. A three phase power system can experience four types of shunt faults and two types of open circuits as shown in Figure 2.1. These faults can be described as follows:

1. shunt faults:

   a. *Three-phase faults*- a three-phase fault resulting from a short circuit between phases a, b, and c (Figure 2.1(a)) or between phases a, b, and c and ground.

   b. *Two-phase faults*- a two-phase fault can be experienced in three ways. One possibility is a short circuit between phase a and phase b. Other possibilities are short circuits between phase b and phase c (Figure 2.1(b)), and between phase c and phase a.

   c. *Two-phase to ground faults*- a two-phase to ground fault can be experienced in three different ways. One possibility is a short circuit between phases a and b to ground. Other possibilities are

short circuits between phases b and c to ground (Figure 2.1(c)), and between phases c and a to ground.

d. *Single phase to ground faults*- a single phase to ground fault can be experienced as a short circuit between ground and any of the three phases (Figure 2.1(d)).

2. Open circuits:

a. *One open conductor*- a single conductor open circuit can be experienced on any one of the three phases (Figure 2.1(e)).

b. *Two open conductors*- a two-conductor open circuit can be experienced in three ways. One possibility is open circuits of phases a and b, open circuits of phases b and c (Figure 2.1(f)) and open circuits of phases c and a.

2.3. Protection of Transmission Lines

Transmission lines are generally protected by distance relays, directional relays or pilot relays. Pilot protection schemes utilize information from both ends of the transmission line being protected. From the method of transmission of information from one end of the protected line to the other, these relays can be classified as: wire pilot protection, carrier pilot protection, microwave pilot protection and fibre optic pilot protection. In wire pilot protection, an auxiliary pair of pilot wires carry the information from one end of the line to the other. Wire pilot protection is generally used for protecting short transmission lines. Carrier pilot protection uses high frequency carrier signals transmitted over the protected line. In the case of microwave pilot protection, the information is transmitted on microwave communication channels. In fibre optic protection, electrical signals are converted to light signals. The converted signals are then transmitted through a fiber optic cable. The fibre optic cable eliminates any electromagnetic interference.

Another family of relays used in line protection are directional relays. These relays sense the direction in which the power flows. Directional relays are used together with distance relays which are not inherently directional. This allows a directional relay to trip for the flow of current in a specified direction only.

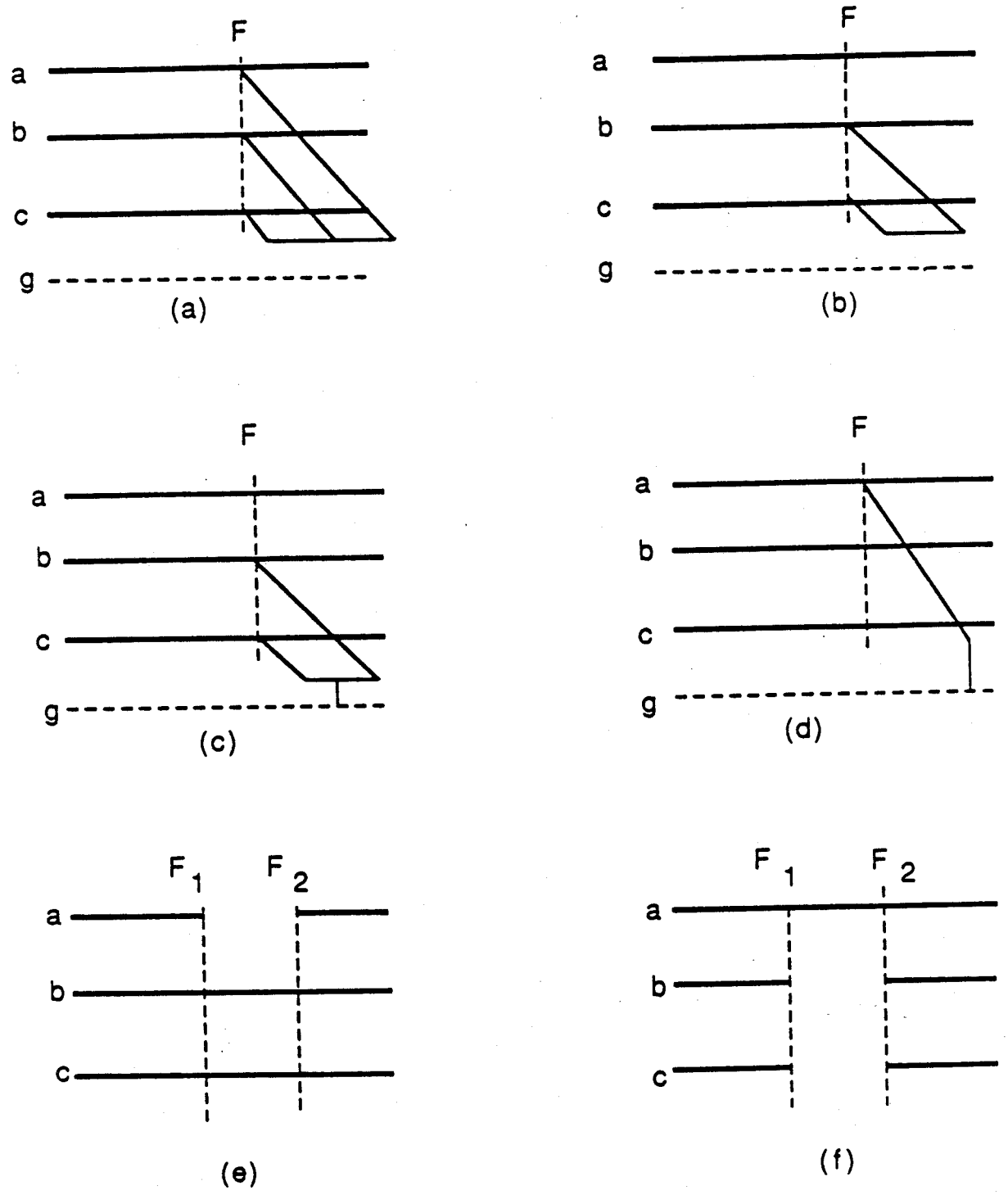

Figure 2.1: Types of transmission line faults.

2.3.1. Distance and Directional Relay Comparators.

The measuring units of distance and directional relays are either amplitude or phase comparators [19]. The operation of an amplitude comparator depends on the magnitudes of its inputs. An amplitude comparator is provided with two inputs, an operating signal and a restraining signal. The comparator operates when the magnitude of the operating signal is larger than the magnitude of the restraining signal. This is mathematically expressed as :

$$|S_0| > |S_R| \tag{2.1}$$

where:

S_0 is the operating signal and

S_R is the restraining signal.

The boundary or threshold condition is specified by $|S_0| = |S_R|$. These relationships are independent of the phase between the operating signal S_0 and the restraining signal S_R.

A phase comparator responds to the phase displacement angle, β, between the input signals. The inputs to a phase comparator can be denoted as S_1 and S_2 with S_1 leading S_2 for positive values of β. Operation is independent of the amplitudes of S_1 and S_2.

Figure 2.2 gives the basic requirements of amplitude and phase comparators. The limiting angles β_1 and β_2 are known as coincidence angles, and symmetrical boundary characteristics are obtained for $\beta_1 = \beta_2$. Thus operation of the phase comparator is usually governed by

$$-90° \leq \beta \leq 90° \tag{2.2}$$

where:

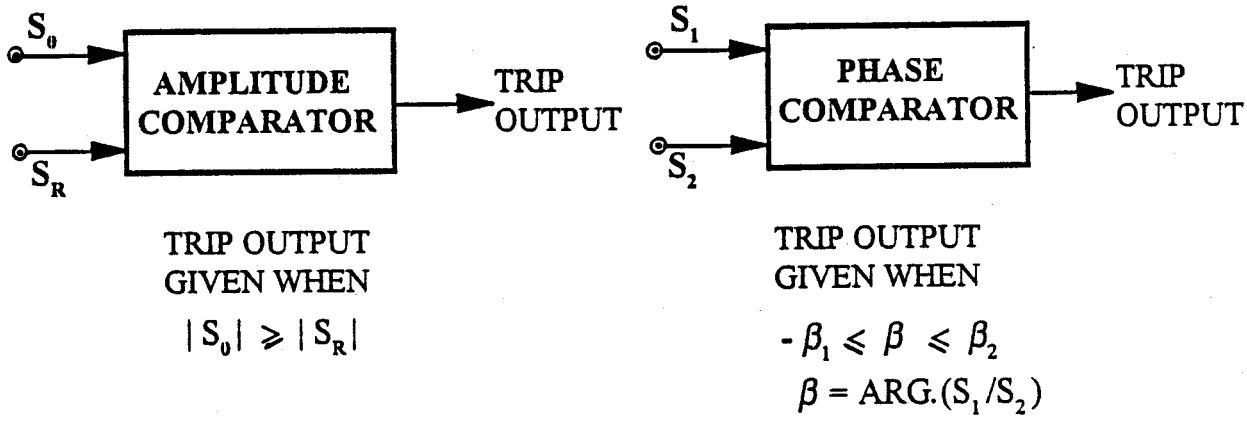

Figure 2.2: Block representation of comparators.

β is the angle between the input signals S_1 and S_2.

Usually, S_0, S_R, S_1 and S_2 are phasors representing signals derived by mixing voltages and currents proportional to the system voltages and currents.

Figure 2.3 shows a typical amplitude comparator that compares the amplitudes of two currents [24]. Bridge connected rectifiers convert a.c inputs I_0 and I_R to equivalent unidirectional currents, i_0 and i_r. The difference between the operating and restraining currents feeds an averaging circuit. The output of the averaging circuit is applied to a polarity detecting circuit. The comparator provides an output when the average of the difference current is positive and exceeds a threshold value.

Figure 2.4 shows the block diagram of a typical phase comparator [24]. A coincidence circuit accepts inputs S_1 and S_2 and provides a positive output when the signals S_1 and S_2 are of the same polarity and a negative output when they are of opposite

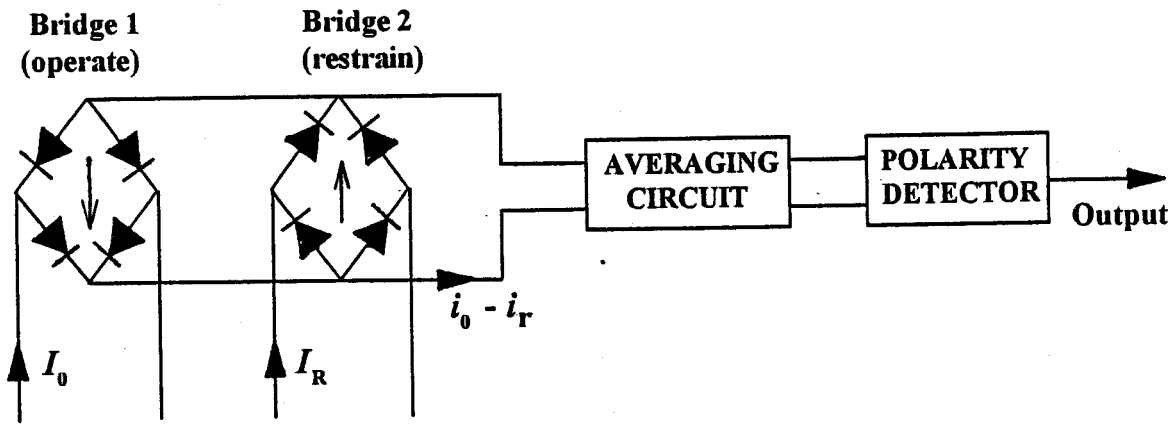

Figure 2.3: A block diagram of a typical amplitude comparator.

Figure 2.4: A block diagram of a typical phase comparator.

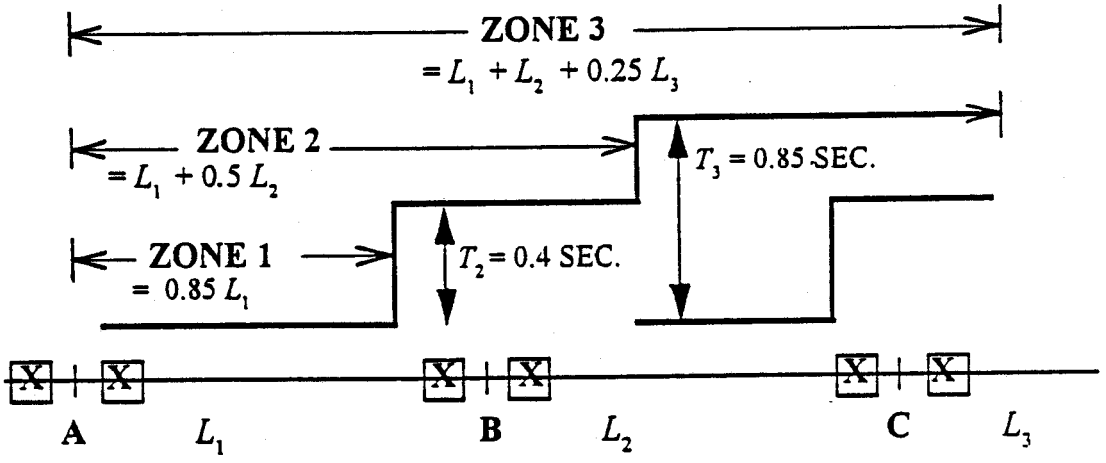

Figure 2.5: Time-distance characteristic of a typical three-zone distance protection scheme.

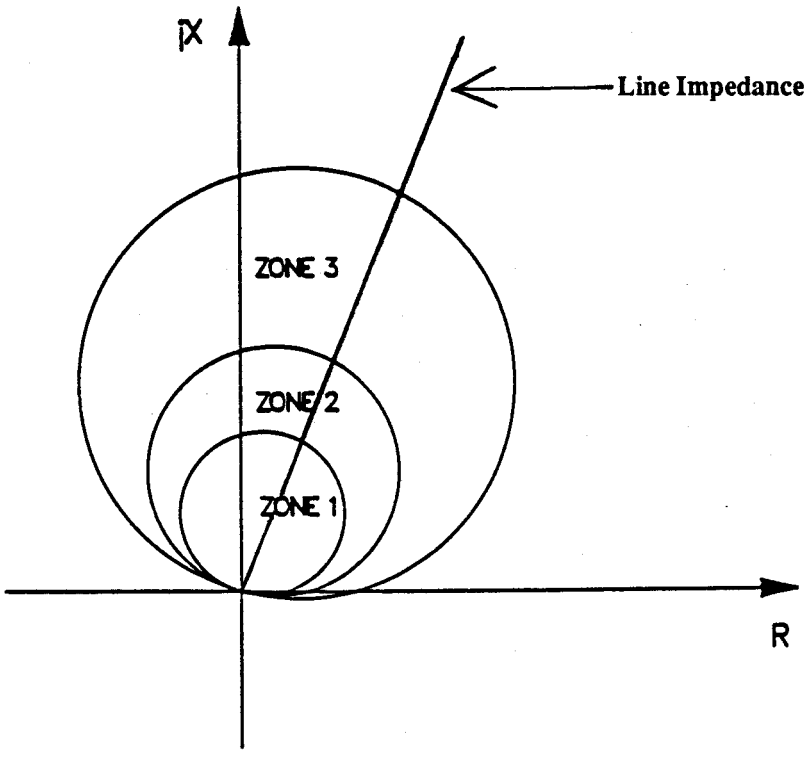

Figure 2.6: Representation of distance relay characteristics in the impedance plane.

polarity. The output of the integrating circuit increases linearly when the input to the circuit is positive and falls at the same rate when the input is negative. The level detector gives a trip signal when the integrator output exceeds a preset value.

2.3.2. Distance Protection

Distance relays are the most commonly used devices for protecting transmission lines [25]. A distance relay essentially calculates the impedance of the protected line from the relay location to the fault. The computed impedance in a distance relay is then compared to the relay settings to determine if the fault is in the protected zone. If a fault lies in the zone of protection, the relay issues a trip command that opens the circuit breakers of the line. The setting value of the measuring element is expressed as a percentage of the total impedance of the protected line.

Three zones of protection are normally established to protect a transmission line section and to provide backup protection for the adjoining sections. Zones of a typical transmission line are shown in Figure 2.5. Zone 1 relays are usually set for approximately 80 to 85 percent of line L_1. The time delay for zone 1 relays, T_1, is so small that zone 1 is considered to be instantaneous. The 20 percent margin provides a safety factor to accommodate overreaching errors due to inaccuracies in relays, current and potential transformers, auxiliary devices and infeed effects [5]. Thus, the high speed protective zone cannot be set to cover the complete length of line, and a reduced line coverage is accepted. Zone 2 relays are set for 100 percent of line L_1 plus approximately 30 to 50 percent of line L_2. The operation of zone 2 is delayed through a timer, T_2. The time delay for zone 2 is typically in the range of 0.30 to 0.40 seconds. Zone 3 relays are set for 100 percent of both lines L_1 and L_2 plus approximately 25 percent of line L_3. The zone 3 relay which also acts as a backup for zone 1 and zone 2 operates through a timer, T_3 to coordinate with zone 2 relays. The time delay for zone 3 relays is about 0.8 seconds. The relays at the far end of the line are similarly coordinated in the opposite direction at each bus. Figure 2.6 depicts the reach of the three zones of distance relays in the impedance plane. The relays operate when the ratio of fault voltage to current falls within the circles describing the relay characteristics.

Measurement is usually done by six relay elements; three being used for phase fault measurements and another three for ground fault measurements. Thus six relay units continuously monitor the transmission line. An important aspect of a distance protection scheme is to select current and voltage signals so that the appropriate impedance presented to a measuring element during a fault is the positive-phase-sequence impedance from the relay location to the fault. The inputs to the distance relay elements are shown in Table 2.1. If the input voltage and current signals are incorrectly chosen, the impedance seen by a measuring element may depart significantly from that corresponding to the impedance of the protected circuit. It is essential that the relay sees the positive-phase-sequence impedance from relay location to fault point irrespective of the fault type. To ensure this, the measuring elements for phase to ground faults, are provided with the phase current which is compensated with the zero-sequence current. For single phase to ground faults, the ratio of the faulted phase voltage and zero sequence compensated phase current is used. The zero sequence compensation factor, K_0 is defined as:

$$K_0 = \frac{(Z_0 - Z_1)}{Z_1}. \tag{2.3}$$

where:

Z_0 is the zero sequence impedance of the line and

Z_1 is the positive sequence impedance of the line.

The three measuring elements provided for phase fault protection are denoted (A-B), (B-C) and (C-A). These relays are expected to respond correctly to three-phase, phase-to-phase, and two phase-to-ground faults. The use of difference quantities eliminates zero-sequence signals to ensure correct measurements.

In absence of a fault resistance, the impedance is directly proportional to the corresponding distance from relay location to fault location and hence the name 'distance

Table 2.1: Inputs to the Distance Relay.

Relay Element	Voltage Input	Current Input
Phase A - G	V_a	$I_a + 3K_0 I_0$
Phase B - G	V_b	$I_b + 3K_0 I_0$
Phase C - G	V_c	$I_c + 3K_0 I_0$
Phase A - B	$V_a - V_b$	$I_a - I_b$
Phase B - C	$V_b - V_c$	$I_b - I_c$
Phase C - A	$V_c - V_a$	$I_c - I_a$

relay'. Distance relays are classified according to the shape of their characteristics in the impedance plane. The following are some of the classifications:

1. Impedance relay
   The characteristic of this type of relay is a circle in the impedance plane with centre at the origin as shown in Figure 2.7(a). This relay is non-directional and operates during reverse faults within the reach of the relay. For effective transmission line protection, a directional relay is used in conjunction with the impedance relay.
2. Admittance relay
   The characteristic of this relay is a circle that passes through the origin as shown in Figure 2.7(b). This relay is inherently directional and the name mho relay also refers to this relay.
3. Reactance relay The characteristic of this relay is a straight line parallel to the resistance axis as shown in Figure 2.7(c).
4. Blinder The characteristic of this relay is a straight line in the impedance plane as shown in Figure 2.7(d).

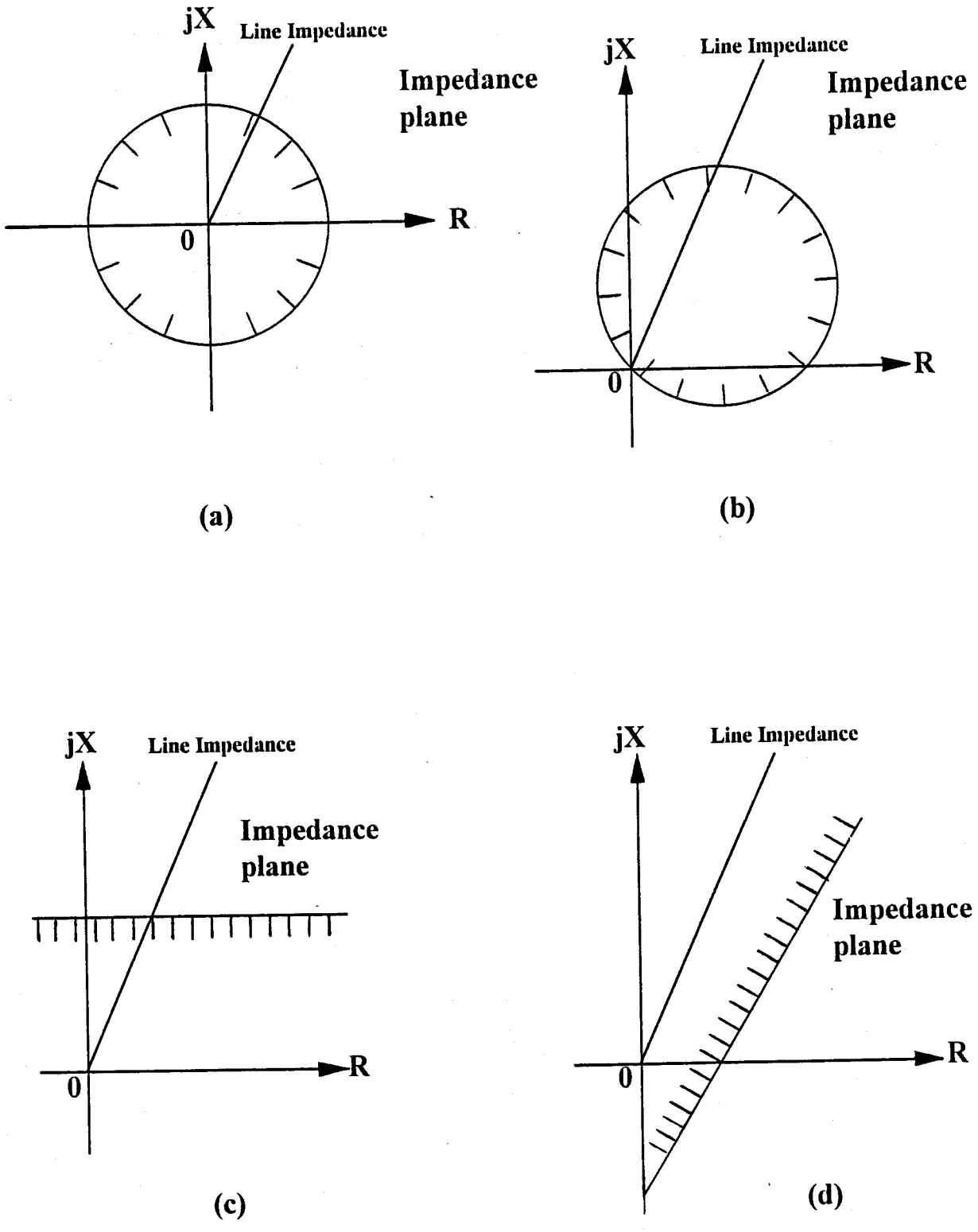

Figure 2.7: Distance relay characteristics: (a) Impedance, (b) Admittance, (c) Reactance and (d) Blinder relays.

Most of the remaining relay characteristics can be obtained by combining the above characteristics. For example, a quadrilateral characteristic can be obtained by using four blinder relays and a suitable logic. Reactance relays are more suitable for protection of short lines. Whereas, the admittance and quadrilateral relays are used for protecting long lines.

2.4. Transformer Terminated Lines

Frequently, in order to economize in switchgear, an arrangement is used whereby a composite feeder consisting of an overhead line terminated in a transformer is switched as a single unit there being no circuit breaker between the line and the transformer. Such arrangements are used in both distribution and transmission networks [9, 26].

High speed protection against phase and earth faults can be provided by distance relays located at the end of the feeder remote from the transformer [13]. As pointed out in the previous section; for a line not terminated with transformer the first zone will be set to reach only 80–85% of the feeder length. In the case of transformer terminated lines, the first zone can be set to cover the whole feeder and reach part way into the transformer. In so doing; it is possible to cover the whole of the feeder without danger of over-reaching to a fault on the low voltage side. As 80–90% of faults in lines are transient, therefore, by deenergizing the line long enough for the fault source to pass, service can be restored by automatically reclosing the breaker. However, transformer terminated lines, should never be reclosed automatically unless there is an assurance that the fault is in the line section [11].

2.5. Summary

A brief description of faults that are experienced by transmission lines has been presented in this chapter. The various kinds of relays used for protecting transmission lines have been discussed. The most commonly used relays in this field are the distance relays.

A distance protection scheme is normally a multi-zone arrangement, in which the

first zone of protection provides instantaneous tripping and faults in subsequent zones are cleared after a time delay. A distance relay measuring element is normally given a reduced line coverage setting for the high speed protective zone to ensure that operation does not take place for external fault just beyond the remote end of the protected circuit. Only in exceptional cases such as the transformer terminated line, will the first zone setting cover the whole line plus part of the transformer.

3. DIGITAL RELAYS

3.1. Introduction

Combinations of different relays and circuit breakers are used in transmission line protection. Power systems have become more complex and this demands that the protective relays be accurate, reliable and take less time to operate. A number of researchers and organizations have been conducting substantial research in the area of computer relaying for the last two decades [16]. Early research in the field of computer relaying considered the use of a central computer for all the relaying functions in a substation [15]. With the advent of microprocessors, the relaying functions within a substation can be distributed and the relays can communicate with each other. The emphasis of research for the past fifteen years has, therefore, been to develop relays using microprocessors.

This chapter discusses the functional details of a digital relay. Advantages of digital relays and the algorithms which can be implemented in the processor to produce numerical quantities from sequences of data samples are described.

3.2. Fundamental Functional Blocks of a Digital Relay

Figure 3.1 shows the block diagram of the basic subsystems of a typical digital relay. These subsystems consist of analog pre-processing, analog to digital conversion, digital processor, relay output, and power supply units. The digital relay receives low level signals proportional to power system voltages and currents via the voltage and current transformers, which are fed into analog pre-processing units.

An analog pre-processing unit consists of auxiliary current and voltage transformers, surge suppression circuits and low-pass filters. The outputs of the auxiliary

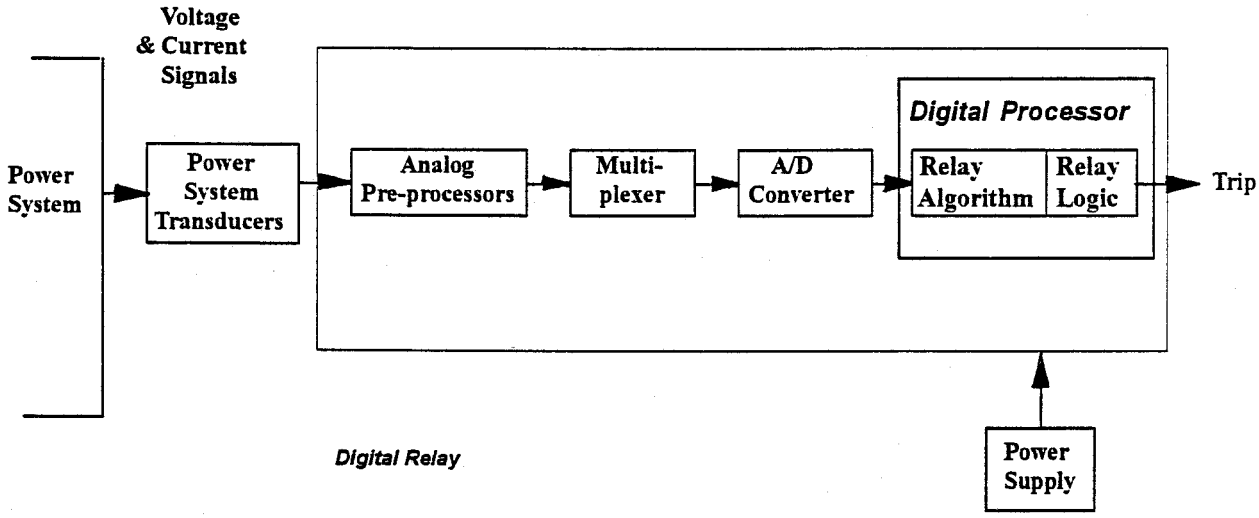

Figure 3.1: Functional block diagram of a typical digital relay.

current transformers are fed into current to voltage converters to convert the current signals to voltage signals. The surge suppression circuits limit the level of voltage signals to protect the relay circuitry. Low-pass filters are used to band limit the input signals to avoid aliasing [27]. The cut-off frequency of the low-pass filter is chosen considering the sampling frequency of the input signals. The outputs of the analog pre-processing units are fed into a multiplexer and into an analog to digital (A/D) converter.

The A/D converter changes the analog signals into digital values. The digitized signals are then fed into a digital processor. The digital processor has two main functions:

1. To evaluate parameters of interest using relay algorithms and
2. To use the computed parameters to decide if there is a fault in the zone of protection or not.

An independent power supply unit, consisting of rectifiers and a set of batteries, supplies power to the relay.

3.3. Benefits of Digital Relaying

Recent advances in the field of micro-processors has enabled digital relays to be viable alternative to electro-mechanical and static relays. While the cost of conventional relays has been increasing, that of digital devices has been decreasing for the last two decades. It is, therefore, logical to say that, in future, digital relays will be more economical to use in power systems than electro-mechanical or static relays. Besides the relaying functions, a digital relay has the ability to perform other tasks, such as self diagnosis and data analysis. This section summarizes some of the advantages of using digital relays.

1. *Flexibility*: Digital relays are more flexible than the conventional relays. They are programmable devices and include multiple characteristics. Revision and modification in digital relay characteristics, necessitated by changes in the operating conditions, can be made through pre-programmed modules. A single general purpose hardware based relay can be designed to perform a variety of protection and control functions with change of the programming only [28]. A number of these functions can be called upon as needed.
2. *Reliability*: Failure rate of digital equipment is higher than the components of conventional relays. However, most digital relays are designed to monitor themselves at regular intervals by exciting the software together with pre-specified data and comparing the results with expected results of a properly functioning device. In the event of deviation of results, the digital relay alerts an operator of the device failure. System reliability can be further increased by the relay checking its hardware at all times and flagging any failures. These features increase the reliability but also increase the hardware and software costs.
3. *Adaptive Capabilities*: A digital relay can be programmed to automatically change its behaviour depending upon its external circumstances which change with time. The basis for the change, can be either local information available directly to the relay, such as load flow in the protected apparatus;

or the change can be initiated from an external source such as a substation operator or a data link from a central system control computer. The change may only be in a specific settings of the relay or a whole new protection routine can be selected when needed [29].

4. *Data-Interface Access*: A digital relaying system can always be equipped with input/output ports through which data and control commands can be exchanged. The pre-fault and post-fault signals can be stored in the relay memory and later transmitted to a central computer through a data link. This information can be used for further investigation that might lead to improved operating practices and relay design.
5. *Mathematical Capabilities*: A digital relay can be programmed to provide any function within the limits of imagination of the designer. Specific protection problems can be broken down into fine details, and each handled separately. For example, many researchers of computer relaying have recognized and proposed equations which can serve as basis for distance protection of transmission lines.

3.4. Digital Relay Algorithms

Digital relay algorithms are programs, in the relay's microprocessor, that use samples of voltages and currents to calculate numerical estimates of parameters needed for power system protection. The algorithms consist of a set of mathematical equations describing the voltage and current waveforms. An adequate model of these waveforms is required in order to obtain an accurate estimation of their parameters by the relay algorithms. These algorithms yield numerical estimates of peak values and phase angles of voltages and currents. The algorithms can be classified according to the mathematical method used and the assumptions made. These algorithms can also be divided based on the window size, i.e.

1. Short window algorithms
2. Long window algorithms

Short window algorithms use fewer samples. The computation time of short window algorithms is smaller than that of long window algorithms but the results of short window algorithms are not as accurate as those of long window algorithms.

Long window algorithms use a large number of samples usually one cycle of $60Hz$ or more. More time is involved in computation since more samples are used in the

estimation. The most desirable feature of long window algorithm is the high degree of accuracy of its estimates. In some situations, computation time can be greatly reduced by computing some of the parameters of the algorithms off-line.

3.4.1. Trigonometric Algorithms

A trigonometric algorithm assumes that the current and voltage waveforms are sinusoids of the fundamental frequency only and that the power system continues to operate at its nominal frequency during application of the algorithm. A voltage signal can be expressed as:

$$v = V_p \sin(\omega_0 t + \theta_v) \tag{3.1}$$

where:

v is the instantaneous value of the voltage,
V_p is the peak value of the voltage,
θ_v is the phase angle,
ω_0 is the nominal angular frequency and
t is time in seconds.

The first derivative of the voltage with respect to time provides Equation (3.2):

$$v' = \omega_0 V_p \cos(\omega_0 t + \theta_v) \tag{3.2}$$

Dividing both sides of this equation with ω_0 provides Equation (3.3):

$$\frac{v'}{\omega_0} = V_p \cos(\omega_0 t + \theta_v) \tag{3.3}$$

Using Equations (3.1) and (3.3), the peak value and phase angle of the voltage signal can be obtained as follows:

$$V_p^2 = v^2 + \left(\frac{v'}{\omega_0}\right)^2 \tag{3.4}$$

$$\omega_0 t + \theta_v = arctan\left(\frac{\omega_0 v}{v'}\right) \tag{3.5}$$

Mann and Morrison [30] estimated the first derivative v' from three consecutive samples. The sampling of the waveforms is done after every interval of ΔT seconds. If actual sampling times are $(k-1)\Delta T$, $k\Delta T$ and $(k+1)\Delta T$ seconds, then estimate of the first derivative at time $k\Delta T$ is mathematically expressed as:

$$v'_k = \frac{v_{k+1} - v_{k-1}}{2\Delta T} \tag{3.6}$$

Gilcrest et al. [31], Rockefeller and Udren [32] used the first and second derivatives of the voltage equation to estimate its peak value and phase angle. The second derivative of the voltage equation is derived as

$$v'' = -\omega_0^2 V_p \sin(\omega_0 t + \theta_v) \tag{3.7}$$

Equations (3.8) and (3.9) give the expressions which were used in References [31] and [32] to estimate the peak value and phase angles.

$$V_p^2 = \left(\frac{v'}{\omega_0}\right)^2 + \left(\frac{v''}{\omega_0^2}\right)^2 \tag{3.8}$$

$$\omega_0 t + \theta_v = arctan\left(\frac{-v''}{\omega_0 v'}\right) \tag{3.9}$$

Equations (3.6) and (3.10) are the mathematical expressions for the first and second derivatives of the voltage signal.

$$v_k'' = \frac{1}{(\Delta T)^2}(v_{k+1} - 2v_k + v_{k-1}) \tag{3.10}$$

Makino and Miki [33] used two samples to determine the peak value and the phase angle of a sinusoid.

3.4.2. Least Error Squares Algorithm

The use of the Least Error Squares technique for estimating the peak value and phase angle of current or voltage phasor was first proposed by Luckett et al [34]. Brooks [35] also used this method assuming that the input signal is a combination of a d.c. component and a fundamental frequency component. Sachdev and Baribeau [36], investigated further and demonstrated that most of the computations can be done off-line. Also they showed that the technique can be applied without pre-specifying the rate of decay of the dc component. This technique is briefly outlined below.

A voltage signal can be expressed by a mathematical model of the form of Equation (3.11).

$$v(t) = K_0 e^{-t/\tau} + \sum_{n=1}^{N} K_m \sin(m\omega_0 t + \theta_m) \tag{3.11}$$

where:

N is the highest order of the harmonic voltage,
K_0 is the magnitude of the decaying d.c. component at $t = 0$,
τ is the time constant of the decaying d.c. component,
K_m is the magnitude of the m^{th} harmonic component and
θ_m is the phase angle of the m^{th} harmonic component.

The model represents a voltage that contains a decaying dc component, a fundamental frequency component and harmonics. Assume the voltage is composed of the fundamental frequency component and a decaying dc component only. Its equation can be defined as follows:

$$v(t)=K_0 e^{-t/\tau} + K_1 \sin(\omega_0 t + \theta_1) \tag{3.12}$$

The exponential of the above equation can be replaced by the first two terms of its Taylor series expansion. Another substitution which can be made is $\cos(\theta_1)\sin(\omega_0 t) + \sin(\theta_1)\cos(\omega_0 t)$ replacing $\sin(\omega_0 t + \theta_1)$ in Equation 3.12. The resulting equation after these substitutions is:

$$v(t) = K_0 - (K_0/\tau)t + (K_1 \cos\theta_1)\sin(\omega_0 t) + K_1 \sin(\theta_1)\cos(\omega_0 t) \tag{3.13}$$

At time $t = t_1$, the voltage equation becomes:

$$v(t_1) = K_0 - (K_0/\tau)t_1 + (K_1\cos\theta_1)\sin(\omega_0 t_1) + (K_1\sin\theta_1)\cos(\omega_0 t_1) \quad (3.14)$$

In linear form the representation of Equation (3.14) is given as:

$$v(t_1) = a_{11}x_1 + a_{12}x_2 + a_{13}x_3 + a_{14}x_4 \quad (3.15)$$

where:

$$x_1 = K_0 \qquad a_{11} = 1$$

$$x_2 = -\frac{K_0}{\tau} \qquad a_{12} = t_1$$

$$x_3 = K_1\cos(\theta_1) \qquad a_{13} = \sin(\omega_0 t_1)$$

$$x_4 = K_1\sin(\theta_1) \qquad a_{14} = \cos(\omega_0 t_1)$$

The next voltage sample arrives at $t_2 = t_1 + \Delta T$. The linear representation of this voltage is given by Equation (3.16)

$$v(t_1 + \Delta T) = a_{21}x_1 + a_{22}x_2 + a_{23}x_3 + a_{24}x_4 \quad (3.16)$$

where:

$$a_{21} = 1 \qquad a_{23} = \sin(\omega_0 t_2)$$

$$a_{22} = t_2 \qquad a_{24} = \cos(\omega_0 t_2)$$

For a preselected time reference and known sampling rate, the values of the *'a'* coefficients become known. Assuming there are *'p'* samples, resulting equations can be expressed in matrix form as follows:

$$[A]\ [X] = [V] \quad (3.17)$$

$$p\times 4\ \ 4\times 1\ \ p\times 1$$

where:

[*A*] is matrix of *'a'* coefficients,
[*X*] is vector of unknowns and
[*V*] is vector of samples.

The vector of unknowns [X] can be determined as follows provided 'p' is greater than four.

$$[X] = [A]^{+}\ [V] \qquad (3.18)$$

$$4\times 1\ \ 4\times p\ \ \ p\times 1$$

where:

$[A]^{+}$ is the left pseudo-inverse of [A].
Its mathematical model is:

$$[A]^{+} = [[A]^{T}\,[A]]^{-1}\,[A]^{T} \qquad (3.19)$$

$$4\times p\quad 4\times p\ p\times 4\ 4\times p$$

The elements of $[A]^{+}$ can be determined off-line. This reduces the on-line calculations necessary for estimating the real and imaginary components of the phasors. The procedure to design a Least Error Squares filter consists of the following steps:

1. Select a suitable model for representing the signal.
2. Linearize the model.
3. Select a sampling rate.
4. Select a data window size and time reference.
5. Express the process in matrix form.
6. Determine the left pseudoinverse of the coefficient matrix.

An important advantage of this approach is that the decaying d.c. component is explicitly filtered out from the input data without prespecifying the X/R ratio of the system.

3.4.3. Correlation Algorithms

The process of correlating an input signal with a pair of orthogonal functions can be used to extract components of selected frequencies from the input signal. Two orthogonal functions commonly used in digital relaying are:

1. Even and odd rectangular waves, and

2. Sine and cosine functions.

A power system signal can also be correlated with itself or with another power system signal. When a signal is correlated with itself it is referred to as auto-correlation while correlating a signal with another is called cross-correlation. The even and odd rectangular waves algorithm correlates a signal with a pair of orthogonal rectangular waves of a specified frequency. The reference rectangular waves are sampled at the frequency that is used for sampling signal waveform. The k^{th} estimate of the real and imaginary part of a voltage phasor extracted from sampled values are obtained using the following equations.

$$V_r(k) = \frac{1}{A}\sum_{n=0}^{m-1} V_{k+n-m+1} Signum(\sin(2\pi\frac{n}{m})) \tag{3.20}$$

$$V_i(k) = \frac{1}{A}\sum_{n=0}^{m-1} V_{k+n-m+1} Signum(\cos(2\pi\frac{n}{m})) \tag{3.21}$$

where:

$$\begin{aligned} Signum(x) &= -1 \quad for\ x < 0 \\ &= 0 \quad for\ x = 0 \\ &= +1 \quad for\ x > 0 \end{aligned}$$

V_r is the real part of the fundamental frequency voltage phasor,
V_i is the imaginary part of the fundamental frequency voltage phasor,
m is the number of samples and

$$A = \sum_{n=0}^{m-1} |\sin(2\pi\frac{n}{m})|$$

The advantage of correlating the signal with an even and odd rectangular waves is that the weighting factors are negative one, zero and positive one. This eliminates multiplication, from the computations.

The Fourier technique, correlates voltage and current signals with sine and cosine functions to estimate their real and imaginary components. This technique can be mathematically described as follows:

$$V_r = \frac{V_p}{\pi}\int_0^{2\pi} \sin(\omega_0 t + \theta_v)\sin(\omega_0 t)d(\omega_0 t) \tag{3.22}$$

$$V_i = \frac{V_p}{\pi}\int_0^{2\pi} \sin(\omega_0 t + \theta_v)\cos(\omega_0 t)d(\omega_0 t) \tag{3.23}$$

where:

V_p is the peak value of the voltage signal,
V_r is the real part of the fundamental frequency voltage phasor,
V_i is the imaginary part of the fundamental frequency voltage phasor and
ω_0 is the nominal frequency of the voltage signals.

In digital relaying, the input signals are sampled at discrete instants of time and, therefore, numerical techniques are used to perform integrations. Using the rectangular rule of integration the k^{th} estimate can be computed as :

$$V_r(k) = \frac{2}{m}\sum_{n=0}^{m-1} V_{k-n+m+1}\sin(2\pi\frac{n}{m}) \tag{3.24}$$

$$V_i(k) = \frac{2}{m}\sum_{n=0}^{m-1} V_{k-n+m+1}\cos(2\pi\frac{n}{m}) \tag{3.25}$$

where:

m is the number of samples in one cycle of $60Hz$.

The peak value and phase angle of the fundamental frequency voltage or current phasor can be obtained from their real and imaginary parts. Figure 3.2 illustrates the use of this technique for computing real and imaginary parts of a $60Hz$ voltage waveform which is sampled 12 times per cycle.

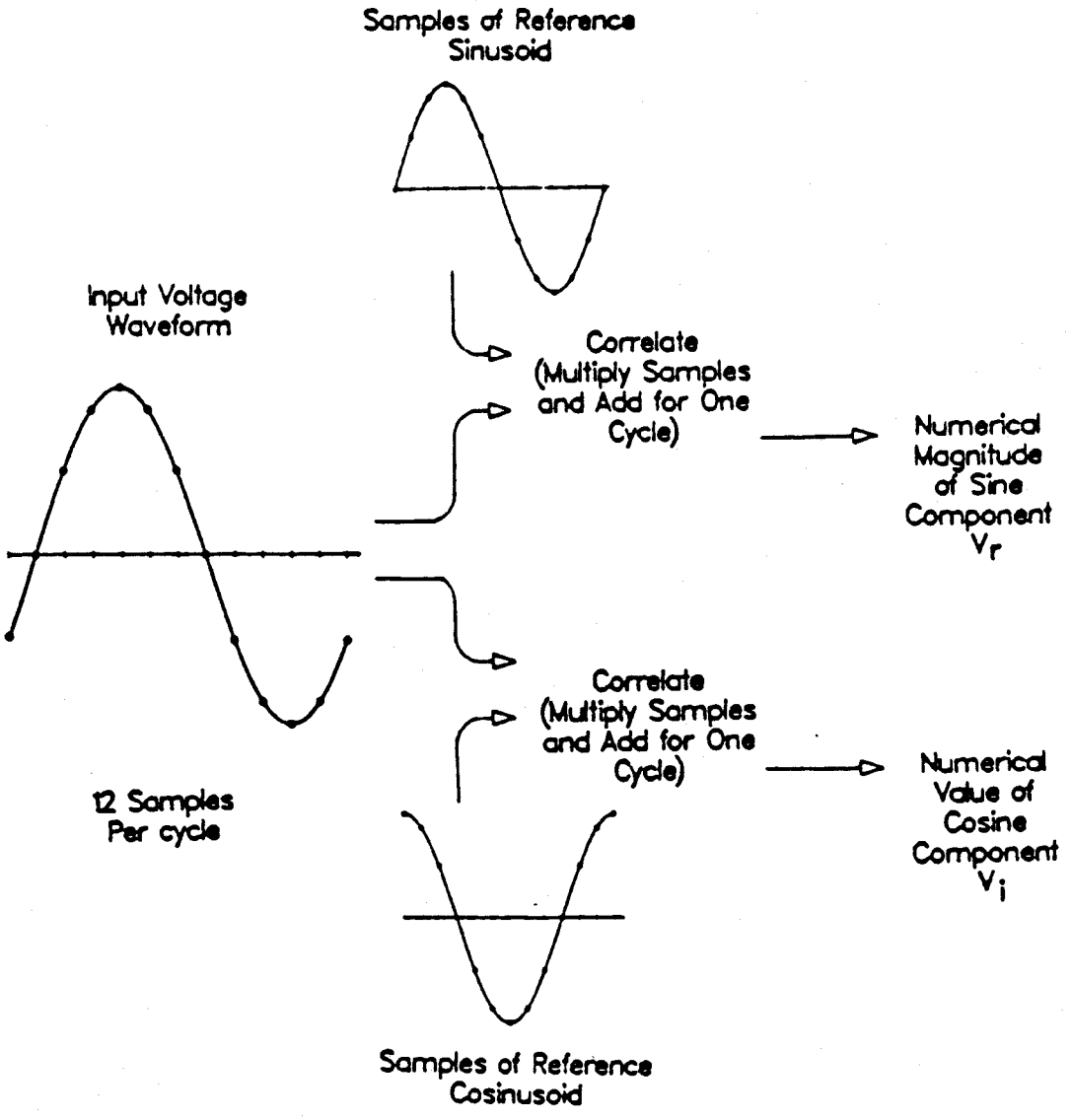

Figure 3.2: The correlation of voltage samples with sine and cosine waves [37].

3.5. Digital Distance Relay Algorithms

With the advent of microprocessors, engineers have developed devices which calculate apparent parameters from sampled data [15, 16]. The digital distance relay algorithms used for this purpose can be divided into two categories. The first category consists of those algorithms which estimate phasors representing the fundamental frequency voltages and currents and then calculate the impedance from the phasor estimates. Digital filters, used for calculating the phasors, are designed to eliminate specified non-fundamental frequency components. The presence of frequencies not considered in the design adversely affects their outputs and, therefore, the estimates of the impedance. The algorithms of second category, model a transmission line in the form of one or more differential equations. These are solved using instantaneous values of voltages and currents [28, 38, 39]; they provide estimates of the apparent parameters of the line.

The impedance plane provides a convenient way of visualizing the results of the calculated impedance estimates. The computed values of impedances for various fault and non- fault conditions are plotted in the plane and compared with the reach characteristics of a digital distance relay.

3.5.1. Impedance Calculation

The algorithms discussed in this section depends on extracting the fundamental frequency components of voltages and currents from the sampled data. Algorithms like the Fourier, Least Error Squares or short-window algorithms can be applied to calculate voltage and current phasors either in rectangular form or polar form. The impedance to the fault is then calculated using these in either polar form, $|Z|\angle\theta$, or in rectangular form, $(R+jX)$. The apparent impedance in rectangular form is calculated using the following expression:

$$Z=R+jX=\frac{(V_rI_r+V_iI_i)}{I_r^2+I_i^2}+j\frac{(V_iI_r-V_rI_i)}{I_r^2+I_i^2} \tag{3.26}$$

where:

Z is the apparent impedance,
V_r is real part of the voltage phasor,
V_i is the imaginary part of the voltage phasor,
I_r is the real part of the current phasor and
I_i is the imaginary part of the current phasor.

3.5.2. Differential Equation Algorithm

In this algorithm parameters of interest are included in the system description rather than the waveform. McInnes and Morrison [38, 40], and other researchers [28, 39, 41] modelled the faulted line as a series R–L circuit. The voltage-current relationship can, therefore, be described as:

$$v(t) = Ri(t) + L\frac{di(t)}{dt} \tag{3.27}$$

where:

$v(t)$ is the instantaneous voltage at relay location ,
$i(t)$ is the instantaneous current at relay location,
R is the resistance of the line from the relay location and
L is the inductance of the line from the relay location.

Solution for R and L parameters is obtained by integration over two successive time periods. Integrations are performed using the trapezoidal rule. The sampled - data expressions for 3 samples are:

$$L = \frac{\Delta t}{2}\left[\frac{(i_k+i_{k-1})(v_{k-1}+v_{k-2})-(i_{k-1}+i_{k-2})(v_k+v_{k-1})}{(i_k+i_{k-1})(i_{k-1}-i_{k-2})-(i_{k-1}+i_{k-2})(i_k-i_{k-1})}\right] \tag{3.28}$$

$$R = \left[\frac{(v_k+v_{k-1})(i_{k-1}-i_{k-2})-(v_{k-1}+v_{k-2})(i_k-i_{k-1})}{(i_k+i_{k-1})(i_{k-1}-i_{k-2})-(i_{k-1}+i_{k-2})(i_k-i_{k-1})}\right] \tag{3.29}$$

where:

R is the resistance of the line upto the fault point as seen from relay location and
L is the inductance of the line upto the fault point as seen from relay location.

The compensating factor K_0 used in the calculation of single phase faults mentioned in the previous chapter, is calculated differently for the differential algorithm. For the inductance estimation it will be:

$$K_0=\frac{L_0-L_1}{L_1} \tag{3.30}$$

and for the resistance it will be:

$$K_0=\frac{R_0-R_1}{R_1} \tag{3.31}$$

where:

L_0 is the zero-sequence of the inductance of the line,
L_1 is the positive-sequence of the inductance of the line,
R_0 is the zero-sequence of the resistance of the line and
R_1 is the positive-sequence of the resistance of the line.

This algorithm described by Equations (3.28) and (3.29) is a short window algorithm and hence is not as selective as a long window algorithm. The model is valid only for lines that are not extremely long, permitting shunt capacitance to be neglected. For long lines, shunt- admittance effects introduce some error. The advantage of this algorithm is that the d.c. offset is not an error signal since it satisfies the differential equation.

3.6. Summary

This chapter has presented the functional blocks of a typical digital relay. The advantages of digital relays over conventional relays (electromechanical and static) have been presented. Digital relays use a set of mathematical equations or relaying algorithms to estimate the parameters of interest for power system protection.

In the case of distance relays for transmission line protection, faults are located by measuring the apparent impedance looking into the transmission line. The measurement is then used to determine whether the fault is in the protection zone. Some of the

algorithms that can be used to estimate the apparent impedance by extracting the fundamental components of the voltage and current phasors have been presented in this chapter. Another form of algorithms which are based on the line model have also been described. The fast and accurate measurement of the apparent impedance is a primary requirement for reliable protection of transmission lines.

4. DIGITAL SIMULATION OF MAGNETIZING INRUSH CURRENT

4.1. Introduction

Transformers are important elements of a power system. These devices are used for changing the levels of voltages suitable for efficient transmission or utilization of electrical power. A transformer consists of a magnetic core built of insulated silicon steel laminations upon which are wound two distinct sets of coils suitably located with respect to each other and are termed the primary and secondary windings. The primary winding is the winding to which the supply voltage is applied irrespective of whether it is the higher or lower voltage winding; the other winding to which the load is directly connected is termed the secondary winding. Its purpose is to transfer electrical energy from one circuit to another, usually without any electrical connection between the two circuits.

If the behaviour of the transformer is to be analyzed, then its mathematical model must be constructed. The transformer, though probably is one of the most familiar component of the power system, it is also one of the most difficult to model accurately. To model a transformer in a transient situation, nonlinear behaviour of its core must be taken into account [2, 42].

This chapter concerns itself with the modelling of magnetizing inrush current in transformers. A discussion of the way transformers are modelled in the EMTDC program, based on the classical theory of coupled circuits, is included [43]. Procedure for modelling of saturation in transformers is also described. The physics of inrush current which occurs during energization of transformers is discussed. Extension of the single-phase transformer models to simulate three-phase transformers is outlined.

Procedure for including the residual flux in simulation of magnetizing inrush current in three-phase transformer is developed. Some simulation results on inrush current in a three phase bank connected in Delta-Wye configuration are also included and discussed in this chapter.

4.2. Magnetizing Inrush Current Phenomenon

This is a transient phenomenon, characteristic of the magnetizing current of the transformer when it is being energized. It may cause a momentary dip in the voltage if the impedance of the source of excitation is considerable. Magnetizing inrush current can be classified according to its causes as follows:

1. *Initial magnetizing inrush current:* This occurs when energizing a transformer after a prior period of de-energization. This has the capacity to produce the maximum magnetizing inrush current [11].
2. *Recovery magnetizing inrush current:* This happens when voltage is returning to normal after a fault or a momentary dip in the voltage. The worst case is a solid three-phase fault near the transformer bank; since the voltage is reduced nearly to zero then suddenly it is restored to normal when the fault has been cleared. This produces inrush current, but its maximum will not be as high as in case 1 because the transformer will be partially energized [11].
3. *Sympathetic magnetizing inrush current:* This occurs when a transformer is connected to a line to be paralleled with a transformer which is already energized, the voltage drop in the line impedance due to inrush current in the transformer being connected appears to the second transformer as a change in line voltage. The result is a 'sympathetic inrush' current flow in the transformer which is already energized. This inrush current will never be as high as initial magnetizing inrush current [44].

If the magnetizing characteristics of a single-phase transformer are as shown in Figure 4.1; the magnetizing current will follow the hysterisis loop to zero when the transformer is switched off retaining a flux density B_r. For M-19 steel core, a value for H_{max} of 160 ampere turns/m results in B_{max}= 1.0T and B_r= 0.64T. Figure 4.2 shows magnetizing current wave I_1 and flux density wave B_1 definitely interrupted at the instant marked by the first dotted line on the left, at which the current was passing through a normal zero value, with the flux at a residual value B_r. If the transformer had not been switched off, both the flux density and current waves would have followed the dotted curves. Since the transformer has been switched off, they both follow the solid horizontal lines, with I_2

at zero and flux density at B_r. If the transformer is re-energized at instant t_1 when the flux density would normally be at its negative maximum value $-B_{max}$; the flux will start at the end of curve B_2 with a residual value B_r and traces the curve B_3. This curve is a sinusoid having a d.c. offset which results in the saturation of the transformer core. The magnetizing current required to produce the flux is drawn from the power system with I_3 being the corresponding current to B_3. This current is remarkably higher than the normal magnetizing current, I_1.

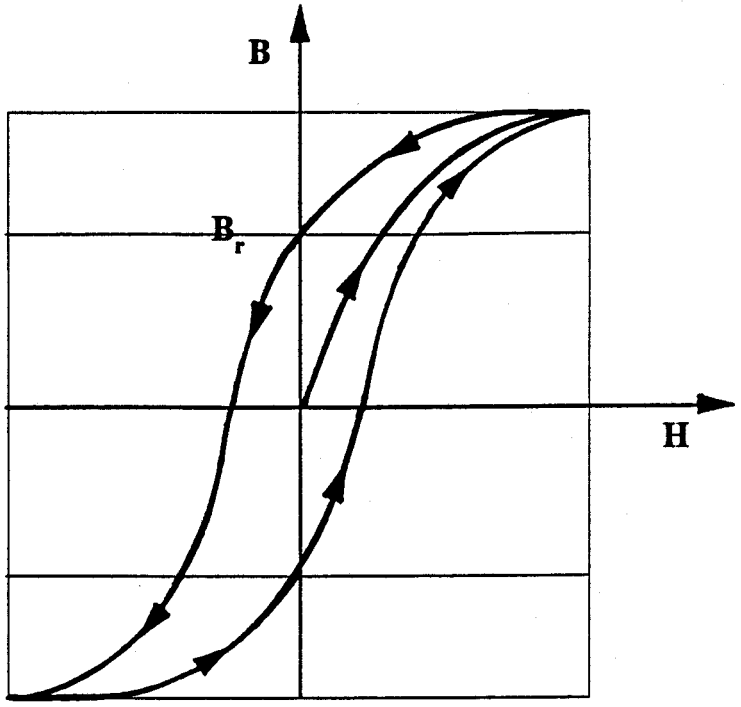

Figure 4.1: Magnetizing characteristics of a typical single-phase power transformer.

Inrush current in three-phase banks is a complicated phenomenon [44, 45]. When transformers in three-phase bank are connected in delta on the side to be energized, the inrush will be exactly the same as for the single-phase transformers if the voltage is maintained at full value. If however, the line impedance is high enough to cause an appreciable drop in voltage when inrush current flows through it, the whole phenomenon becomes complex. The inrush current into one phase only can approach the theoretical maximum because the time of closing the circuit will be the correct instant to cause

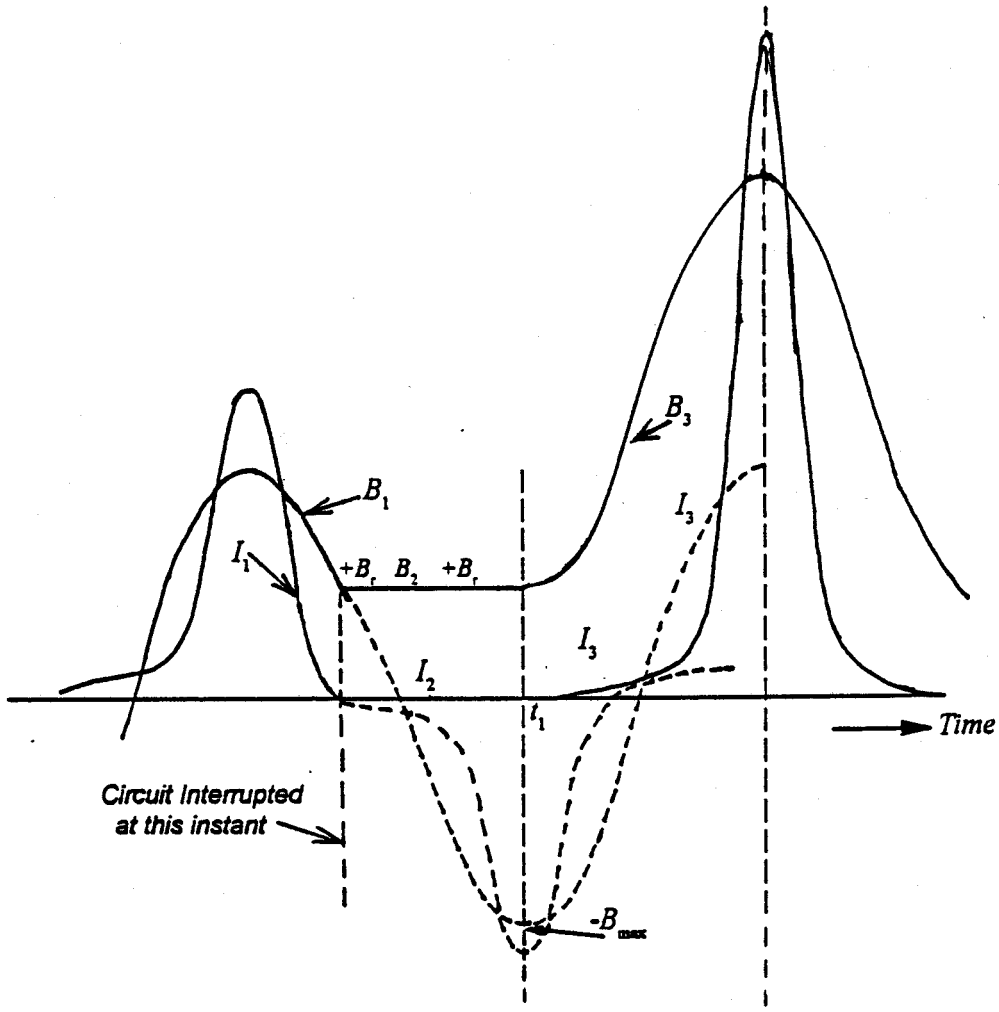

Figure 4.2: Residual flux density and inrush current phenomenon.

maximum inrush current in only one phase. The other two phases, being displaced in time by 120°, will draw much less current. The currents in the three lines will then have three entirely different values, the voltage drops in the three lines will be different, and the voltages at the transformer terminals will likewise be different for each phase.

4.3. Factors Which Determine the Magnitude of Inrush Current

The initial value of the current taken on no-load by the transformer at the instant of switching on is principally determined by the point of the voltage wave at which switching on occurs, but it is also dependent on the magnitude and polarity of the residual magnetism which may be left in the core after the transformer is switched off [46]. In studying inrush current, it is better to determine the flux in the magnetic circuit first and then derive the current from the flux. This procedure is preferable because the flux does not depart much from a sine wave even though the current is usually distorted.

If the secondary of a transformer is open, the differential equation for the circuit, neglecting the winding resistance, can be written as follows:

$$e = n_1 \frac{d\phi}{dt} \tag{4.1}$$

where:

e is the instantaneous value of supply voltage,
ϕ is the instantaneous flux threading primary winding and
n_1 is the number of primary turns.

Consider that the supply voltage is sinusoidal as:

$$e = \sqrt{2}E\sin(\omega t + \lambda) \tag{4.2}$$

where:

E = rms value of supply voltage and
$\omega = 2\pi f$

Substituting the value of e in Equation (4.1) provides

$$\sqrt{2}E\sin(\omega t + \lambda) = n_1\frac{d\phi}{dt}. \tag{4.3}$$

Solving the above differential equation provides

$$\phi = -\sqrt{2}\frac{E}{\omega n_1}\cos(\omega t + \lambda) + \phi_t. \tag{4.4}$$

In this solution, $(-\sqrt{2}E/\omega n_1)\cos(\omega t + \lambda)$ is the normal steady-state flux in the transformer core. The second term, ϕ_t, represents a transient component of flux, the magnitude of which depends upon the instant at which the transformer is energized, the normal maximum flux and the residual flux in the core at the time the transformer is

energized. Under steady-state conditions this component is equal to zero. Equation (4.4) can be rewritten as:

$$\phi = -\phi_m \cos(\omega t + \lambda) + \phi_t \tag{4.5}$$

where:

$$\phi_m = \sqrt{2}\frac{E}{\omega n_1} \tag{4.6}$$

At $t=0$

$$\phi_0 = -\phi_m \cos\lambda + \phi_{t0} \tag{4.7}$$

where:

ϕ_0 is the transformer residual flux,
$-\phi_m \cos\lambda$ is the steady-state flux and
ϕ_{t0} is the initial transient flux

In the above equation the angle λ depends upon the instantaneous value of the supply voltage at the instant the transformer is energized. If the transformer is energized at zero voltage, λ is equal to 0, whereas, if it is energized at where the supply voltage is at a positive maximum, λ is equal to 90°.

Assume that a transformer having zero residual flux is energized when the supply voltage is at a positive maximum. For these conditions, ϕ_0 and $\cos\lambda$ are both equal to zero so ϕ_{t0} is also equal to zero. As is assumed there is no residual magnetism in the core, the desired conditions are obtained which produce the normal steady time distribution of the flux and there would be no transient. That is, at the instant of switching on, the flux starts from zero, rises to the normal maximum in one direction, falls to zero, rises to the normal maximum in the opposite direction and again reaches zero, the wave being symmetrically disposed about the zero axis. The no-load current, therefore, pursues its normal course and does not exceed the magnitude of the normal no-load current.

However, if a transformer having zero residual flux is energized at zero supply voltage the following conditions exist:

$$\lambda=0 \tag{4.8}$$
$$-\phi_m\cos\lambda=-\phi_m \tag{4.9}$$
$$\phi_0=0 \tag{4.10}$$
$$\phi_{t0}=\phi_m \tag{4.11}$$

Substituting ϕ_{t0} in Equation (4.5) provides

$$\phi=-\phi_m\cos(\omega t)+\phi_m. \tag{4.12}$$

Under normal conditions the magnetic flux in the core, being 90° out of phase with the voltage, reaches its peak value when the voltage passes through zero. Due to this phase displacement it is necessary for the flux to vary from a maximum in one direction to a maximum in the opposite direction in order to produce one half cycle of the required back e.m.f in the primary winding, so that the total flux produced during the half cycle correspondes to twice the maximum flux density. At the instant of switching in there being no residual magnetism in the core, the flux must start from zero, and to maintain the first half cycle of the voltage wave it must reach a value corresponding to twice the normal maximum flux density. As the magnitude of no-load current is dependent upon the flux density, the maximum initial transient current may be as high as 8 to 30 times the full-load current. The total flux wave consists of a sinusoidal flux plus a d-c flux [45, 46, 47].

Not all the flux is carried by the core. The core can carry only a flux ϕ_{sat} corresponding to its saturation; the rest is carried by space [44]. As a result, during saturation the current is limited only by the impedance which the coil would have with the core removed. This impedance is principally a reactance and the inductance in the line simply adds to this air-core reactance of the coil in limiting the inrush current.

In addition to the time point of energization with relation to the flux requirements, are the size of the transformer, the size of the power system source, type of iron in the transformer and *L/R* ratio of the transformer and system.

4.4. Modelling of Single-Phase Transformers

The fundamental principal from which the theory of transformer modelling in EMTDC is based on, comes from the well-known voltage equations for coupled circuits [43]:

$$v_1 = R_1 i_1 + L_1 \frac{di_1}{dt} + M_{12} \frac{di_2}{dt}. \tag{4.13}$$

$$v_2 = R_2 i_2 + L_2 \frac{di_2}{dt} + M_{21} \frac{di_1}{dt}. \tag{4.14}$$

where:

Subscripts 1 and 2 refer to the primary and secondary windings in a two mutually coupled winding,
v_1 and v_2 are the instantaneous terminal voltages,
i_1 and i_2 are the instantaneous currents,
R_1 and R_2 are the winding resistances,
L_1 and L_2 are the self-inductances of the windings and
M_{12} and M_{21} are the mutual inductances assumed equal.

The resistance of the transformer windings is so small that the voltage drop in resistance due to the exciting current is negligible compared with the terminal voltage. In a power-system transformer at no load, normal voltage, and normal frequency, the value of this voltage drop in the excited winding is usually less than 0.1 per cent of the effective value of the applied voltage [43]. For such a condition, it is sufficiently accurate to neglect the resistance drop and equate the terminal voltage, v, to the counter electromotive force e induced by the changing flux in the winding. The relation between the maximum values of the induced voltage and flux can then be expressed as:

$$E_{max} = \omega N \phi_{max} = 2\pi f N \phi_{max}. \tag{4.15}$$

where:

E_{max} is the maximum generated voltage,
ϕ_{max} is the maximum flux,
N is the number of turns in the winding and
f is the frequency of the applied voltage.

The effective value E of the generated voltage becomes:

$$E=\frac{2\pi}{\sqrt{2}}fN\phi_{max}=4.44fN\phi_{max} \tag{4.16}$$

This equation gives the effective or rms value of the voltage generated by a sinusoidally varying flux and the maximum value of the flux. The induced voltage leads the flux by 90°. The coupling circuit between the windings, showing the terminal voltages expressed in terms of the induced voltages, is shown in Figure 4.3.

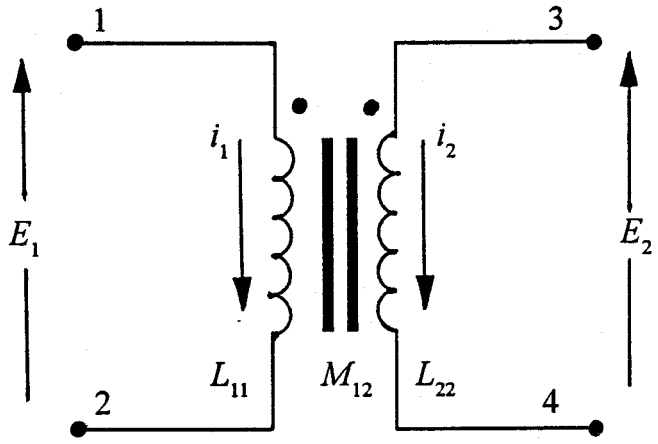

Figure 4.3: Two mutually coupled windings.

Equations (4.13) and (4.14) can also be expressed in matrix form as follows:

$$\begin{bmatrix} E_1 \\ E_2 \end{bmatrix} = \begin{bmatrix} L_{11} & M_{12} \\ M_{12} & L_{22} \end{bmatrix} \frac{d}{dt} \begin{bmatrix} i_1 \\ i_2 \end{bmatrix} \tag{4.17}$$

where:

E_1 is the voltage across the primary winding,
E_2 is the voltage across the secondary winding,

L_{11} and L_{22} are the self inductances of the primary
and secondary windings respectively and
M_{12} is the mutual inductance between the two windings.

The inversion of the inductance matrix in Equation (4.17) enables the winding currents i_1 and i_2 to be calculated, i.e.

$$\frac{d}{dt}\begin{bmatrix} i_1 \\ i_2 \end{bmatrix} = \frac{1}{\Delta}\begin{bmatrix} L_{22} & -M_{12} \\ -M_{12} & L_{11} \end{bmatrix}\begin{bmatrix} E_1 \\ E_2 \end{bmatrix} \tag{4.18}$$

where:

$\Delta = L_{11}L_{22} - M_{12}^2 = L_{11}L_{22}(1 - K_{12}^2)$
$K_{12} = M_{12}/\sqrt{L_{11}L_{22}}$
and it is called the coupling coefficient.

The constant K is a useful quantity in coupled-circuit theory and is one for ideal transformer. A utility in the EMTDC program uses the open-circuit and short-circuit tests to calculate the self inductance L_{11} or L_{22} and mutual inductance M respectively. In open-circuit test, one winding is open-circuited and a voltage at rated frequency is applied to the other winding giving the self inductance as follows:

$$L_{xx} = \frac{V_x}{\omega I_x} \tag{4.19}$$

where:

I_x is the magnetizing current,
V_x is the rated rms voltage,
L_{xx} is the self inductance of the winding having the applied voltage and
ω is the nominal angular frequency.

As for the short-circuit test, one winding is short circuited across its terminals and a reduced voltage of a magnitude to cause a specific value of current, usually rated current,

to flow in the short-circuited winding is applied. The mutual inductance can then be calculated from the general equation:

$$M_{xy}=K_{xy}\sqrt{L_{xx}L_{yy}}. \tag{4.20}$$

where:

M_{xy} is the mutual inductance,
K_{xy} is the coupling coefficient and
L_{xx} and L_{yy} being the self inductances of the windings respectively.

4.5. Modelling Saturation in Single-Phase Transformers

Saturation in the transformer is modelled by current sources across the windings [42, 43, 44]. The use of a current source in modelling saturation is an approximate way of adding saturation to mutually coupled windings. More sophisticated saturation models are reported in the literature but they have the disadvantage that the data is not easily available to make use of them [42, 48]. The saturation model using a current source for a two winding single-phase transformer is shown in Figure 4.4. The magnetizing current is injected into the network through the use of the Norton interface current [42].

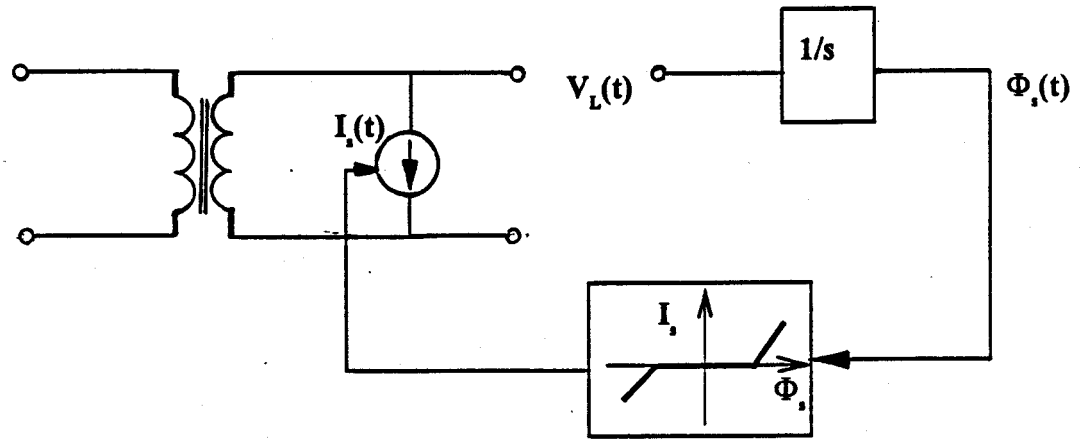

Figure 4.4: Single phase transformer saturation modelling with a current source across the winding.

The current $I_s(t)$ is a function of the winding voltage, V_L. The winding flux $\Phi_s(t)$ is calculated by assuming that the current $I_s(t)$ is the current in the non-linear saturating inductance $L_s(t)$ so that:

$$\Phi_s(t)=L_s(t)I_s(t) \tag{4.21}$$

This equation results in the curve shown in Figure 4.5 where the flux is shown as a function of the current. The air core inductance L_A is drawn as a straight line meeting the flux axis at Φ_k. L_s represents the actual saturation characteristics curve of the single phase transformer since the inductance starts to depend on the current in the coil only when the core starts to saturate [49]. Φ_m and I_m are the peak magnetizing flux and current respectively at rated voltage defining the sharpness of the knee point of the saturation curve.

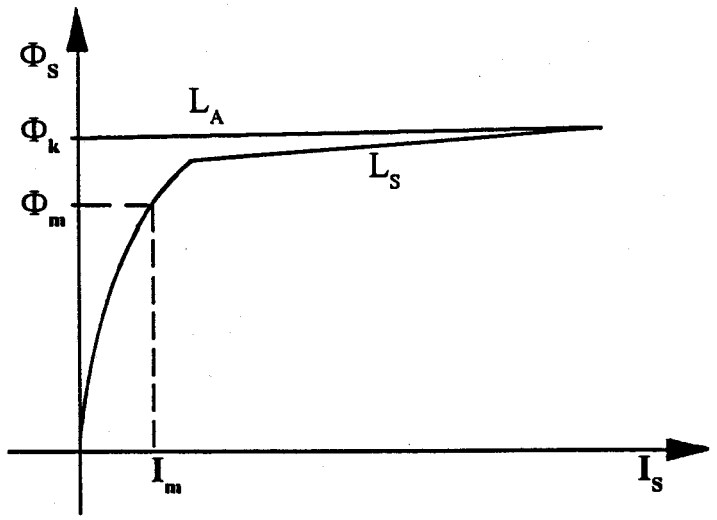

Figure 4.5: Saturation characteristic of a transformer

Provided the values of L_A, Φ_k, Φ_m, and I_m are known, the equation for the current in the non-linear saturating inductance L_s is given by:

$$I_s=\left[\frac{\sqrt{(\Phi_s-\Phi_k)^2+4DLA}+(\Phi_s-\Phi_k)}{2LA}\right]-\frac{D}{\Phi_k} \tag{4.22}$$

where:

$$A=\frac{L_A}{\Phi_k^2}$$

$$B=\frac{[L_A I_m - \Phi_m]}{\Phi_k}$$

$$C=I_m[I_m L_A - \Phi_m+\Phi_k]$$

$$D=\frac{-B-\sqrt{B^2-4AC}}{2A}$$

The flux $\Phi_s(t)$ is calculated as a function of the integral of the winding voltage, $V_L(t)$ i.e.

$$\Phi_s(t)=\int V_L(t)dt \qquad (4.23)$$

4.6. Extension of Single-Phase to Three-Phase Transformer Modelling

In this project, a three-phase transformer is modelled by connecting three single-phase unit transformers having the same parameters to form the desired connections. It is assumed that there is no magnetic coupling between windings of different phases in the three-phase bank . Only coupling between the windings within the same phase is considered. The air core reactance of the transformer is taken as twice the positive-sequence leakage reactance. Saturation in the three-phase bank transformer is modelled equally to a single-phase transformer in all the three phases. The fluxes, both normal and transient, in a three-phase bank flow just as freely as in a single-phase bank, without any complication from saturation or otherwise.

Since in the modelling of the transformer banks it is assumed that no coupling

between windings of different phases exist; the following analysis on flux distribution in the core becomes valid. Consider the flux equations in the three phases for a steady state situation to be:

$$\phi_A=\phi_m\sin(\omega t) \tag{4.24}$$
$$\phi_B=\phi_m\sin(\omega t-120°) \tag{4.25}$$
$$\phi_C=\phi_m\sin(\omega t+120°) \tag{4.26}$$

where:

ϕ_A is flux in phase A,
ϕ_B is flux in phase B,
ϕ_C is flux in phase C and
ϕ_m is the maximum flux.

Assuming that phase A is experiencing positive maximum flux then:

$$\omega t=90° \tag{4.27}$$
$$\phi_A=\phi_m\sin(90°)=\phi_m \tag{4.28}$$
$$\phi_B=\phi_m\sin(90°-120°)=-\frac{\phi_m}{2} \tag{4.29}$$
$$\phi_C=\phi_m\sin(90°+120°)=-\frac{\phi_m}{2} \tag{4.30}$$

Secondly if phase B is the one experiencing positive maximum flux then:

$$\omega t=210° \tag{4.31}$$
$$\phi_A=\phi_m\sin(210°)=-\frac{\phi_m}{2} \tag{4.32}$$
$$\phi_B=\phi_m\sin(210°-120°)=\phi_m \tag{4.33}$$
$$\phi_C=\phi_m\sin(210°+120°)=-\frac{\phi_m}{2} \tag{4.34}$$

Finally if phase C is the one experiencing the maximum positive flux then:

$$\omega t = 330° \tag{4.35}$$

$$\phi_A = \phi_m \sin(330°)) = -\frac{\phi_m}{2} \tag{4.36}$$

$$\phi_B = \phi_m \sin(330° - 120°) = -\frac{\phi_m}{2} \tag{4.37}$$

$$\phi_C = \phi_m \sin(330° + 120°) = \phi_m \tag{4.38}$$

A similar analysis can be done for negative maximum flux.

4.7. Simulation Results

The transformer model described and used in this project belongs to a class of models which can accurately reproduce the response of a transformer at which the short-circuit and open-circuit tests are made; namely, at power frequency through the use of the equivalent networks [2, 42, 49]. The transformer model used is shown in Figure 4.6.

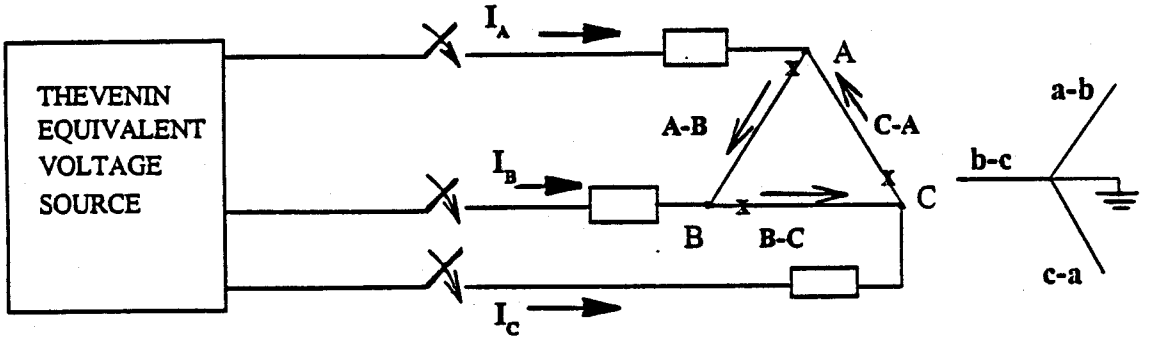

Figure 4.6: The transformer model constructed.

The electrical parameters of the model are given in Table 4.1. Using the utility in EMTDC, data for a single core of a transformer were generated and used to build a three phase transformer model from single phase units. In the constructed three phase transformer model, the winding losses are approximated by external resistors connected

Table 4.1: Transformer data.

Connection of winding	Rated Voltage (*KV*)	Capacity (*MVA*)	Positive sequence reactance (%)	Magnetizing current for both winding (%)	System base frequency (*HZ*)
$\Delta - Y_{\perp}$	138/13.8	120	10	2.5	60

in series with the winding [43, 44]. The subroutine which models and controls three phase transformer saturation has been modified so as to read and record the calculated flux. High resistors are connected to ground on the delta winding to help maintain numerical stability. The model has been used successfully to simulate the current transient known as magnetizing inrush current or simply inrush current which occurs during switching on of transformers. The rated potential difference at rated frequency was applied to the primary terminals with the secondary open circuited for the initial studies conducted. This is modelled by connecting very high resistance to ground on the wye winding [42, 43, 44, 45].

In this project, initial studies on inrush current were done using the above described transformer model. The following observations were made from the results obtained from the transformer model.

1. The exciting current in the three phase banks is very complex and the closing of the three-phase switch contacts which initiates the inrush current is never simultaneous [44]. If the instant is most favourable for one of the phases, it will be unfavourable to the other two. Inrush currents are therefore experienced in at least two phases as shown in Figure 4.7.
2. *Wave shape of inrush current:* The waveform of inrush current is completely offset and alternate half cycles are none existent as shown in Figures 4.7 and 4.8 for the line inrush currents and winding inrush currents respectively. The wave shape of later cycles are very different from that of the initial one. The waveshape depends on the connections of the winding,

and the instant at which the circuit is interrupted. Figure 4.10 shows the different shapes when the circuit was interrupted at a different time from that specified in Figure 4.7. It is not sinusoidal like the corresponding flux (Figure 4.9) for inrush current of Figure 4.7 because of the distortion due to the saturation of the transformer core.

3. *Successive peaks of inrush current*: The resistance of the winding (modelled as an external resistance) contributes an appreciable part of the voltage drop so that the flux does not have to rise quite high. The resistance voltage drop represents a net decrease in flux required, according to the relation

$$iR=e=N\frac{d\phi}{dt} \tag{4.39}$$

so that

$$\phi=\int\frac{iR}{N}dt \tag{4.40}$$

where ϕ represents the flux that would have been required to contribute the voltage actually contributed by the *iR* drop. This means there is a net decrease in the total flux in each cycle so that the inrush current finally decays to zero when the excess flux becomes negligible. This decay depends on the amount of resistance in the winding. Figure 4.11 shows the effect of increasing the value of external resistance to almost five times the value used in simulating inrush current of Figure 4.7.

4. *Rate of decay of the inrush current:* Rate of decay is very fast during the first few cycles and progressively slower thereafter. This is evident nearly in all the figures presented on inrush currents. The manner of decay is not exponential but, it maintains its character of being a pulsating direct current, one pulse every cycle.

5. *Effect of residual magnetism on inrush current*: The residual magnetization in the three cores are of uncertain magnitudes and directions for they depend on the instant of the cycle at which the transformer circuit has previously been interrupted [44]. To obtain the flux, one of the subroutine within the EMTDC which injects current in the windings was modified so as to record the calculated flux. Also, a combination of equations were added to the output subroutine so as to be able to output the flux data to an output file. The residual flux in each case was obtained by switching out the transformer (using a snapshot to retain residual flux data at that instant) and then switching back in the transformer at any time of interest. Figures 4.12 and 4.13 show the residual flux and the corresponding magnetizing inrush current. Generally, the effect of the residual magnetization is that of increasing the inrush current as compared to when there is no residual magnetism as illustrated for inrush current in Figures 4.7 and 4.9

The residual flux values in this case are:

a. Flux in phase A-B = -0.008394 kWb.

b. Flux in phase B-C = 0.01652 kWb.

c. Flux in phase C-A = -0.008128 kWb.

Exact determination of inrush current will usually not be feasible. Indeed all that can be decided is the probability that inrush current will exceed some value.

4.8. Some Measures to Reduce Inrush Current

An objection to the inrush current is the mechanical forces which are exerted between coils at the instant of switching in. For, if a conductor carries current, a magnetic field is set up round the conductor in the form of concentric circles, the density of the field at any point being directly proportional to the current in the conductor and inversely proportional to the distance between the conductor and the point considered. If two conductors both carrying current are in close proximity to each other, they will each be subjected to a force. If the current in both conductors is in the same direction, then, the magnetic fields will produce a force of attraction between the conductors, while with currents, flowing in opposite directions, a repulsive force will be set up [46].

For ordinary power transformer it has been suggested that the residual magnetism may be minimized if the load on the transformer is switched off before the primary circuit is opened. In this case, when the transformer is finally switched out of circuit the only current flowing will be the normal no-load current which will be lagging behind the applied voltage by an angle usually between 70° and 90°. As it is generally found that a circuit breaker opens a circuit at or near zero current, this will correspond to a point at or near the maximum point on the voltage wave so that the flux in the core will be nearly zero [46]. If the transformer is switched out of circuit on load, zero current will, in the case of a non-inductive load, correspond nearly to zero voltage, so that the residual magnetism left in the core would be a maximum; but the more inductive the load, the less likelihood is there of switching out at zero voltage.

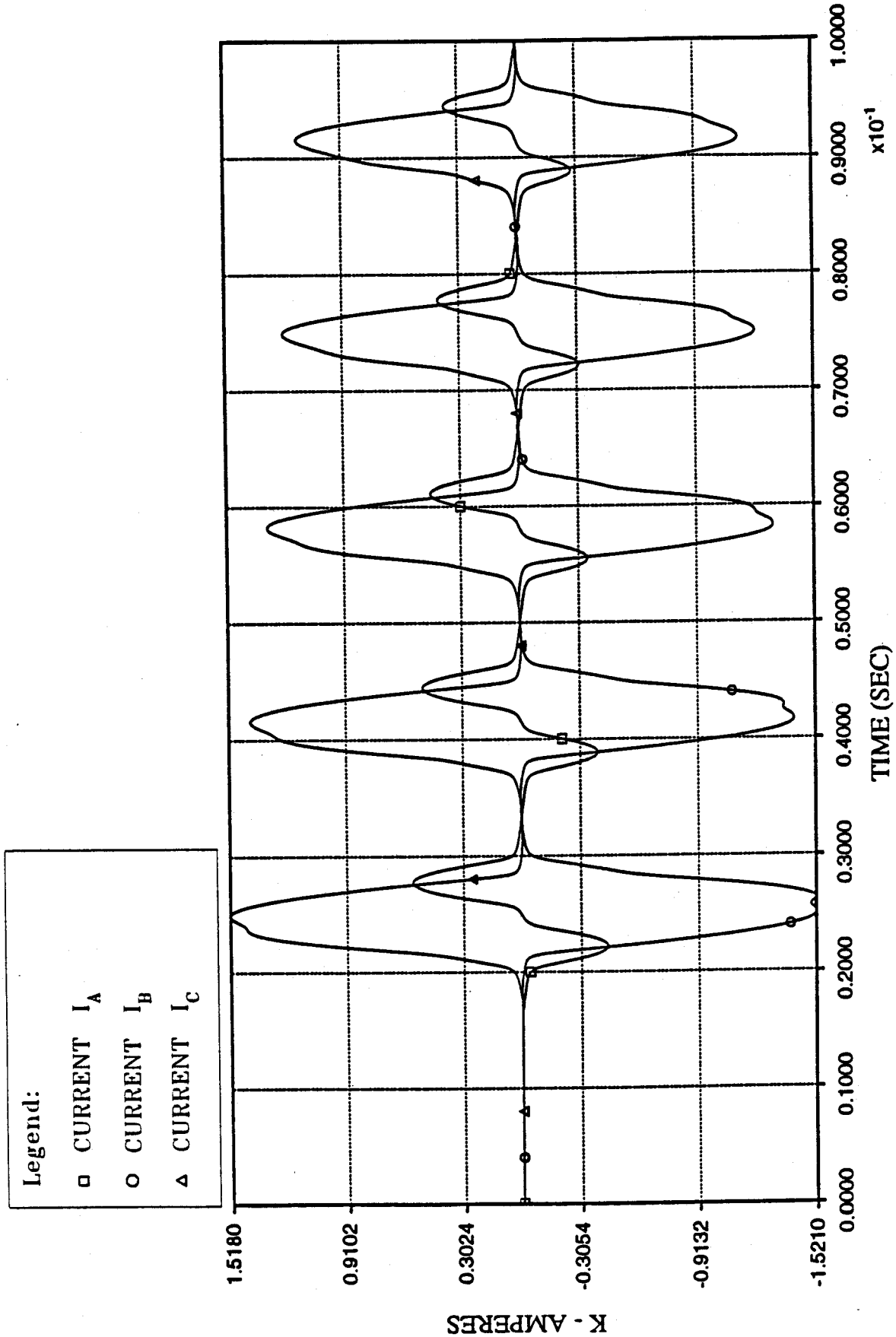

Figure 4.7: Inrush current during switching in of the transformer at 0.0167 seconds showing inrush current at least in two of the phases.

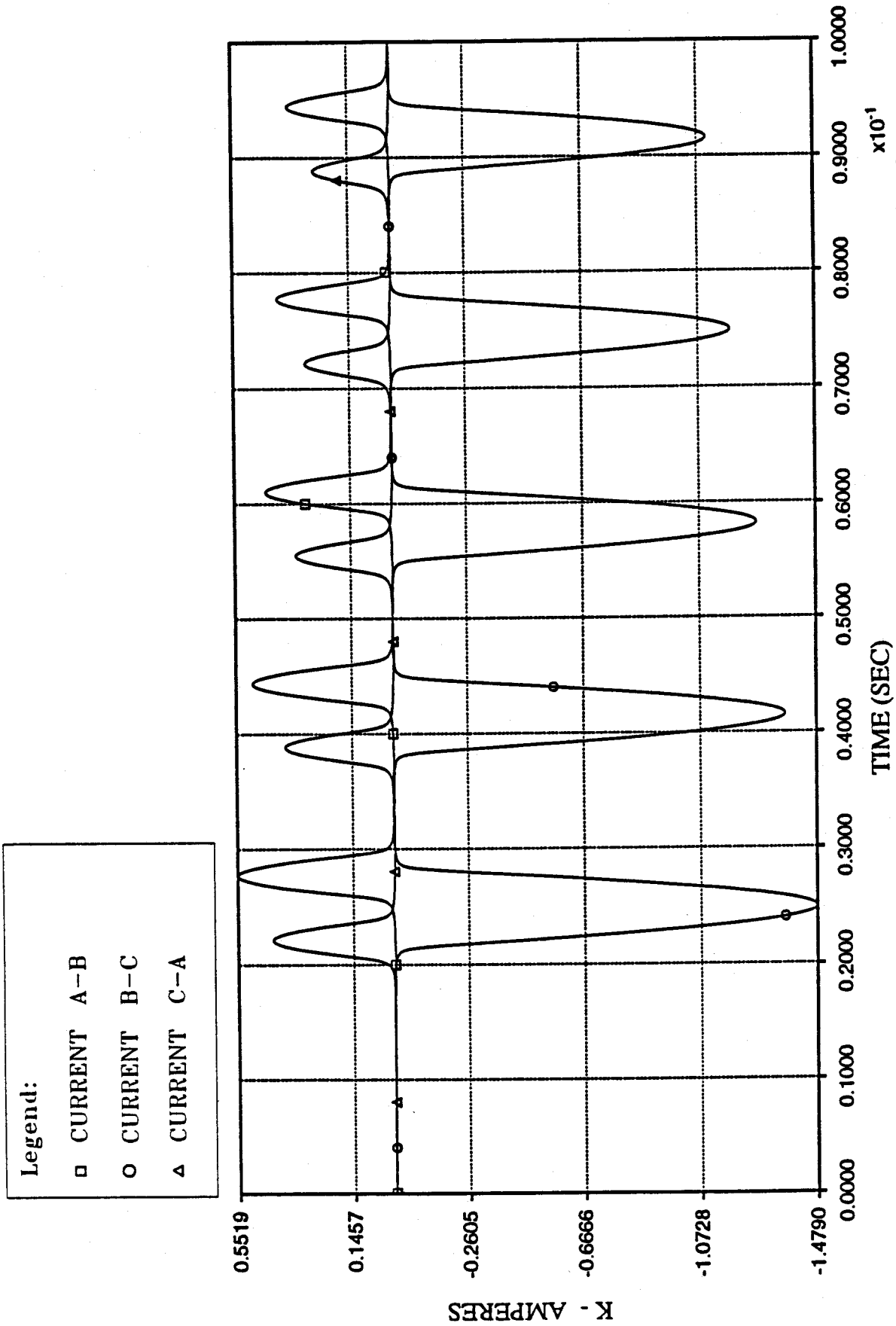

Figure 4.8: Inrush current in the delta winding during the switching in of transformer at 0.0167 seconds.

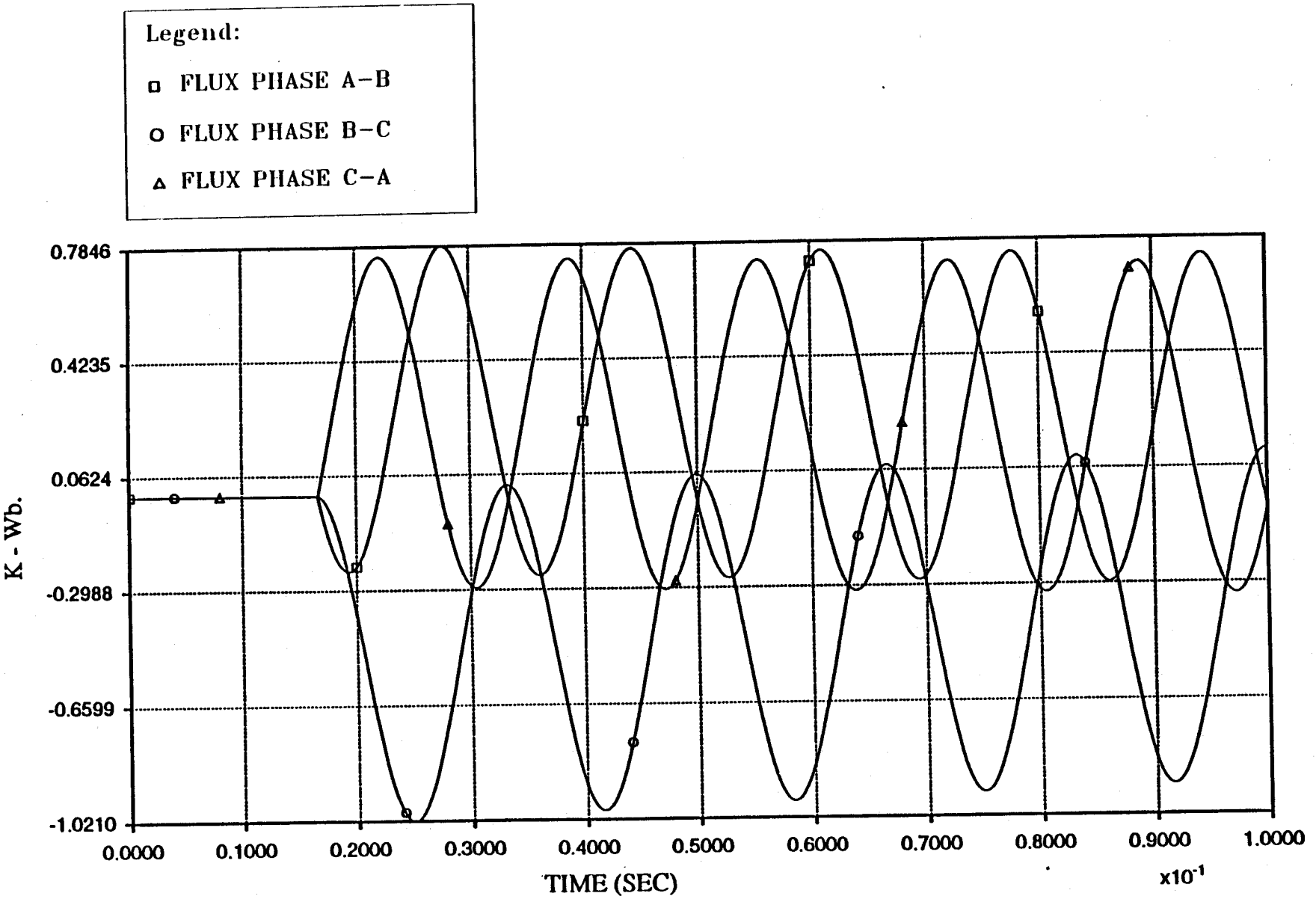

Figure 4.9: The corresponding flux when there is no residual magnetism during switching in of the transformer at 0.0167 seconds.

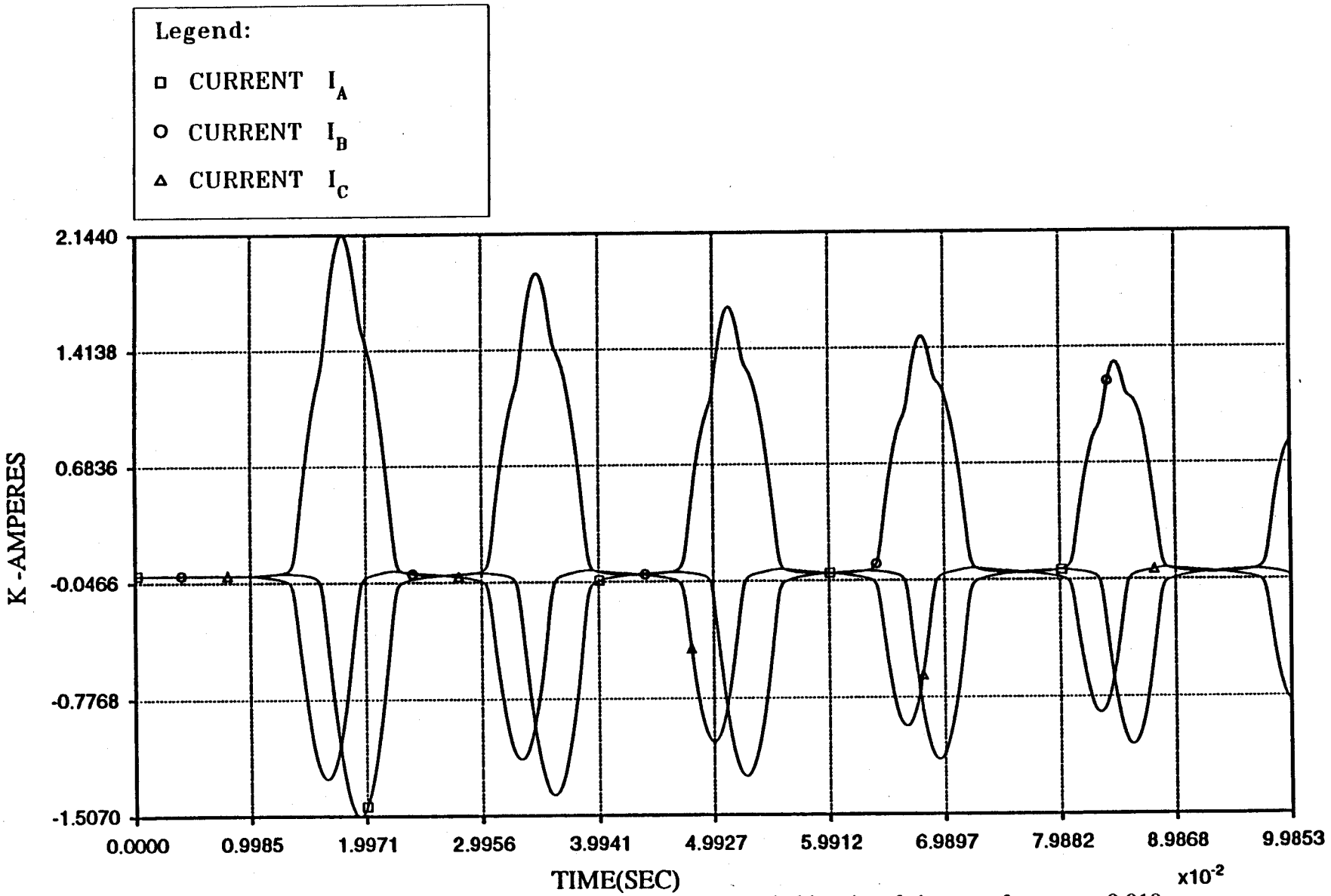

Figure 4.10: Inrush current during switching in of the transformer at 0.010 seconds, showing the different shapes.

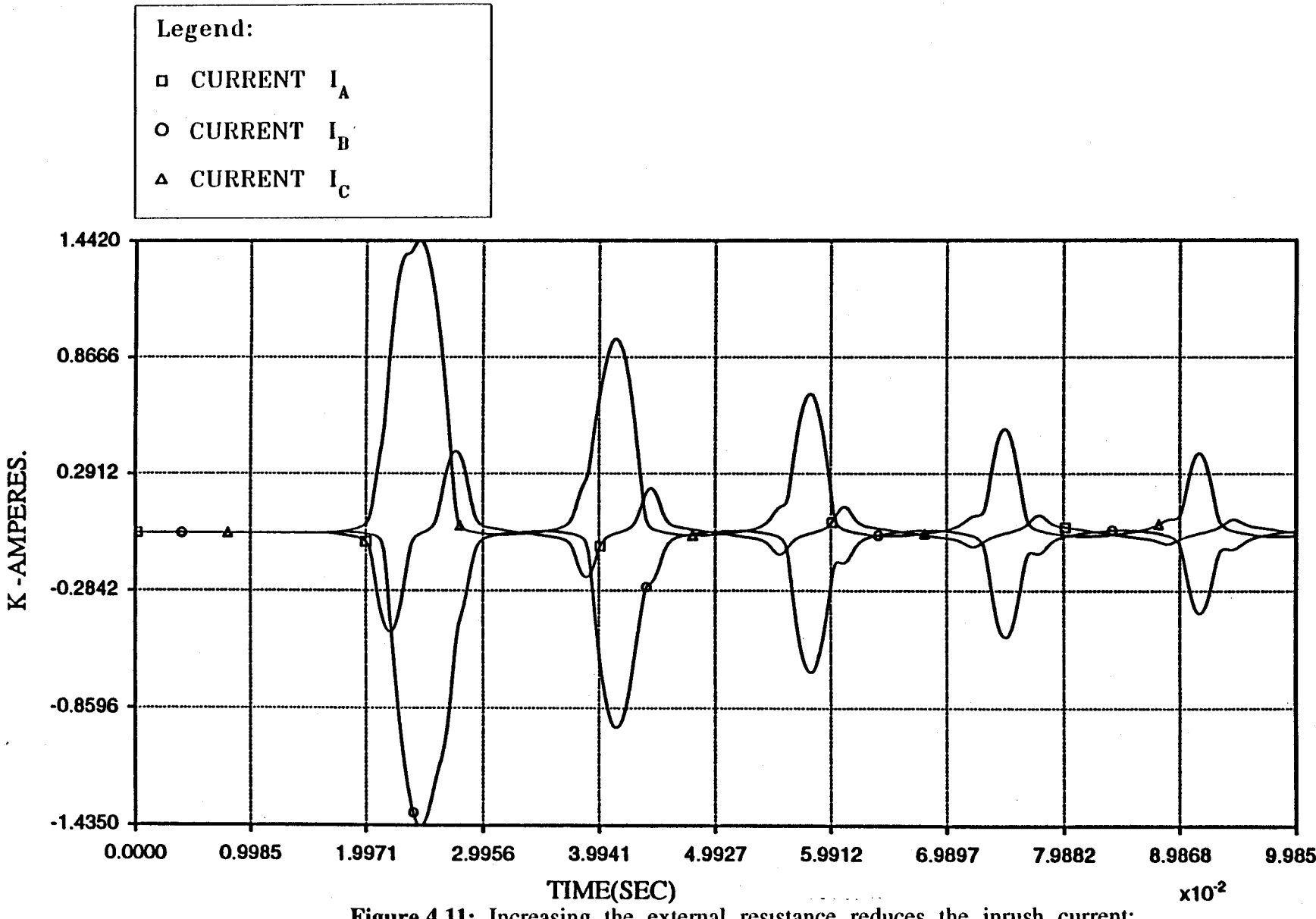

Figure 4.11: Increasing the external resistance reduces the inrush current; switching in of the transformer at 0.0167 seconds.

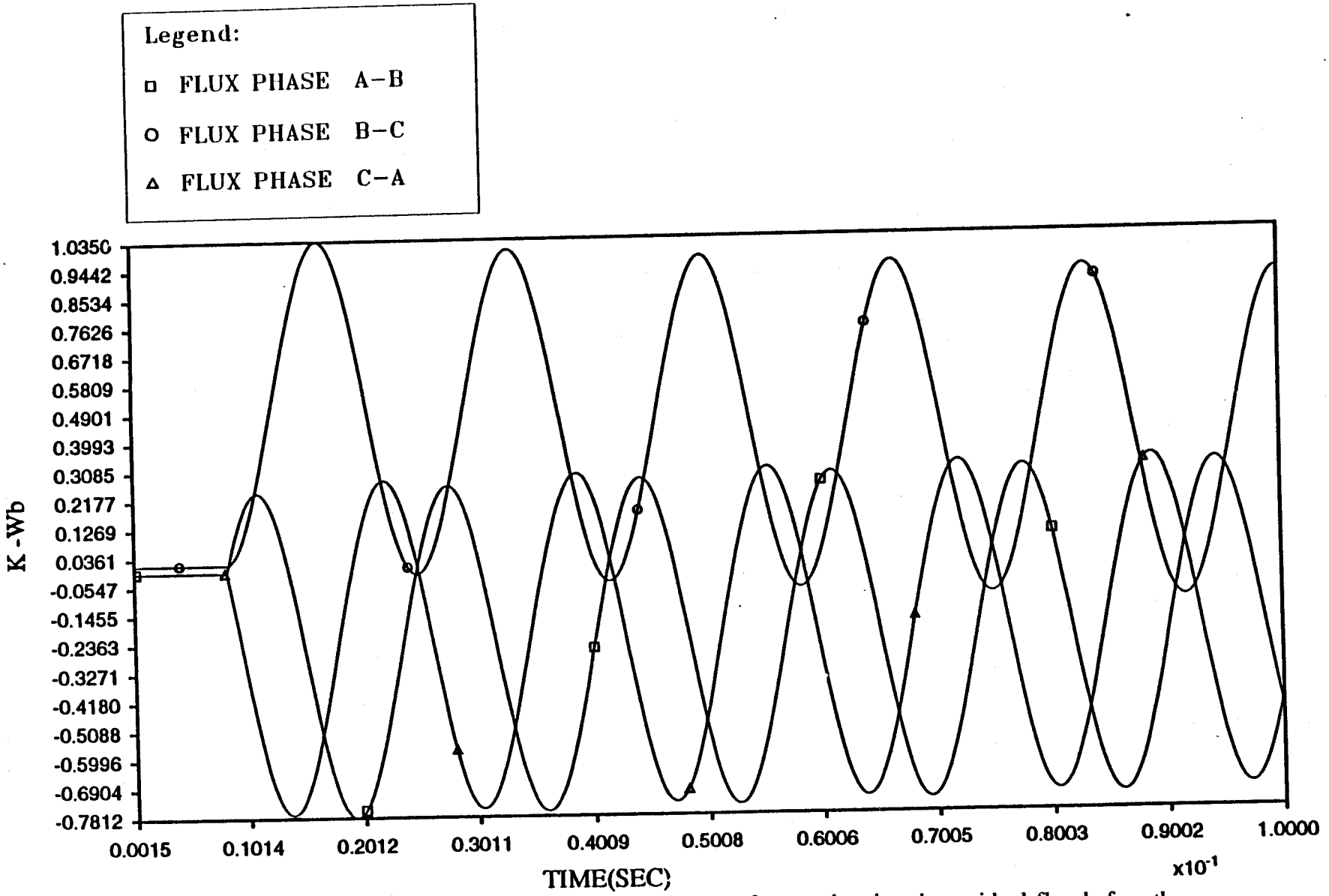

Figure 4.12: The flux in the transformer showing the residual flux before the transformer is switched in; switching in at 0.00835 seconds.

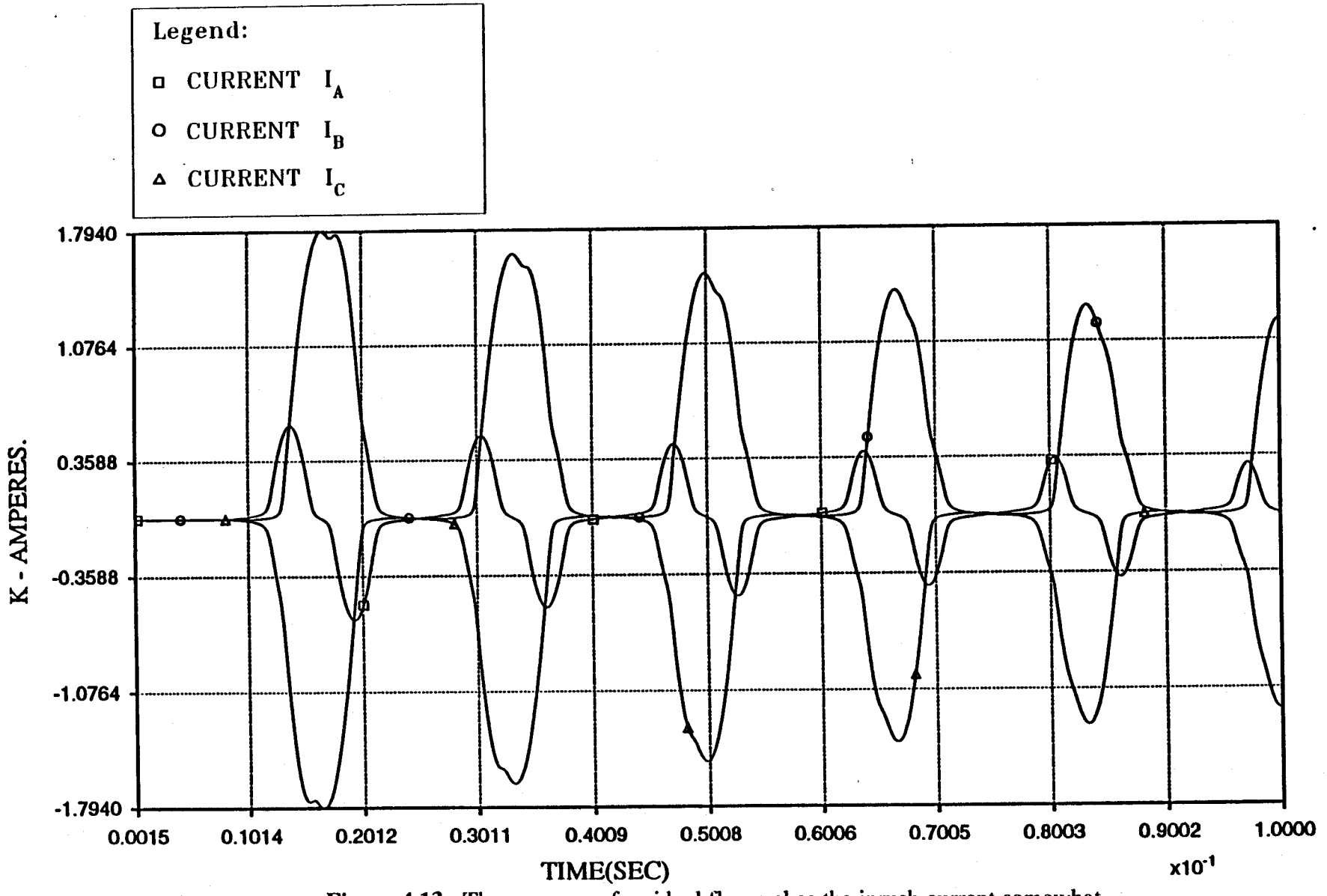

Figure 4.13: The presence of residual flux makes the inrush current somewhat greater or less than if there was no residual flux. In this case it is greater; switching in at 0.00835 seconds.

Theoretically also, the residual magnetism can be eliminated by gradually reducing the applied voltage before switching the transformer out of circuit. Among the disadvantages of inrush current are the operation of differential relays, tripping of main switches and blowing of fuses, but while these are often annoying, they are not serious because the probability of the occurrence of the theoretical maximum inrush current is relatively small [45]. One reason is that they correspond to the closing of the circuit at zero point of the voltage wave, whereas it is more likely that the circuit will be completed nearer the maximum of the voltage wave by the bridging of the gap. Closing of contacts is generally accompanied by sparking. Another reason is that the terminal voltage of the transformer generally drops under a high inrush current. A third reason is that the switching periods which give rise to high inrush currents constitute a small fraction of the total cycle. Experience also shows that actual values are generally far below theoretical maximum values.

Fault protection for transformers is obtained principally by differential type relays. Inrush current appears as an internal fault to the differentially-connected relays. Several methods of desensitizing these relays during inrush current are reported in the literature [11, 50]

4.9. Summary

This chapter has presented the inrush current phenomenon experienced during switching in of transformers. Results from the simulated transformer model using the EMTDC have also been presented. In the transformer models used, for simulation studies, it is assumed that there is no inter-phase magnetic coupling in the three-phase banks. This simplifies the analysis of flux distribution in three-phase banks. Power transformers are operated normally near the knee of saturation curve, so the additional flux requirement of zero-voltage-wave energization plus any residual flux will definitely saturate the core and increase the inrush current.

Suppression of inrush current is not easily achieved in practice. Some of the measures to reduce inrush current have been discussed in this chapter. The problem of inrush current could be studied at greater length and more exact answers obtained but

some of the uncertainties outlined will effectively prevent any calculated solution from being reliable. On transformer terminated lines, it is possible to have a high inrush current upon energizing the feeder. The evaluation of the performance of a digital distance relay protecting a transformer terminated line in the presence of this transient is the focus of the next chapter.

5. EVALUATION OF DIGITAL DISTANCE RELAY ALGORITHMS FOR PROTECTING A TRANSFORMER TERMINATED LINE

5.1. Introduction

A procedure for simulating inrush currents has been presented in Chapter 4. This chapter examines the performance of digital distance relay algorithms for protecting a transformer terminated line. Four algorithms, namely, Mann and Morrison short window, Fourier, Least Error Squares and *R–L* algorithms are used in the studies. The algorithms were selected from each of the categories discussed in Chapter 3. Frequency response of some of these algorithms is presented in this chapter so as to explain the nature of the results included in this chapter.

5.2. Model of the Power System Selected for the Studies

Figure 5.1 shows the test system which was simulated for the studies. The system consists of one Thevenin equivalent source representing the power system and transformer *TR* linked by a transmission line. The transformer was modelled using the procedure presented in the previous chapter. The electrical parameters are given in Tables 5.1 and 5.2. The transmission line was represented as multiphase distributed parameter elements [42].

The figure also shows a relay located at the feeder remote from the transformer *TR* for protecting the line and the transformer. The first zone was set to 100% of the line impedance plus 50% of the impedance of transformer *TR*. Although this zone is set 'half-way into the transformer', it should not be taken as if half the winding will be protected. In reality, the effects of auto-transformer action and variations in the effective impedance of the winding with fault position prevent this, making the amount of the

winding beyond the terminals which is protected very small [13]. The inputs to the digital distance relay are as presented in Chapter 2.

The transformer was switched in under the following conditions:

1. Without any fault on primary terminals of the transformer or far end of the line.
2. With different faults (one fault at a time) on primary terminals of the transformer or far end of the line.

In case of no fault, different levels of inrush current were obtained by switching in and out the transformer at different times of interest so as to retain some residual magnetism.

The shunt faults on the system were simulated by closing the switches at the desired time. Transient data was recorded at the relay location using sampling frequency of $23040Hz$. The output consisted of voltages and currents as functions of time. All values were expressed in per unit (p.u.) on the following base quantities:

1. Base voltage = $230KV$
2. Base capacity = $100MVA$

The voltages and currents presented to the relay during a fault contain transient frequency components such as decaying d.c., harmonics of $60Hz$ and other high frequency components. Depending on the rate at which the voltages and currents are sampled, some of the high frequency components if not filtered can appear approximately to belong to the power frequency ($60Hz$). This misrepresentation can cause digital relays to arrive at incorrect interpretations increasing the chances of making bad decisions. A low pass filter was therefore used to band-limit the voltages and currents to reduce the errors due to the high frequency signals [16, 51].

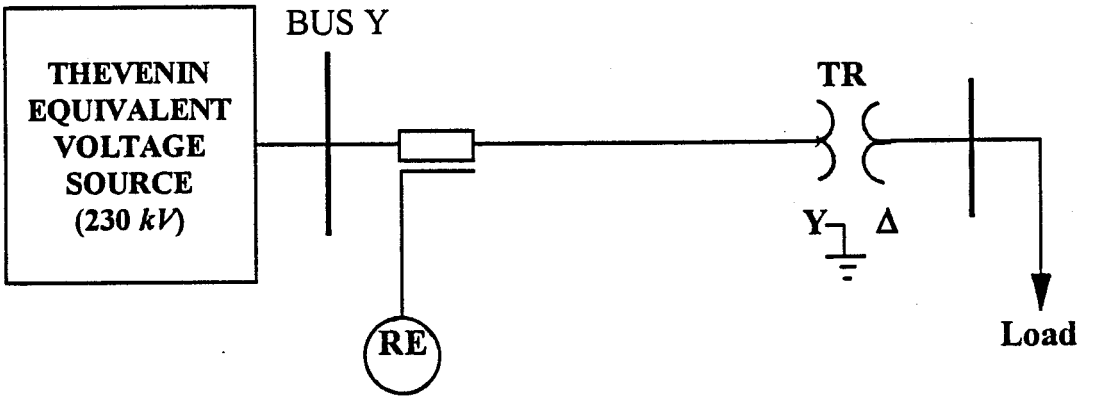

Figure 5.1: The schematic diagram of the test system.

Table 5.1: Thevenin Equivalent Source and Transmission line data.

Series Impedance (p.u)		Shunt Admittance (p.u.)	
Positive and Negative Sequence	Zero Sequence	Positive and Negative Sequence	Zero Sequence
0.0021646 + j0.01626	0. 01385 + j 0.05115	0.0 + j0. 062744	0.0 + j0. 037443
Length of the line (*km*): 25			
Thevenin Equivalent Voltage Source	Rated Voltage	Source Impedance	
	230 *kV*	0.01 + j0.100	

Table 5.2: Data for the transformer and load.

Connection of winding	Rated Voltage (*KV*)	Capacity (*MVA*)	Positive Sequence reactance (%)	Magnetizing current for both winding (%)	System base frequency (*HZ*)	Capacity of load (*MW*)
$Y_{\perp}-\Delta$	230/13.8	100	10	2.5	60	76.18

5.2.1. Design of a Low Pass Filter

A fourth order filter was designed by cascading four first order filters so as to obtain a better roll-off characteristic. The transfer function of the cascaded fourth order low-pass filter is:

$$H(s)=\{\frac{k}{(s+k)}\}^4 \tag{5.1}$$

where:
k is a constant.
s is the Laplace operator.

The frequency response of the filter is obtained by replacing the Laplace operator, s by $j\omega$. Equation (5.1) then becomes:

$$H(j\omega)=\{\frac{k}{(j\omega+k)}\}^4 \tag{5.2}$$

Defining the cut-off frequency as the frequency at which the magnitude of the gain drops from 1.00 in the passband to 0.707, the magnitude of the voltage gain at the cut-off frequency, ω_c, becomes:

$$|\frac{k}{j\omega_c+k}|^4=\frac{1}{\sqrt{2}} \tag{5.3}$$

Using the bilinear transformation [52], which maps the s plane to the z plane, the digital equivalent of an analog filter can be obtained, i.e.

$$s \rightarrow \{2f_s[\frac{1-z^{-1}}{1+z^{-1}}]\} \tag{5.4}$$

where:

f_s is the sampling frequency.

The relationship which exists between the cut-off frequency of the analog low-pass filter and cut-off frequency of its equivalent digital filter can be expressed as follows [52]:

$$\omega_{dc}=2f_s arctan\{\frac{\omega_{ac}}{2f_s}\} \tag{5.5}$$

where:

ω_{ac} is the cut-off frequency of the analog filter and

ω_{dc} is the cut-off frequency of the equivalent digital filter.

In this project, the sampling frequency of the filtered data, used as input to the relay algorithm was set at 720*Hz*. This frequency was derived from the acquisition sample rate of 23040 samples per second by the low pass filter. A cut-off frequency of 360*Hz* was selected in designing the low pass-filter. At this cut-off frequency $k=5200$. The transfer function of the fourth order filter is therefore expressed by:

$$H(s)=\{\frac{5200}{s+5200}\}^4 \tag{5.6}$$

By substituting the value of the sampling rate in Equation (5.4) and using Equation (5.1) and re-arranging, the transfer function of the fourth order digital filter is expressed as follows:

$$H(z)=\{\frac{0.101404(1+z^{-1})}{1-0.797192z^{-1}}\}^4 \tag{5.7}$$

Expanding the above equation and replacing $H(z)$ by the ratio of the output, $Y(z)$ to the input, $X(z)$, the equation becomes:

$$\frac{Y(z)}{X(z)}=\frac{1.0574\times10^{-4}(1+4z^{-1}+6z^{-2}+4z^{-3}+z^{-4})}{1-3.18877z^{-1}+3.81309z^{-2}-2.02651z^{-3}+0.40388z^{-4}} \tag{5.8}$$

This fourth order recursive filter in terms of the samples of a continuous waveform is:

$$\begin{aligned} y(n)= & \ 0.0001057\{x(n)+4x(n-1)+6x(n-2)+4x(n-3)+x(n-4) \\ & +3.1888y(n-1)-3.8131y(n-2)+2.0265y(n-3)-0.4039y(n-4)\} \end{aligned} \tag{5.9}$$

The frequency response of this filter is shown in Figure 5.2.

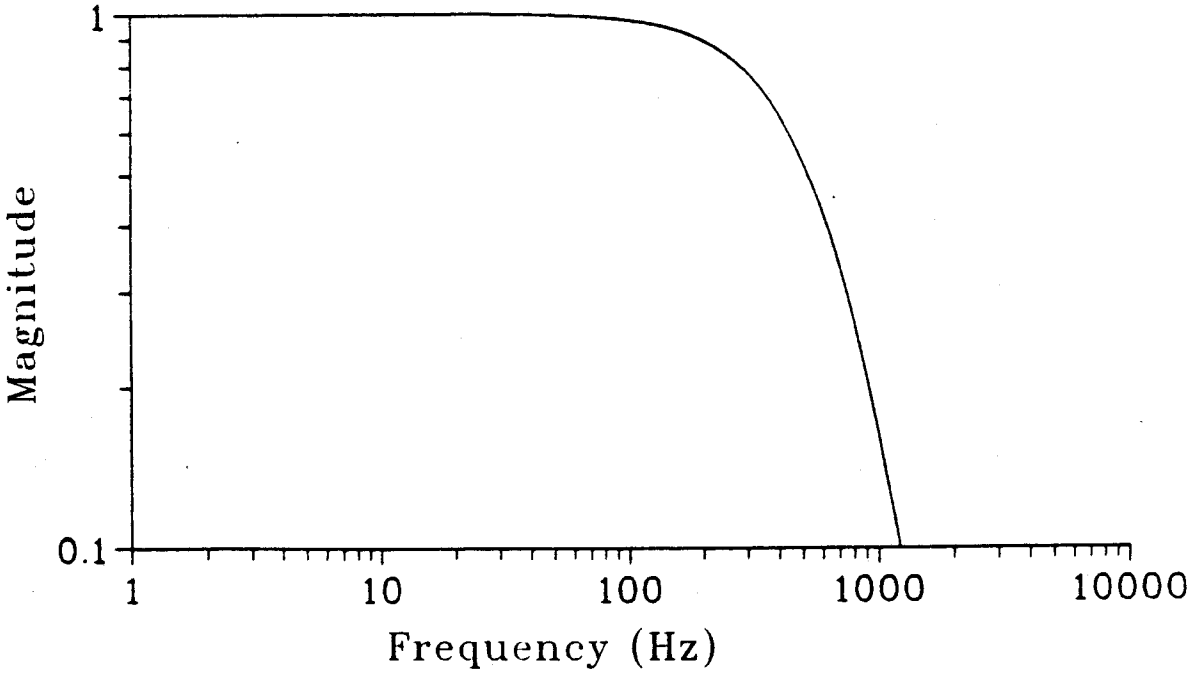

Figure 5.2: The frequency response of the fourth order filter.

5.2.2. Processing of Sampled Data

The filter described in the previous section was used to band limit the voltages and currents recorded at the relay location. The filter also converted the sampling frequency of 23040 samples per second to 720 samples per second as inputs for the relay algorithms. Figures 5.3 and 5.4 show the waveforms of the phase voltages and currents before filtering sampled at the relay location during inrush current provoked by the energization of transformer, *TR*. It is clear that distortions have been remarkably reduced in the waveforms shown in Figures 5.5 and 5.6 after filtering.

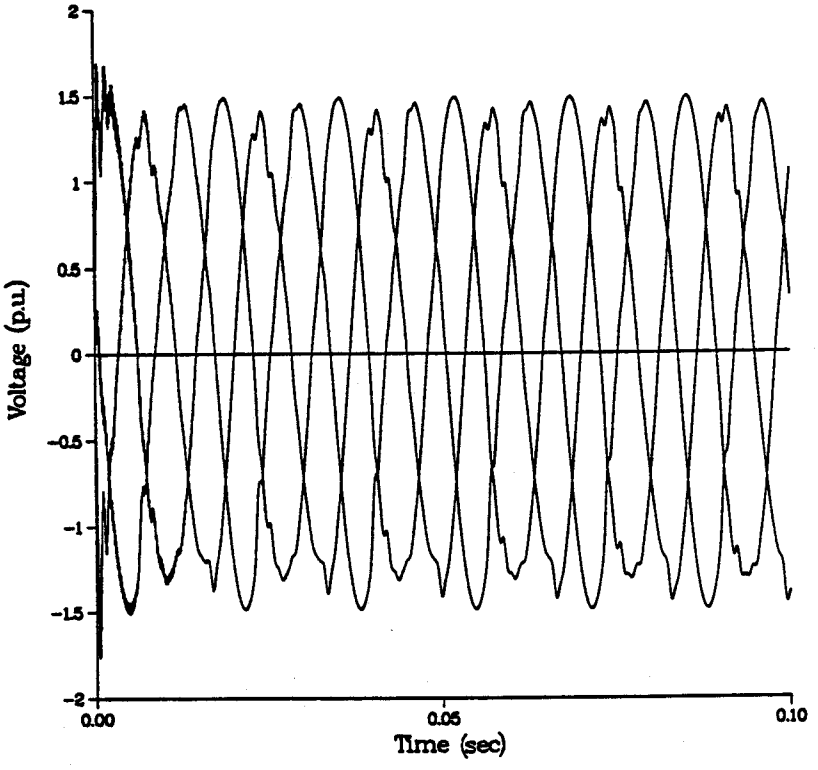

Figure 5.3: Voltage before filtering at relay location during inrush current.

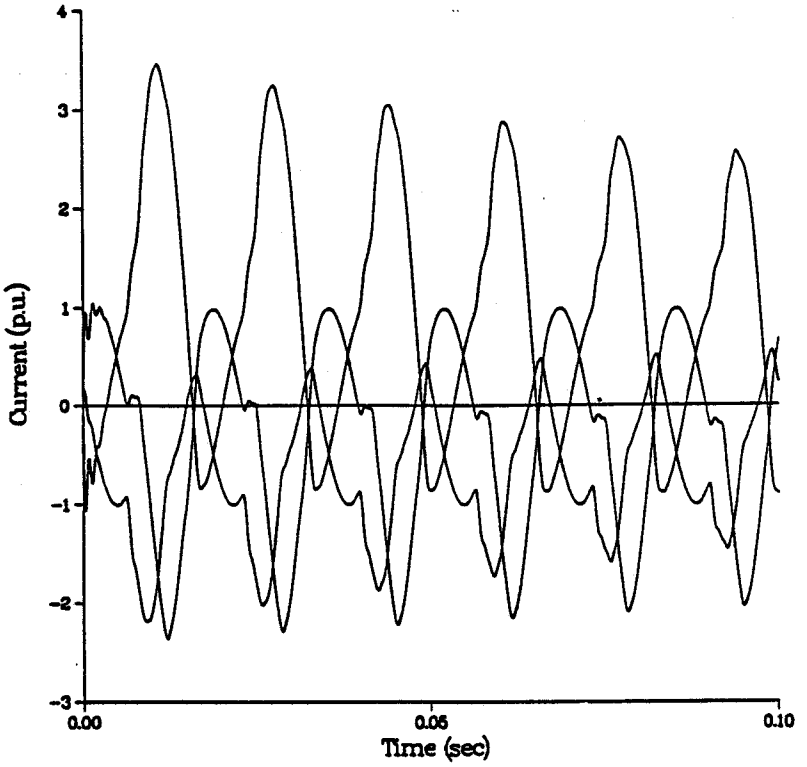

Figure 5.4: Inrush current before filtering at relay location.

5.2.3. The Design and Frequency Response of the Digital Algorithms

The filtering characteristics of an algorithm can be evaluated through the frequency response. The algorithms for the distance protection based on the extraction of the fundamental components are non- recursive digital filters. These filters use a finite number of samples to provide the required output.

In the z domain, the transfer function of a non-recursive digital filter is given by [52]:

$$H(z) = \sum_{n=0}^{m} c_n z^{-n} \tag{5.10}$$

where:

c_n are the filter coefficients and

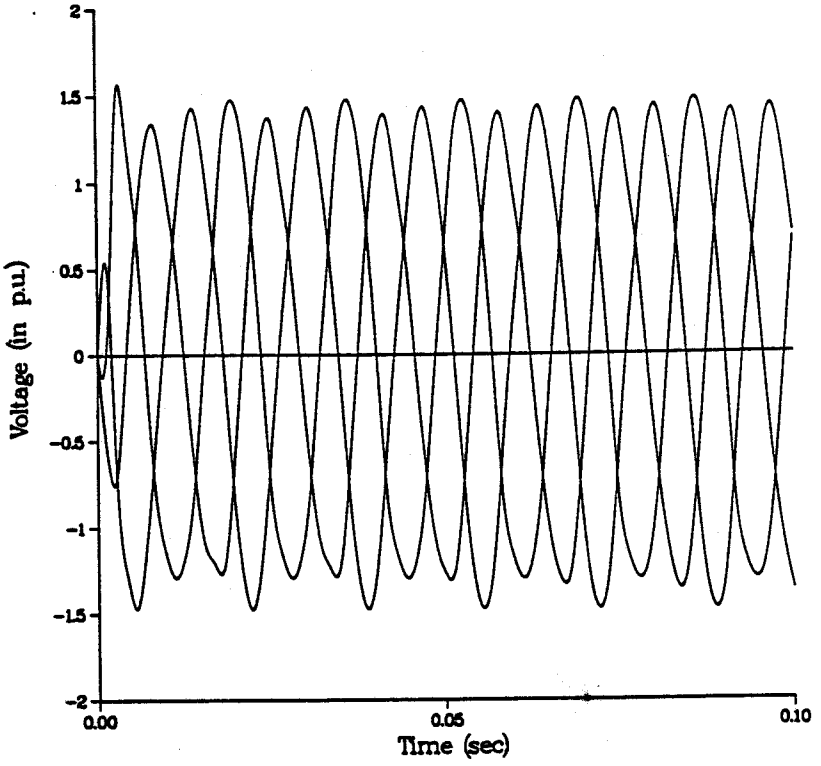

Figure 5.5: Voltage after filtering at relay location during inrush current.

z is a z-transform operator.

To transfer this function into frequency domain z is replaced by $e^{j\omega\Delta T}$ resulting in the following transformed function:

$$H(\omega) = \sum_{n=0}^{m} c_n e^{-j\omega n\Delta T} \tag{5.11}$$

Generally, $H(\omega)$ is complex and can be expressed as:

$$H(\omega) = |H(\omega)|(e^{j\theta_\omega}) \tag{5.12}$$

where:

$\theta_\omega = arg\{H(\omega)\}$

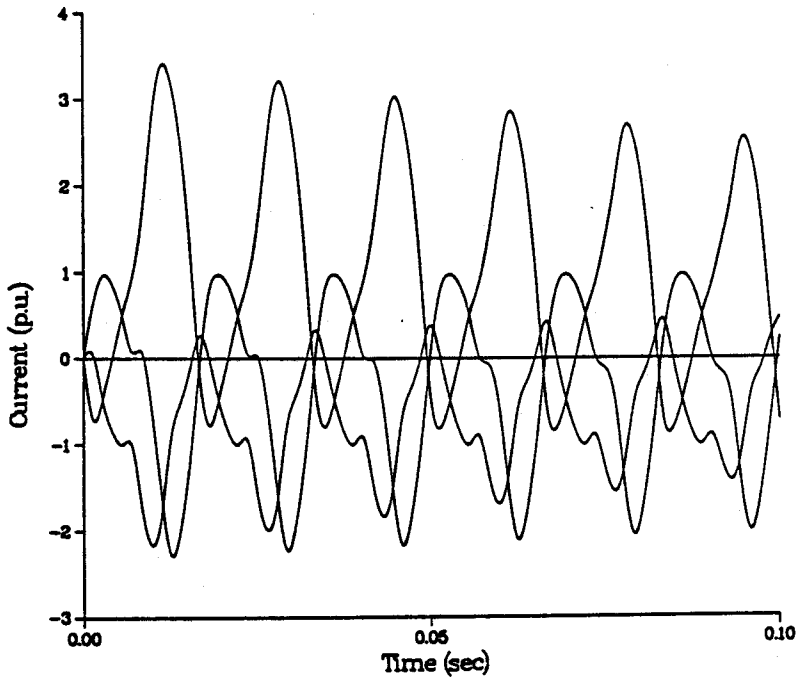

Figure 5.6: Inrush current after filtering at relay location.

The algorithms used for estimating the phasors use two filters. The filter which estimates the real part of a phasor is called the cosine filter and the one which estimates the imaginary part of a phasor is referred to as a sine filter. The analysis of the frequency response of some of the non-recursive algorithms used in this project was done.

The coefficients of the filters of the full-cycle Fourier algorithm are:

$$[C]_r=[0.0000\ 0.0833\ 0.1443\ 0.1667\ 0.1443\ 0.0833\ 0.0000\ -0.0833\ -0.1443\ -0.1667\ -0.1443\ -0.0833] \quad (5.13)$$

$$[C]_i=[0.1667\ 0.1443\ 0.0833\ 0.0000\ -0.0833\ -0.1443\ -0.1667\ -0.1443\ -0.0833\ 0.0000\ 0.0833\ 0.1443] \quad (5.14)$$

where:

$[C]_r$ are the coefficients of the filter that estimates the real part of the phasors and

$[C]_i$ are the coefficients of the filter that estimates the imaginary part of the phasors.

The frequency responses of the sine and cosine filters of the Fourier algorithm, obtained using Equation (5.11) and the filter coefficients are shown in Figures 5.7 and 5.8. These figures reflect the fact that higher harmonics are attenuated by the algorithm. Also the non-decaying part of the d.c. (frequency equal to zero) signal is also attenuated.

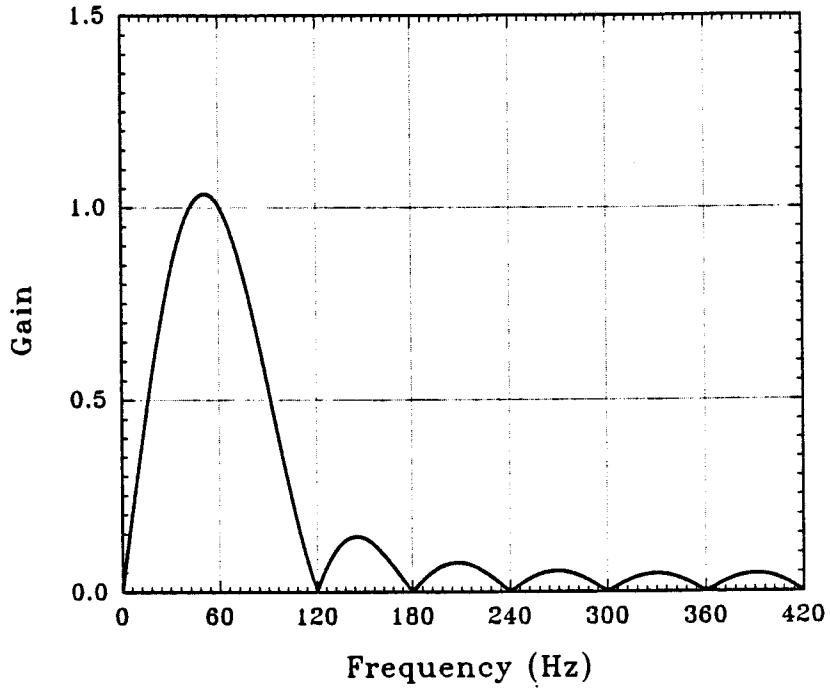

Figure 5.7: Frequency response of the Sine filter of the Fourier algorithm.

The other frequency response analysed was for the Least Error Squares algorithm. In this project, a 13-sample Least Error Squares algorithm is used in which the decaying d.c. is modelled by the first two terms of its Taylor series expansion and the remaining

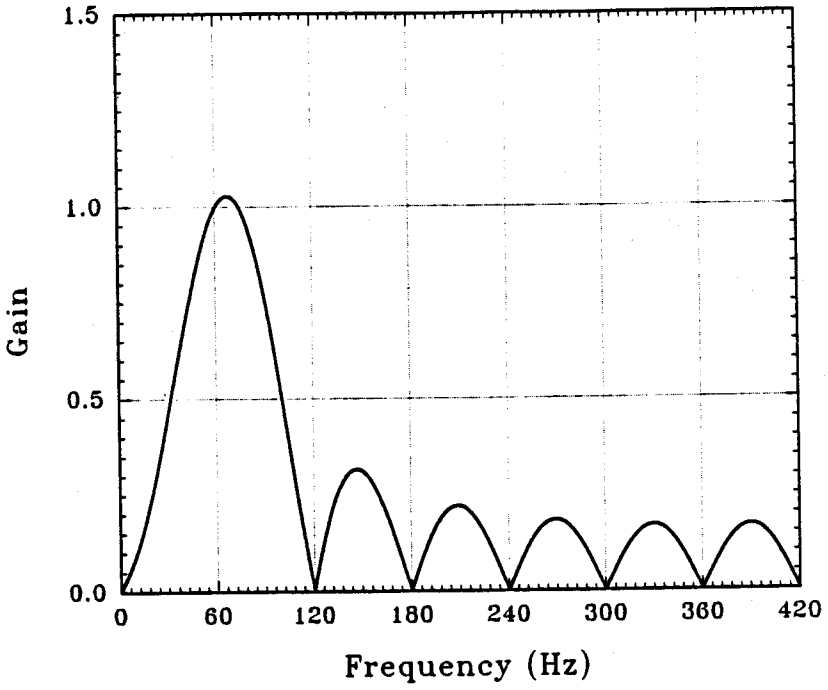

Figure 5.8: Frequency response of the Cosine filter of the Fourier algorithm.

signal is modelled as sinusoids of the fundamental frequency, and the second, third, fourth and fifth harmonics. The coefficients for the sine and cosine filters are:

$$[C]_r=[0.3110\ -0.0833\ -0.1443\ -0.1667\ -0.1443\ -0.0833\ 0.0000\ 0.0833\ 0.1443\ 0.1667\ 0.1443\ 0.0833\ -0.3110] \quad (5.15)$$

$$[C]_i=[-0.0870\ -0.1371\ -0.0906\ 0.0072\ 0.0761\ 0.1516\ 0.1594\ 0.1516\ 0.0761\ 0.0072\ -0.0906\ -0.1371\ -0.0870] \quad (5.16)$$

where:

$[C]_r$ are the coefficients of the filter that estimates the real part of the phasors and

$[C]_i$ are the coefficients of the filter that estimates the imaginary part of the phasors.

The frequency responses of the filters were also obtained using Equation (5.11) and the filter coefficients. Figures 5.9 and 5.10 show the frequency responses of the sine and cosine filters respectively. These figures show that both filters attenuate the non-decaying component of the d.c. as well as the harmonic frequencies.

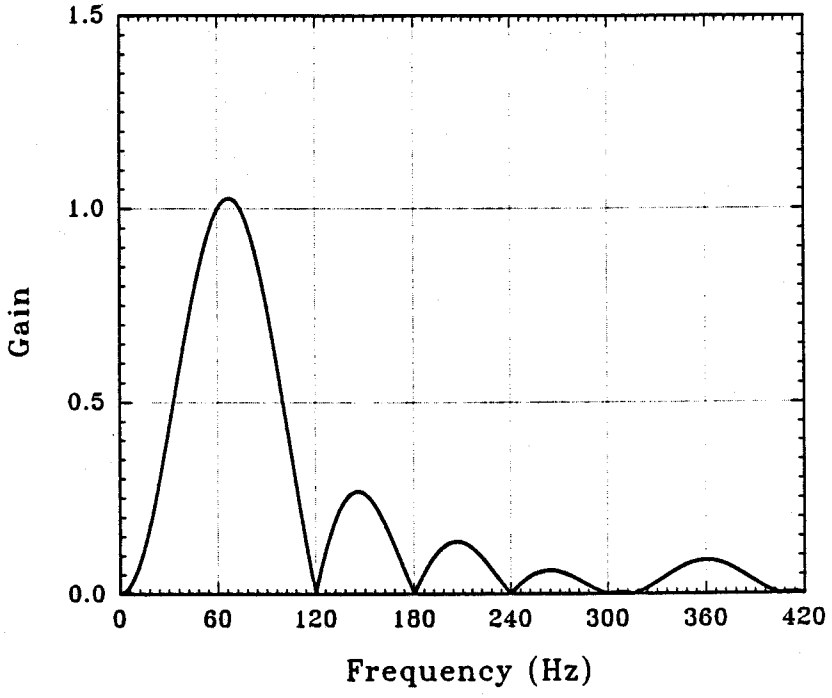

Figure 5.9: Frequency response of the Sine filter of the Least Error Squares algorithm.

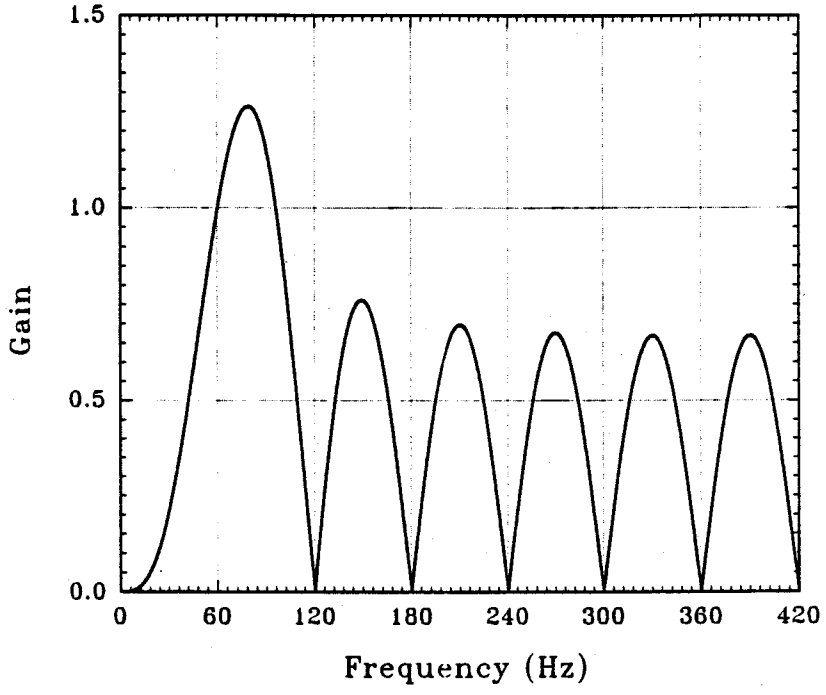

Figure 5.10: Frequency response of the Cosine filter of the Least Error Squares algorithm.

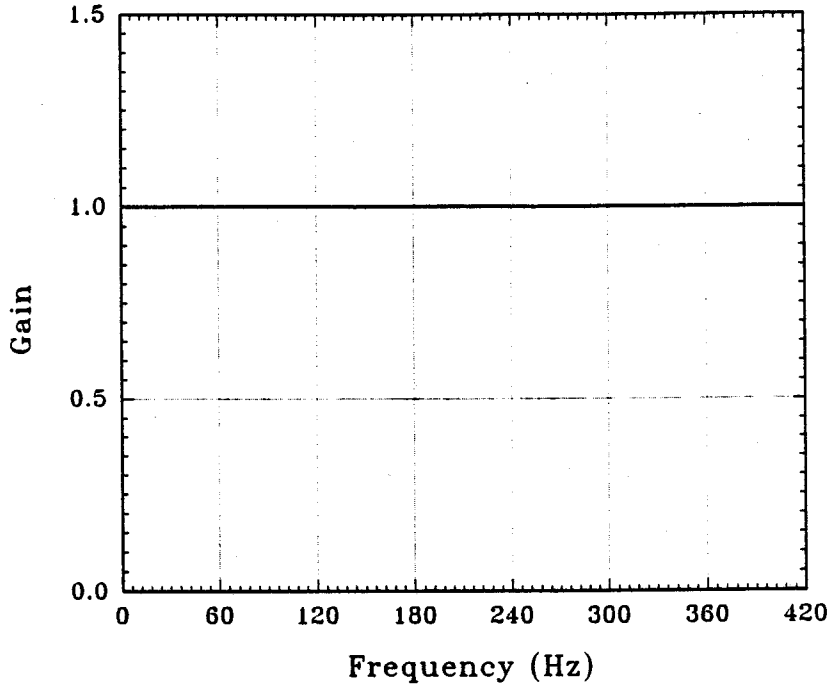

Figure 5.11: Frequency response of the Sine filter of the Mann and Morrison short window algorithm.

The frequency response of the Mann and Morrison algorithm is shown in Figures 5.11 and 5.12. The sine filter allows all frequencies to pass which can be a source of error in phasor estimation. The cosine filter amplifies the second, third and fourth harmonics and allows the fifth harmonic to pass. This can also increase the error in phasor estimation. The transfer function of the sine filter is deduced from a direct sample and is expressed as follows:

$$H(\omega) \doteq 1.0 \tag{5.17}$$

For the cosine filter the transfer function is given by:

$$H(z) = \frac{(z^{+1} - z^{+1})}{2(\omega_0 \Delta T)} \tag{5.18}$$

$$H(w) = \frac{(e^{j\omega\Delta T} - e^{-j\omega\Delta T})}{2\omega_0 \Delta T} \tag{5.19}$$

At sampling frequency of $720Hz$:

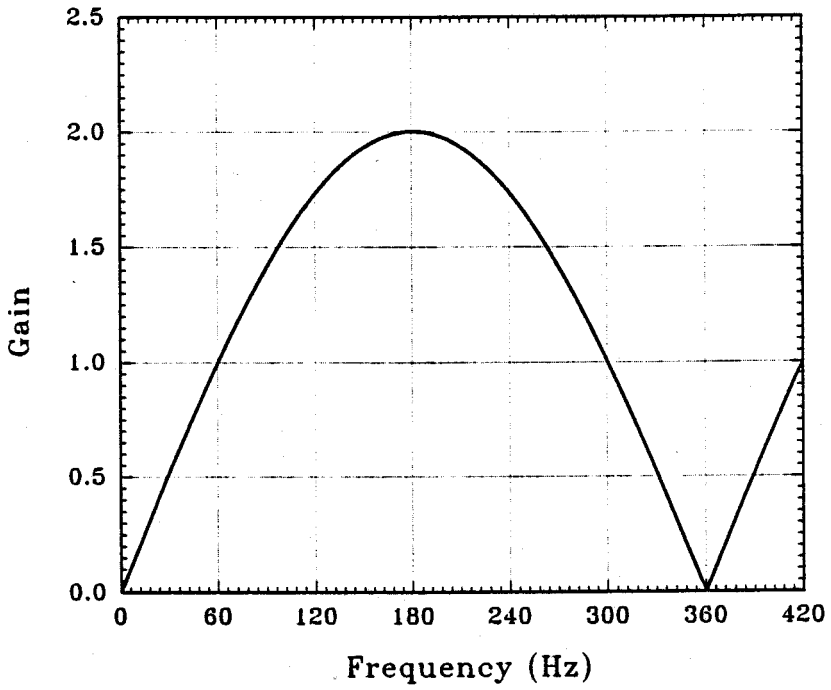

Figure 5.12: Frequency response of the Cosine filter of the Mann and Morrison short window algorithm.

$$H(\omega) = j2\sin(\omega\Delta T) \tag{5.20}$$

The algorithms which extracted the fundamental frequency components used the equation already discussed in Chapter 3 to determine the apparent impedance estimates. The *R–L* algorithm also used equations described in Chapter 3 for estimating the apparent inductance and resistance of a line.

5.3. Dynamic Response of the Digital Distance Relay Algorithms

The dynamic response of the distance relay algorithms shows the manner in which the relay responds to a change in the power system during inrush current and inrush current closed into fault. The Fourier, Least Error Squares, *R–L* and Mann and Morrison short window algorithms were used in the studies reported in this section. A program which maps the setting characteristics of a mho distance relay discussed in Chapter 2 was developed so as to assess the response of the algorithms.

5.3.1. Inrush Current Only

When the various inrush current levels and voltages were presented to the relay simulations using the different algorithms, it was found that the calculated impedance varied drastically over a cycle. This was expected since the reactance of the transformer varies due to saturation during inrush current. Figures 5.13 through 5.16 show the trajectories of the estimated apparent impedancs of the ground elements using different algorithms. The Least Error Squares algorithm suppresses the decaying d.c. and as a result, the movements of calculated impedances are least as is shown in Figure 5.13. However, the decaying d.c. affects the impedance estimates of the Fourier and Mann and Morrison algorithms as illustrated in Figures 5.14 and 5.16 respectively. In addtion, the impedance estimates of the Mann and Morrison algorithm are affected by the presence of harmonics. These harmonics also affect impedance estimates obtained using the R-L algorithm as shown in Figure 5.15.

Figures 5.17 through 5.20 show the trajectories of the estimated apparent impedances of the phase elements. The characteristics of the results are almost the same as for the ground elements with the short window algorithms showing the most pronounced movements. The Fourier algorithm though it is affected by d.c. offsets, it always converges onto the same results with Least Error Squares algorithm. Figures 5.21 through 5.28 show the results of increasing the impedance of the Thevenin source to almost ten times the original value of the impedance of the source under which the results of Figures 5.13 through 5.20 were obtained. These results show that there is no significant change from those presented before. The seen impedances in all cases did not enter the tripping zones of the relay.

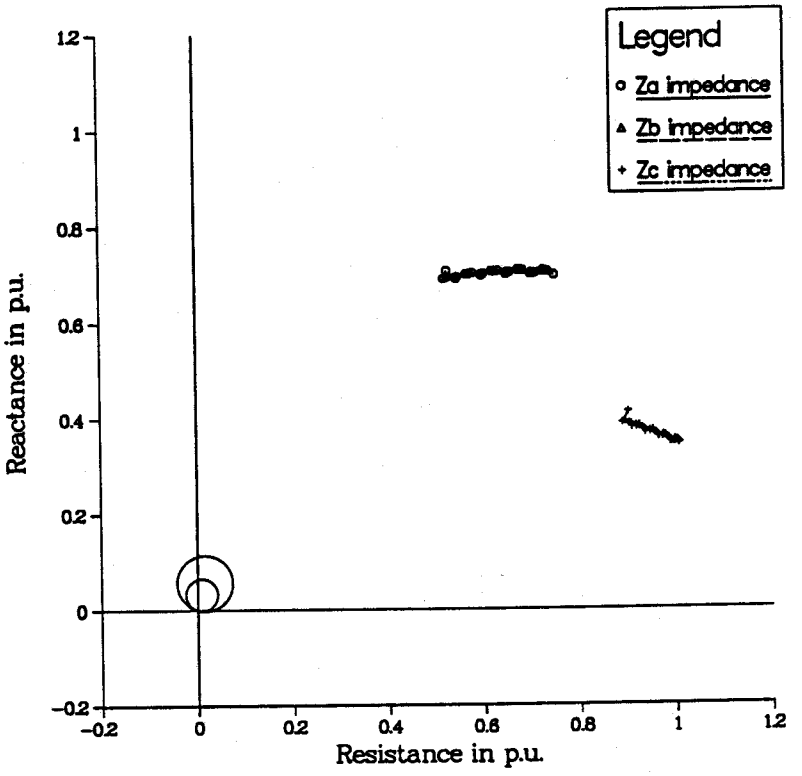

Figure 5.13: Trajectory of impedance estimates of the ground elements during inrush current using the Least Error Squares algorithm.

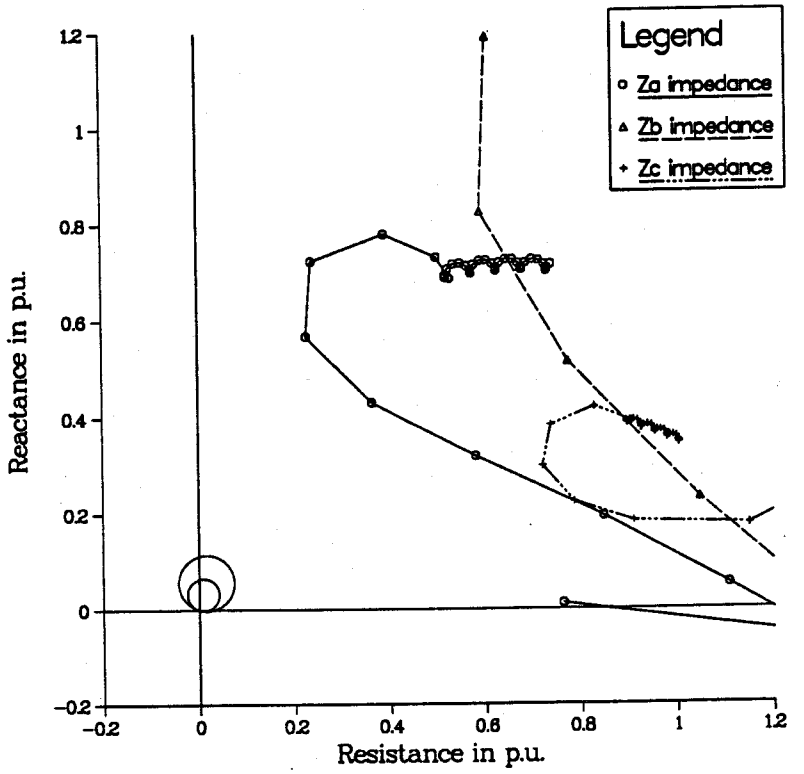

Figure 5.14: Trajectory of impedance estimates of the ground elements during inrush current using the Fourier algorithm.

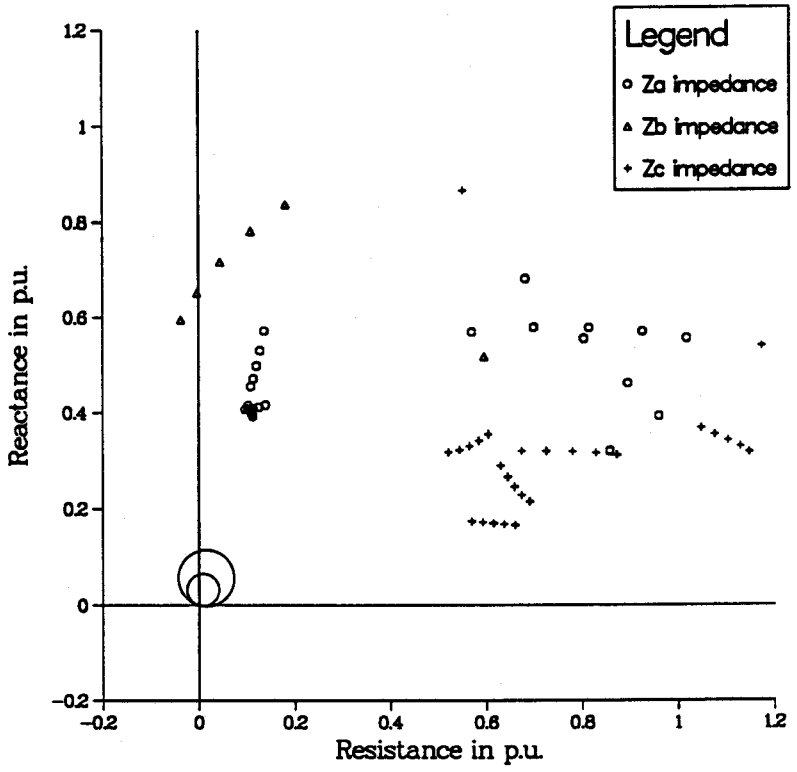

Figure 5.15: Trajectory of impedance estimates of the ground elements during inrush current using the R-L algorithm.

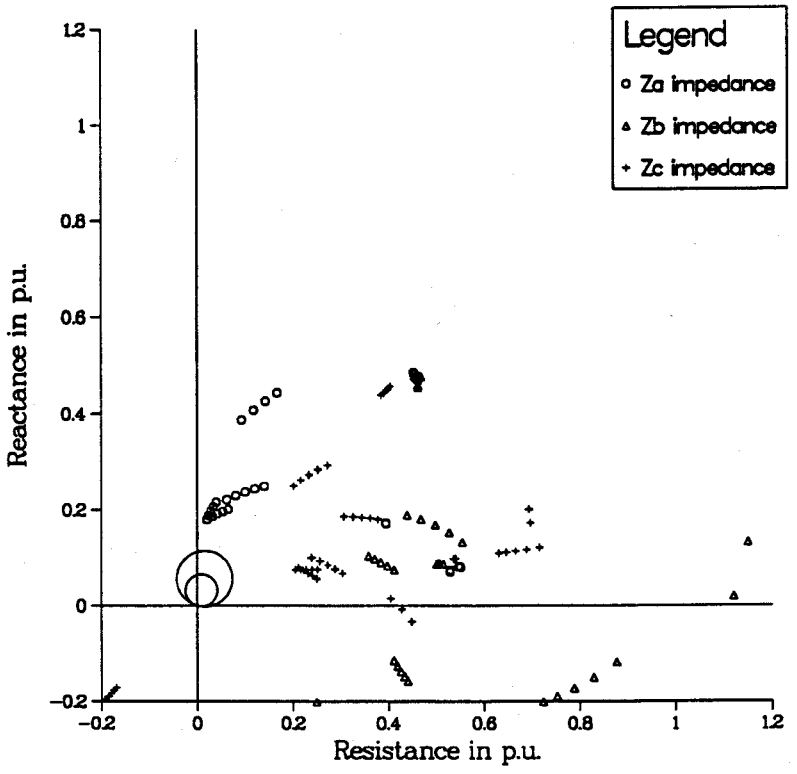

Figure 5.16: Trajectory of impedance estimates of the ground elements during inrush current using Mann and Morrison short window algorithm.

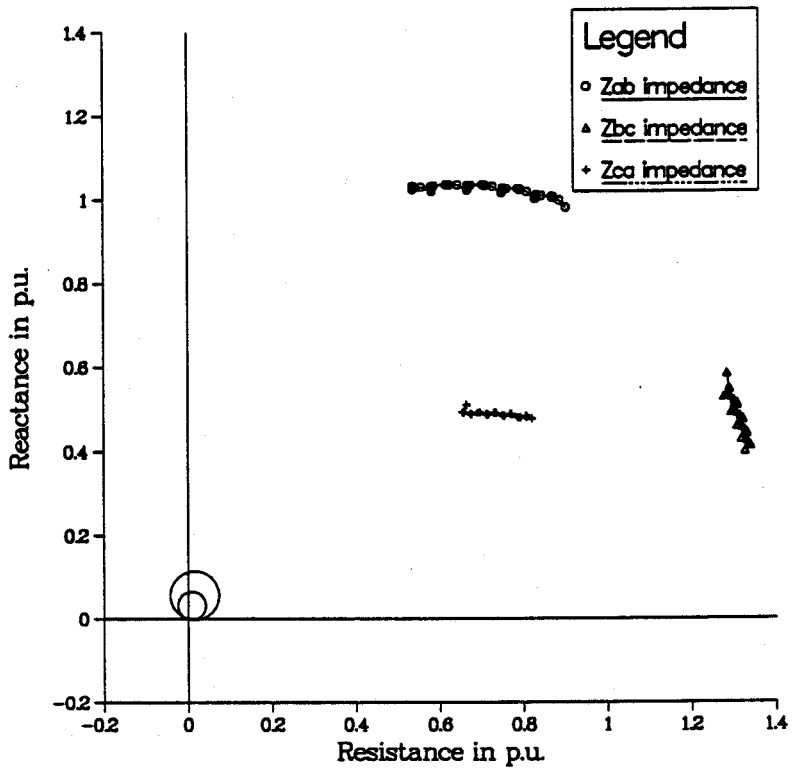

Figure 5.17: Trajectory of impedance estimates of the phase elements during inrush current using the Least Error Squares algorithm.

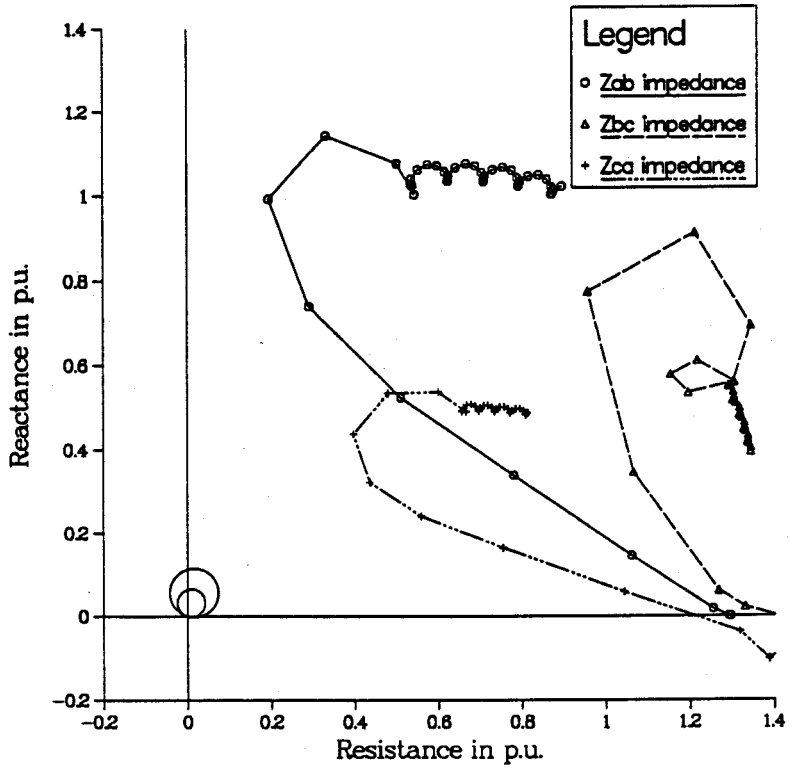

Figure 5.18: Trajectory of impedance estimates of the phase elements during inrush current using the Fourier algorithm.

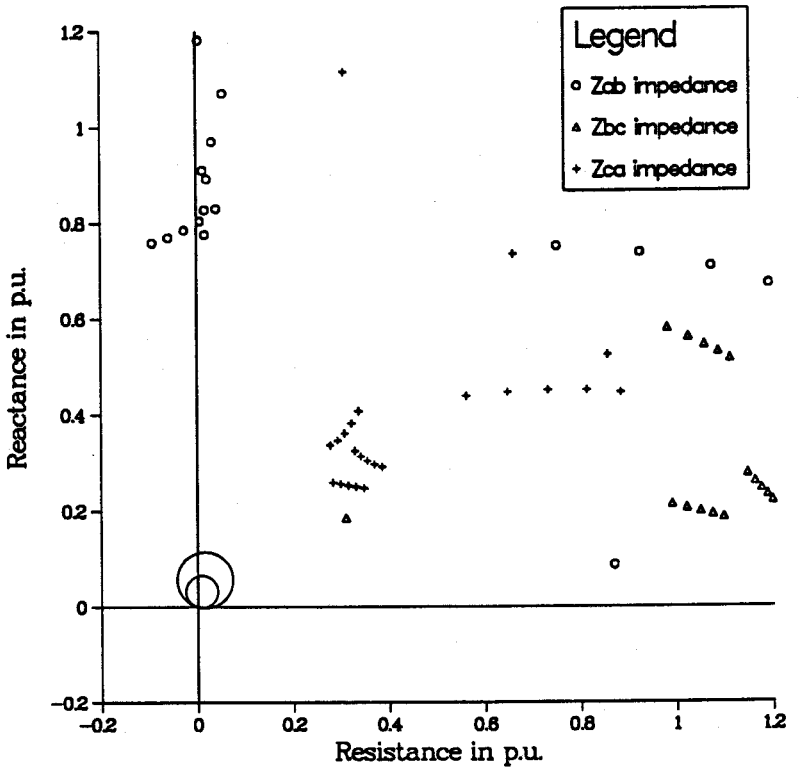

Figure 5.19: Trajectory of impedance estimates of the phase elements during inrush current using the R-L algorithm.

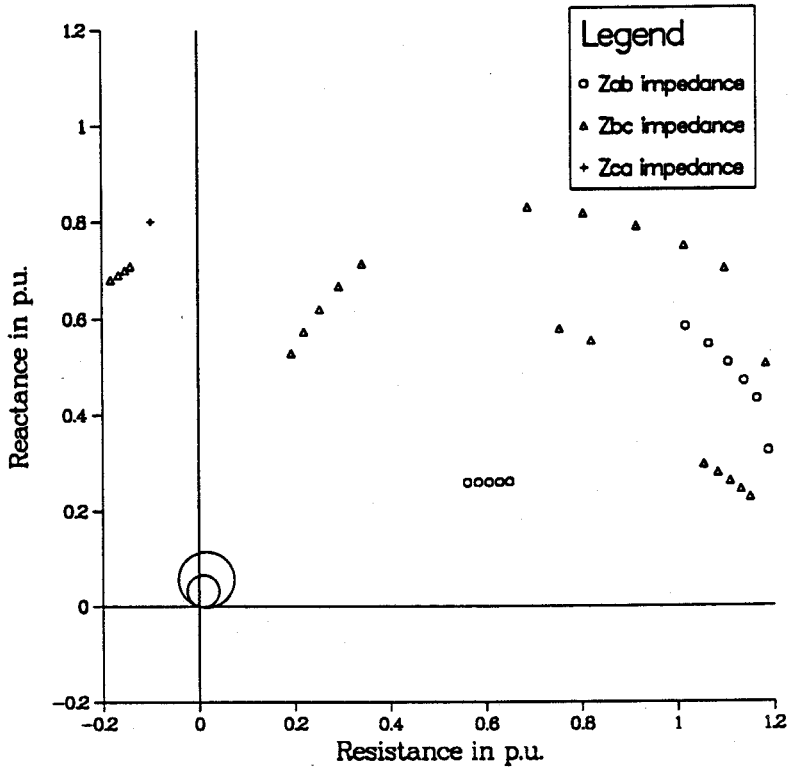

Figure 5.20: Trajectory of impedance estimates of the phase elements during inrush current using Mann and Morrison short window algorithm.

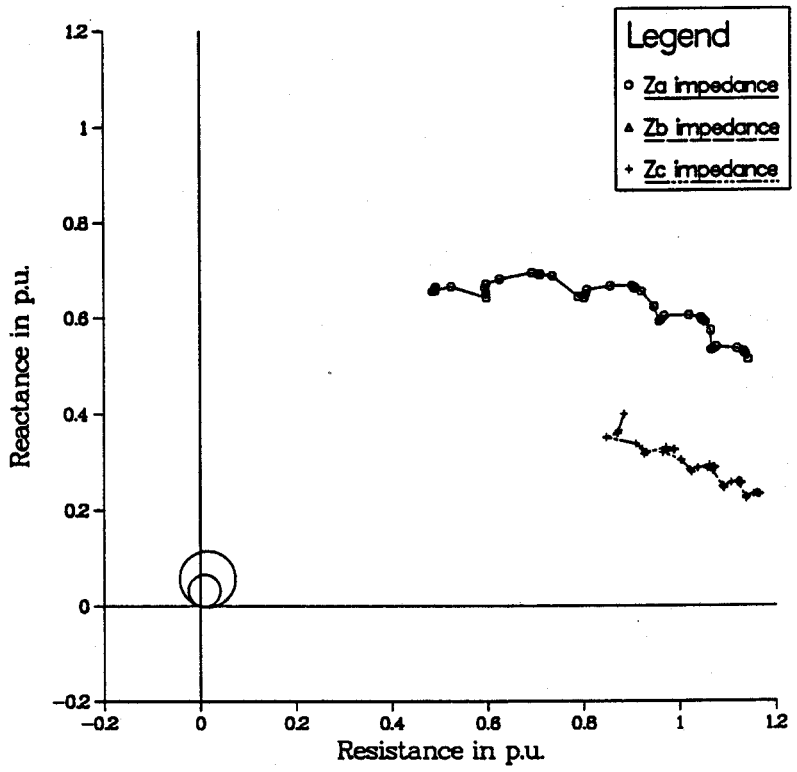

Figure 5.21: Trajectory of impedance estimates of the ground elements during inrush current using the Least Error Squares algorithm with source impedance increased.

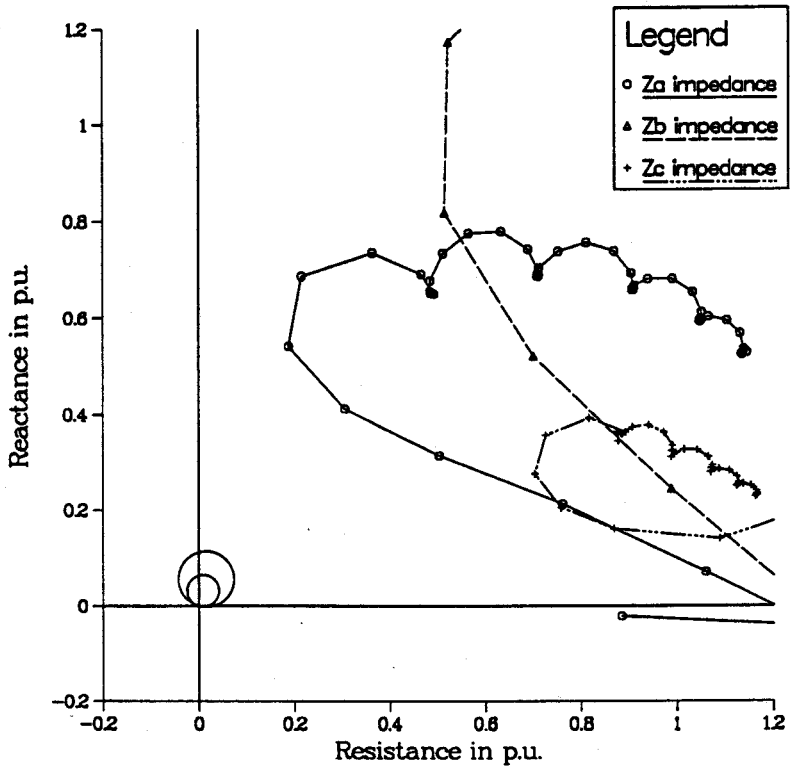

Figure 5.22: Trajectory of impedance estimates of the ground elements during inrush current using the Fourier algorithm with source impedance increased.

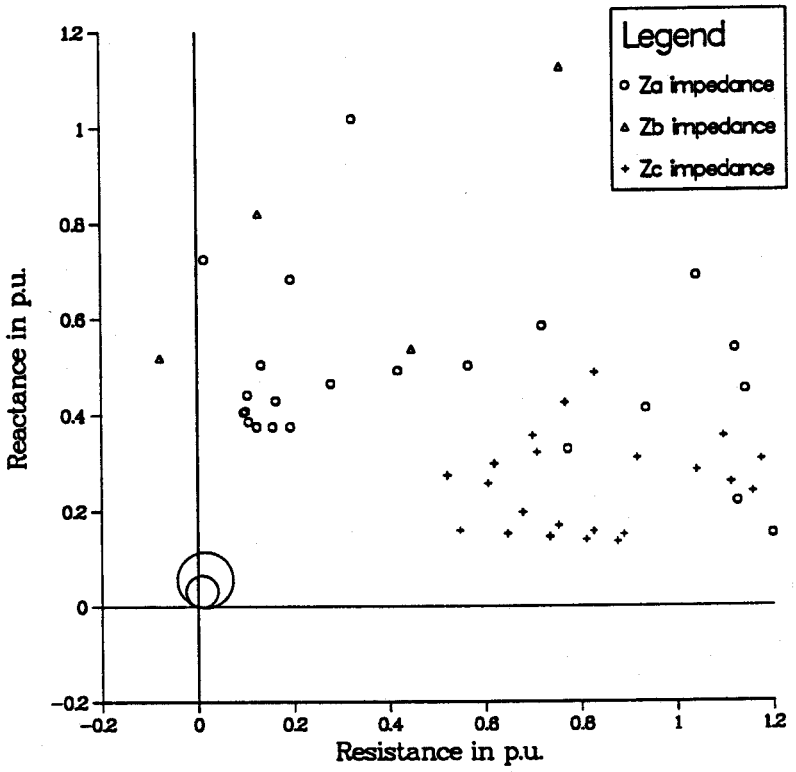

Figure 5.23: Trajectory of impedance estimates of the ground elements during inrush current using the R-L algorithm with source impedance increased.

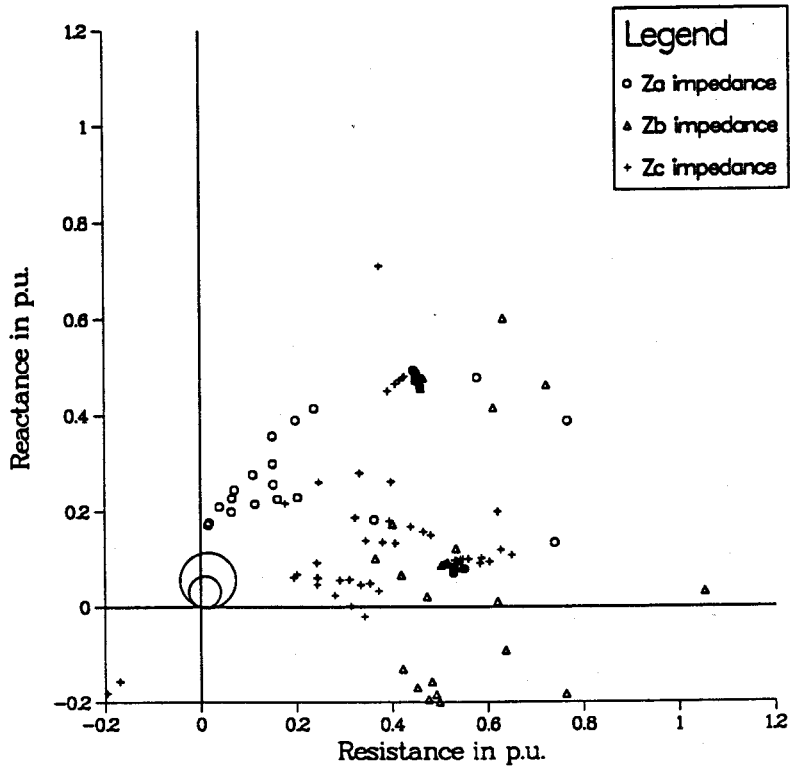

Figure 5.24: Trajectory of impedance estimates of the ground elements during inrush current using Mann and Morrison short window algorithm with source impedance increased.

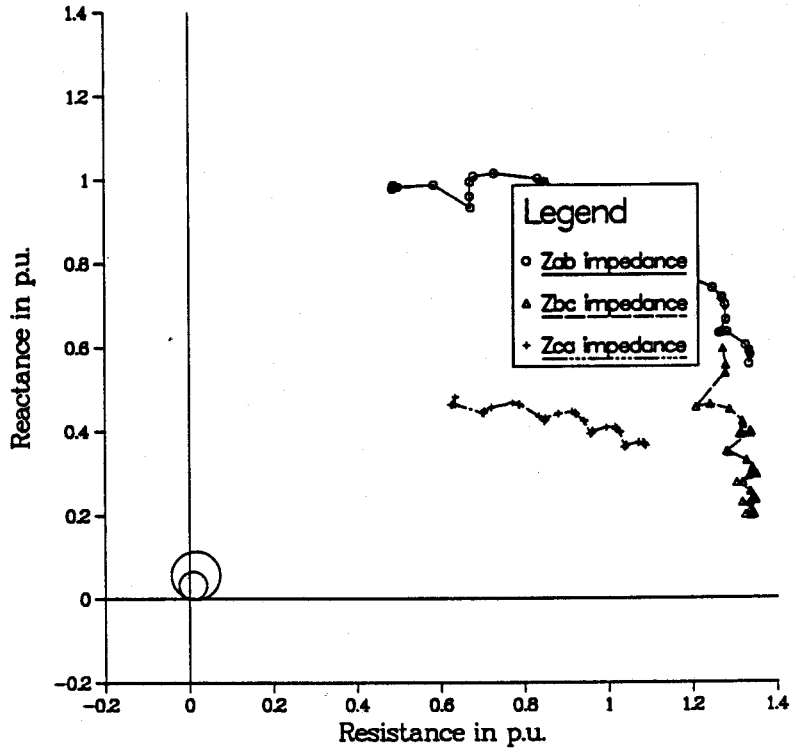

Figure 5.25: Trajectory of impedance estimates of the phase elements during inrush current using the Least Error Squares algorithm with source impedance increased.

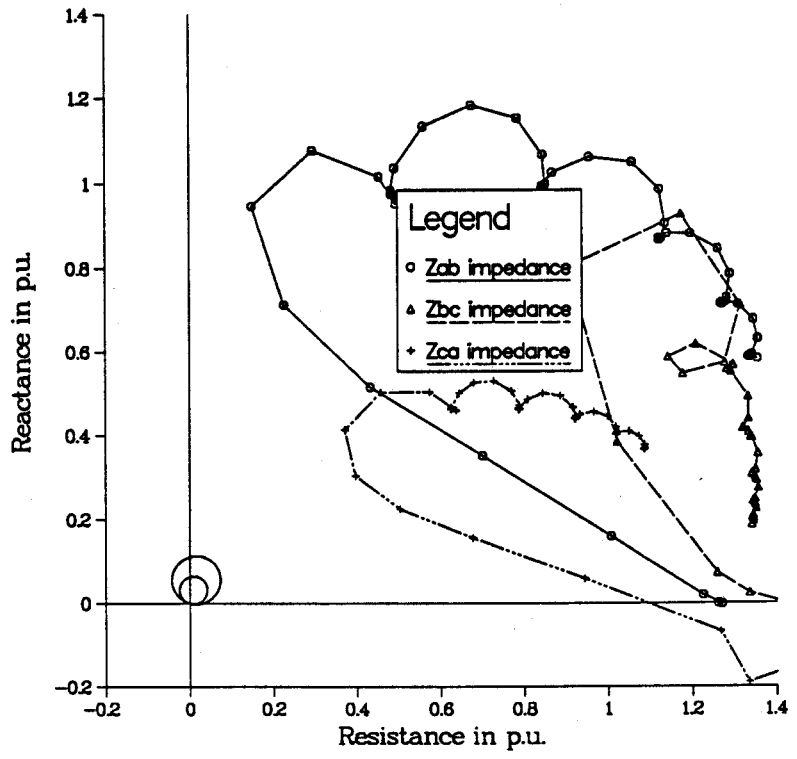

Figure 5.26: Trajectory of impedance estimates of the phase elements during inrush current using the Fourier algorithm with source impedance increased.

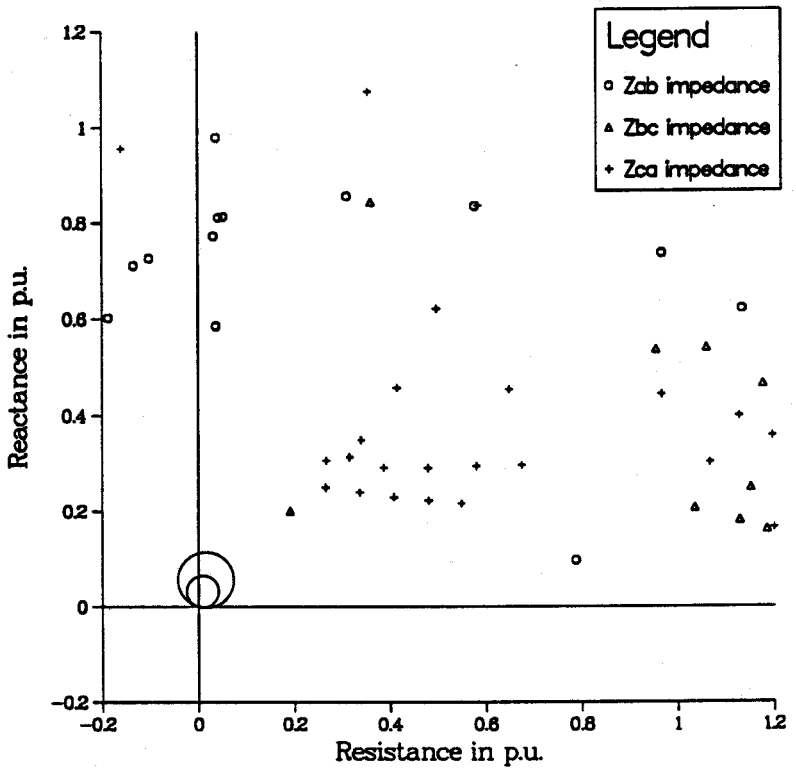

Figure 5.27: Trajectory of impedance estimates of the phase elements during inrush current using the R-L algorithm with source impedance increased.

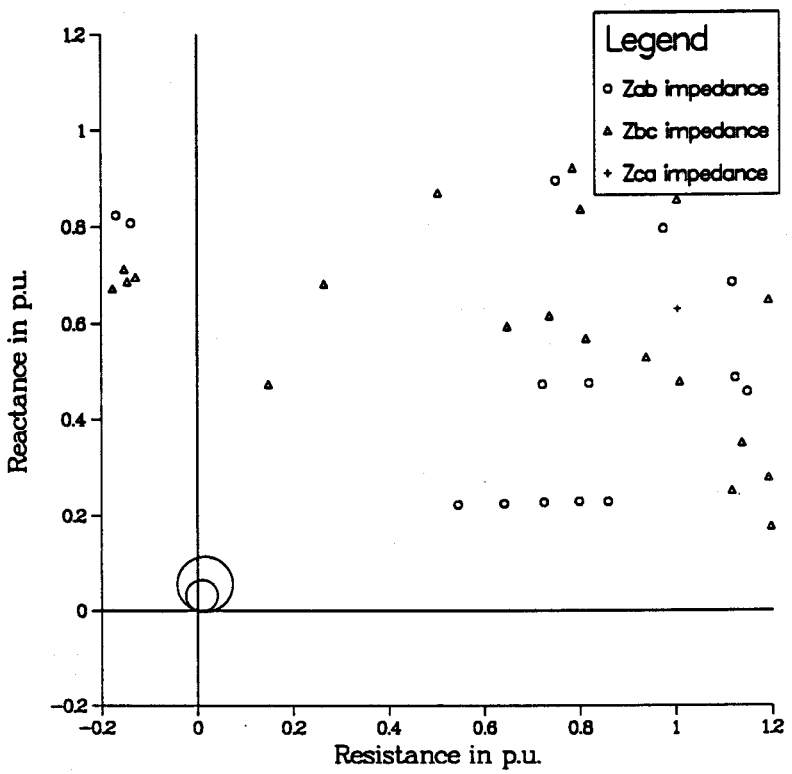

Figure 5.28: Trajectory of impedance estimates of the phase elements during inrush current using Mann and Morrison short window algorithm with source impedance increased.

5.3.2. Inrush Current with a Single Phase to Ground Fault

The impedances seen by the ground fault elements using different algorithms are shown in Figures 5.29 through 5.32. The figures show that the trajectories of the phase A impedance estimates end in the correct zone of the relay and will, therefore, issue a trip command. The estimates of the short window algorithms are not consistent and this can cause the relay to reach a wrong decision. The long window algorithms accurately detect the fault though the Fourier algorithm is slower in settling down to the final value than the Least Error Squares algorithm. The impedance estimates of the phase elements are shown in Figures 5.33 through 5.36 and they do not enter the operating zone of the relay. Apart from the A-G element, none of the other elements operate.

5.3.3. Inrush Current with a Phase to Phase Fault

The results for a phase A to phase B fault are presented in this section. The impedances seen by the ground fault elements are shown in Figures 5.37 through 5.40. None of the impedance estimates of different algorithms settle in the operating zone of the relay. The estimates obtained from the Fourier, R-L and Mann and Morrison algorithms show that the impedance estimates of the ground elements pass through the operating zones of the relay. This might provoke tripping in case of fast relays. Figures 5.41 through 5.44 show the impedance estimates obtained from the phase elements. The trajectories of the impedance estimates obtained using voltages and currents from phase A and phase B end in the correct operating zone of the relay. A trip command will, therefore, be issued. The impedance estimates obtained using the Least Error Squares algorithm is the fastest in settling down to the final value because of the suppression of the d.c. offsets.

In case of the ground elements, the impedance estimates of the Fourier and Mann and Morrison algorithms are affected by the d.c. offsets. The impedance estimates obtained from the Mann and Morrison algorithm are affected by the presence of harmonics. These harmonics, also affect the impedance estimates of the R-L algorithm.

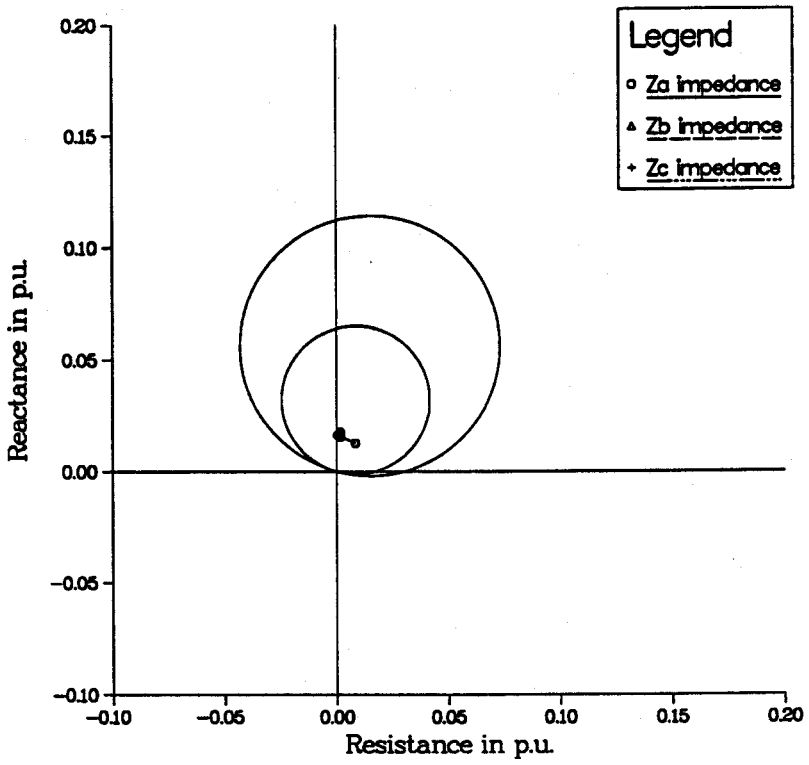

Figure 5.29: Trajectory of impedance estimates of the ground elements for a single-phase to ground fault using the Least Error Squares algorithm.

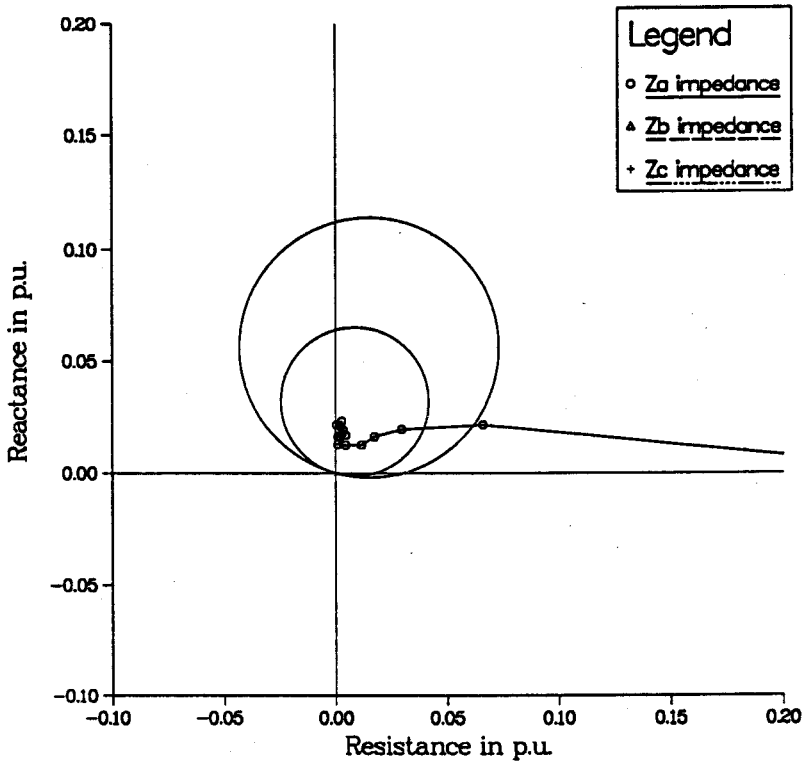

Figure 5.30: Trajectory of impedance estimates of the ground elements for a single-phase to ground fault using the Fourier algorithm.

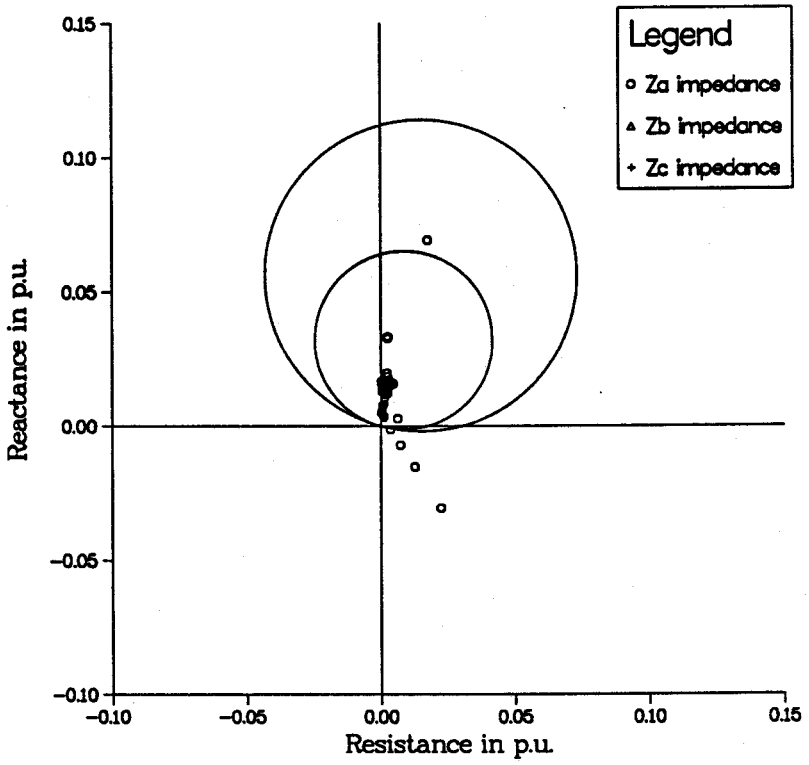

Figure 5.31: Trajectory of impedance estimates of the ground elements for a single-phase to ground fault using the R-L algorithm.

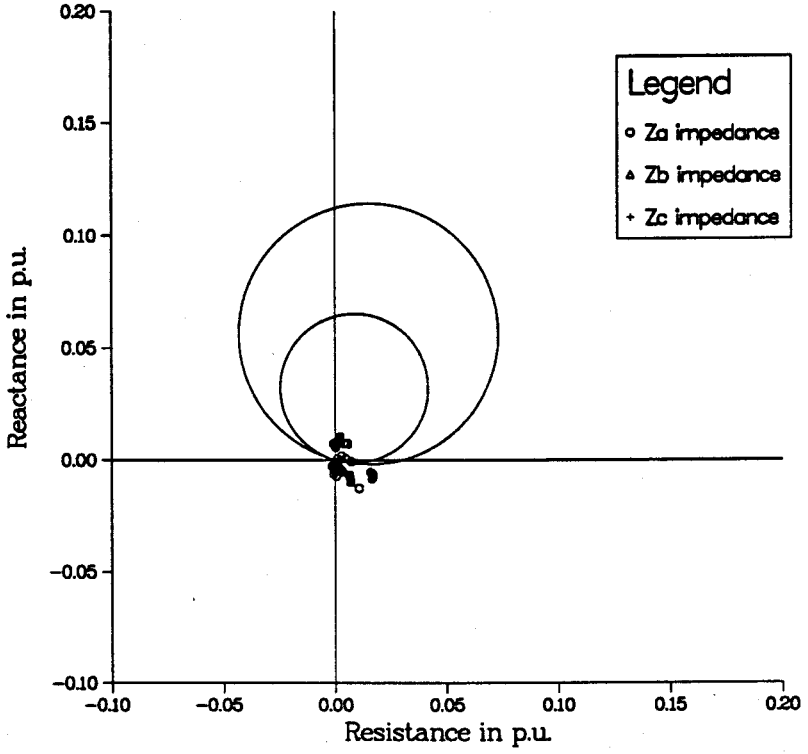

Figure 5.32: Trajectory of impedance estimates of the ground elements for a single-phase to ground fault using Mann and Morrison short window algorithm.

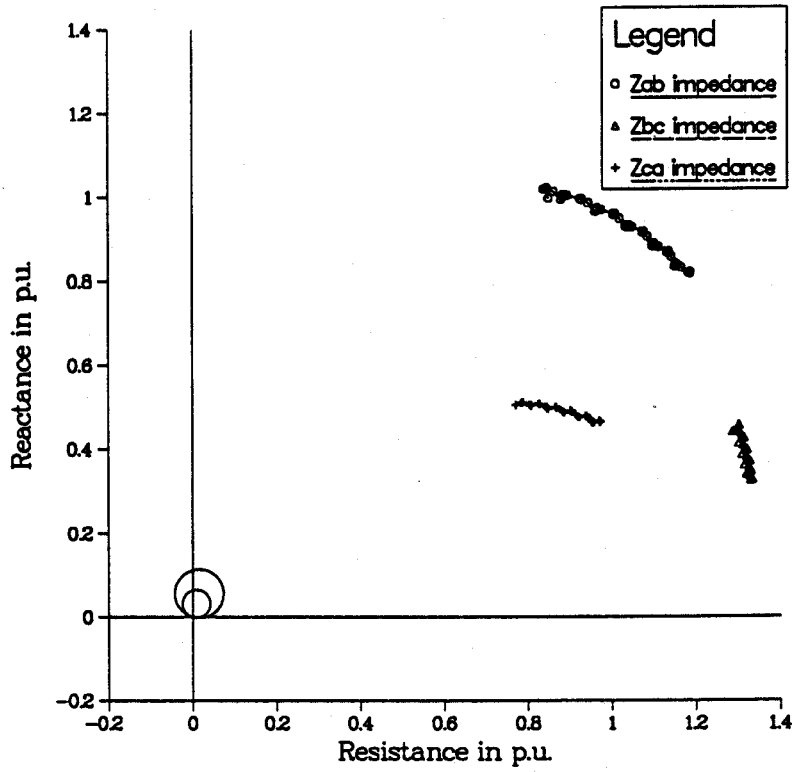

Figure 5.33: Trajectory of impedance estimates of the phase elements for a single-phase to ground fault using the Least Error Squares algorithm.

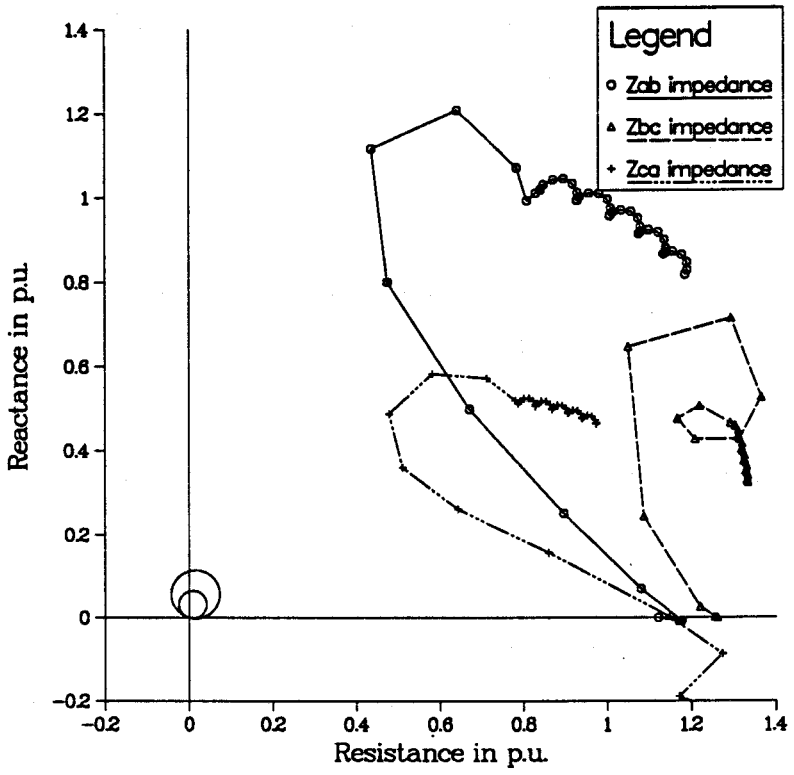

Figure 5.34: Trajectory of impedance estimates of the phase elements for a single-phase to ground fault using the Fourier algorithm.

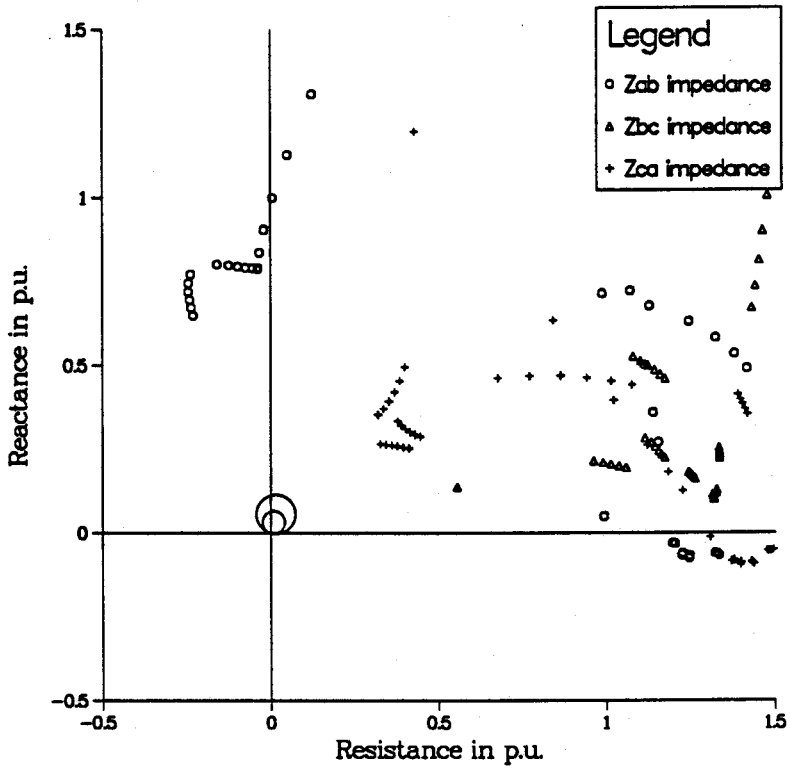

Figure 5.35: Trajectory of impedance estimates of the phase elements for a single-phase to ground fault using the R-L algorithm.

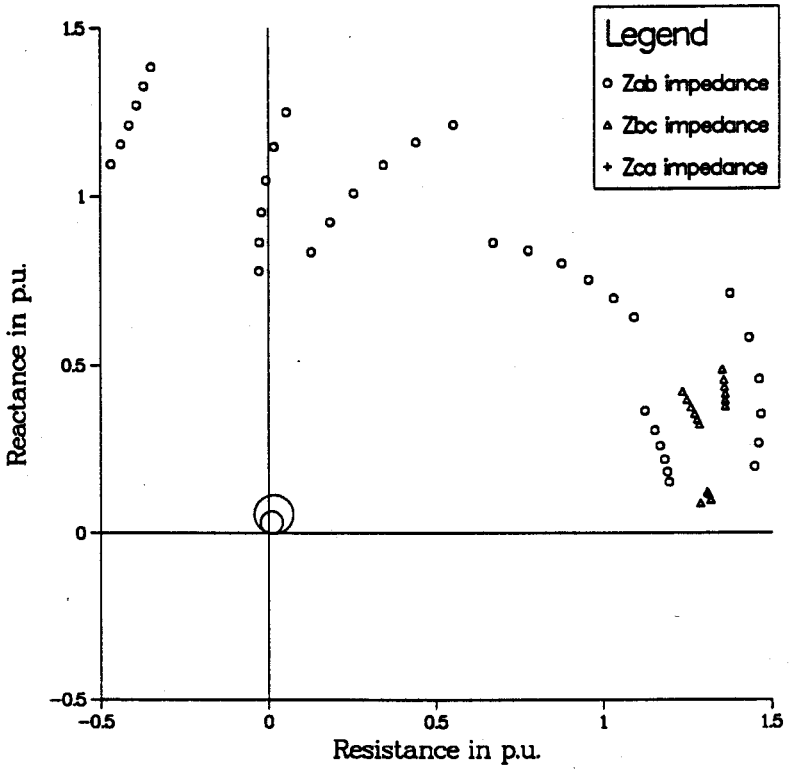

Figure 5.36: Trajectory of impedance estimates of the phase elements for a single-phase to ground fault using Mann and Morrison short window algorithm.

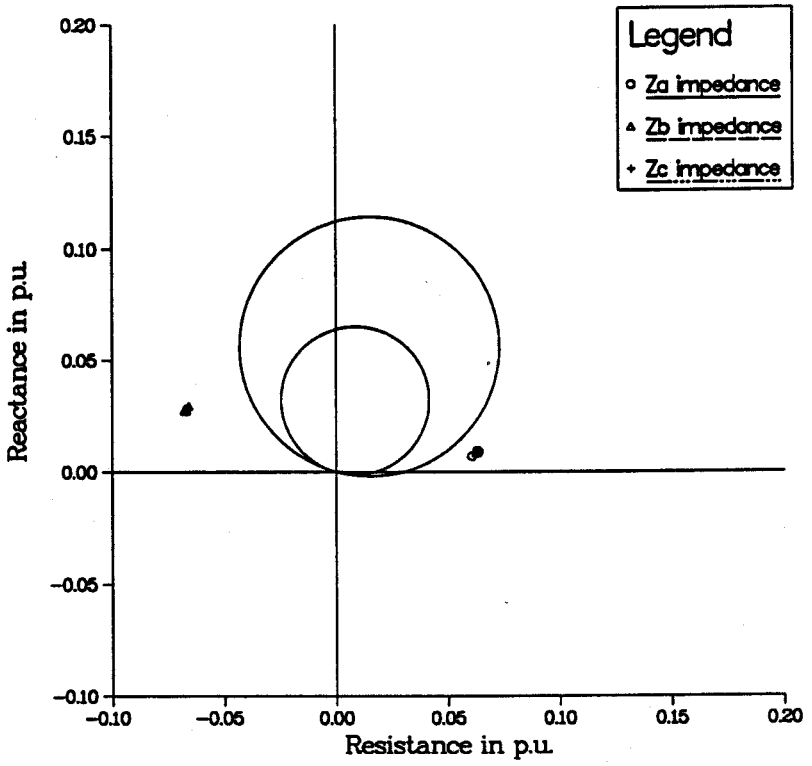

Figure 5.37: Trajectory of impedance estimates of the ground elements for a phase-phase fault using the Least Error Squares algorithm.

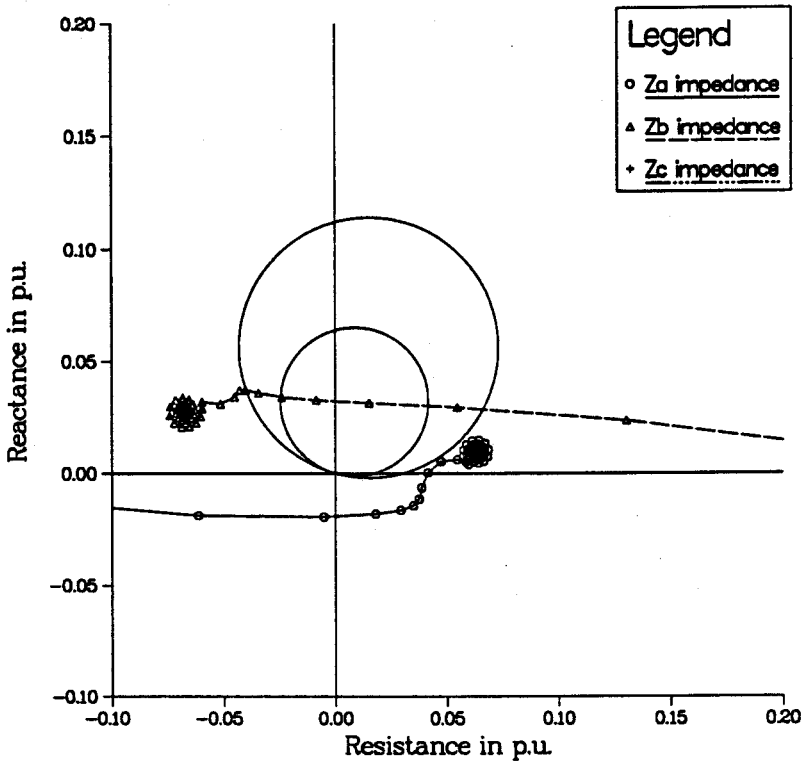

Figure 5.38: Trajectory of impedance estimates of the ground elements for a phase-phase fault using the Fourier algorithm.

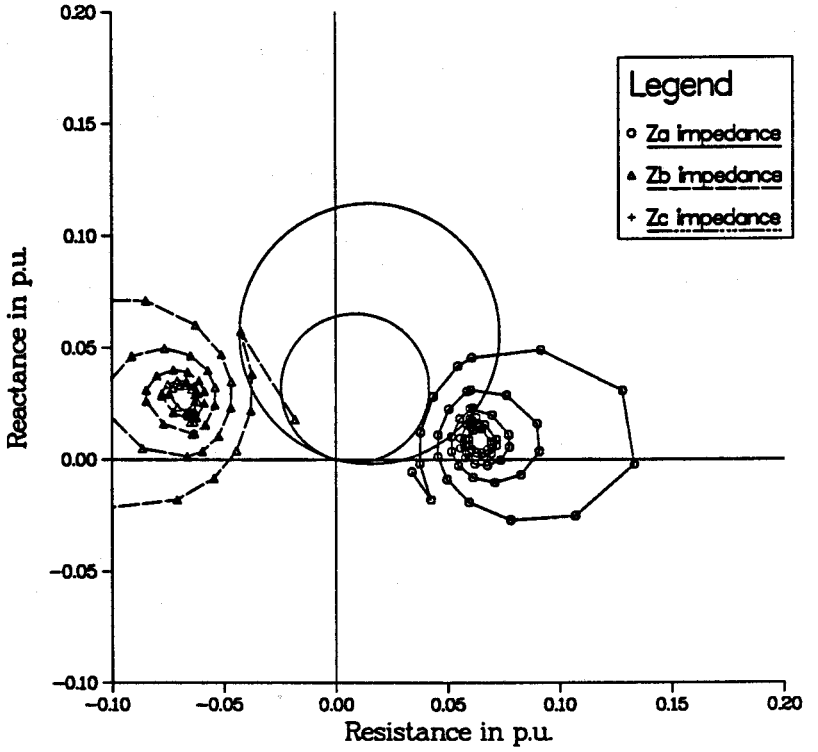

Figure 5.39: Trajectory of impedance estimates of the ground elements for a phase-phase fault using the R-L algorithm.

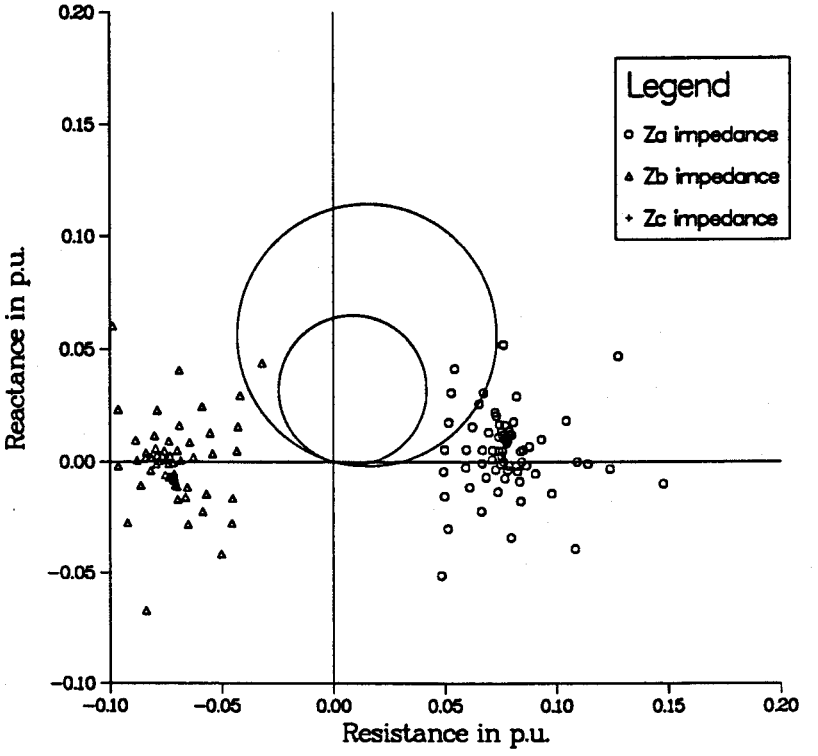

Figure 5.40: Trajectory of impedance estimates of the ground elements for a phase-phase fault using Mann and Morrison short window algorithm.

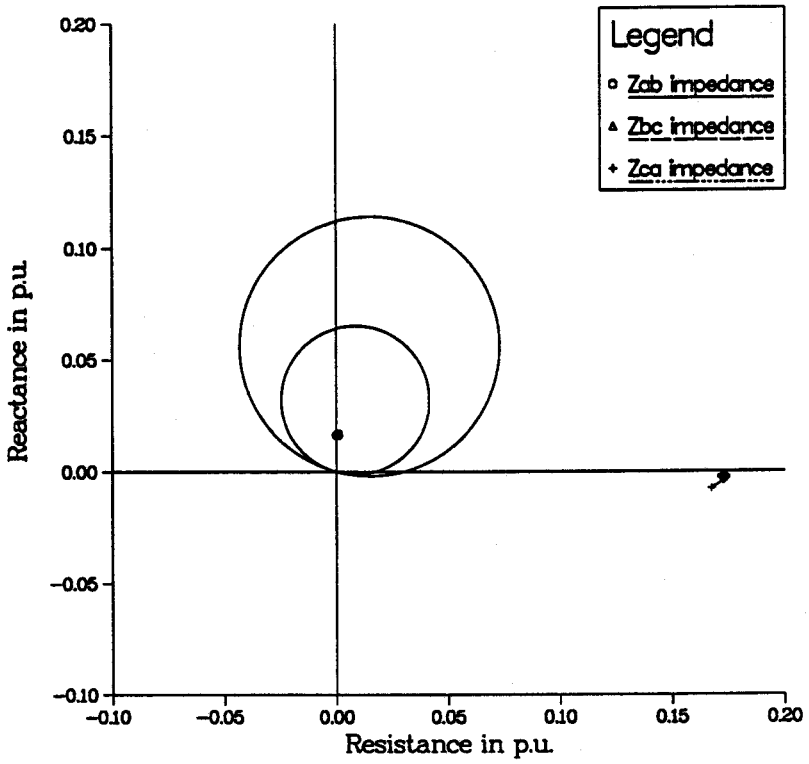

Figure 5.41: Trajectory of impedance estimates of the phase elements for a phase-phase fault using the Least Error Squares algorithm.

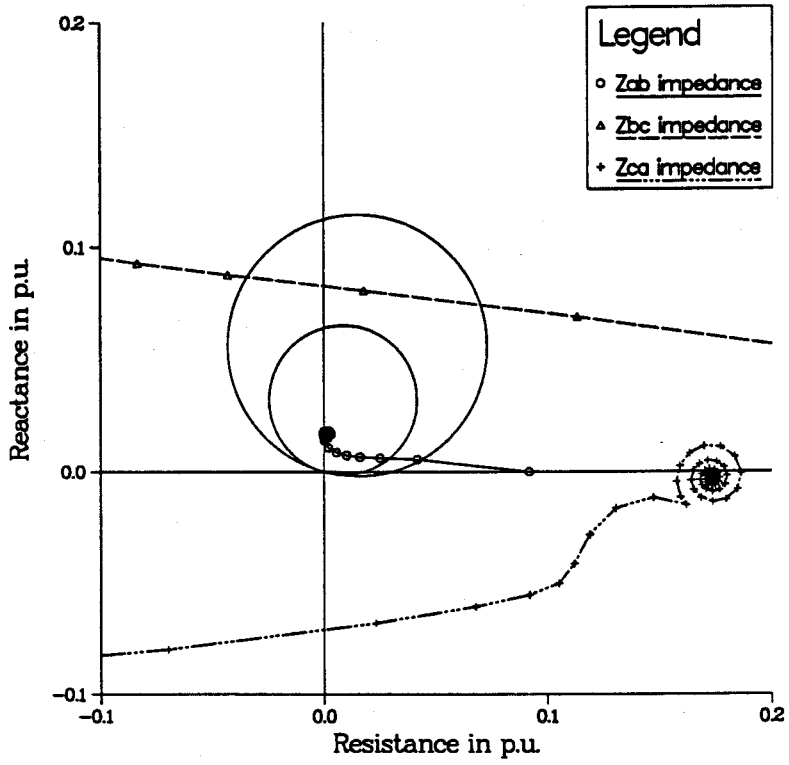

Figure 5.42: Trajectory of impedance estimates of the phase elements for a phase-phase fault using the Fourier algorithm.

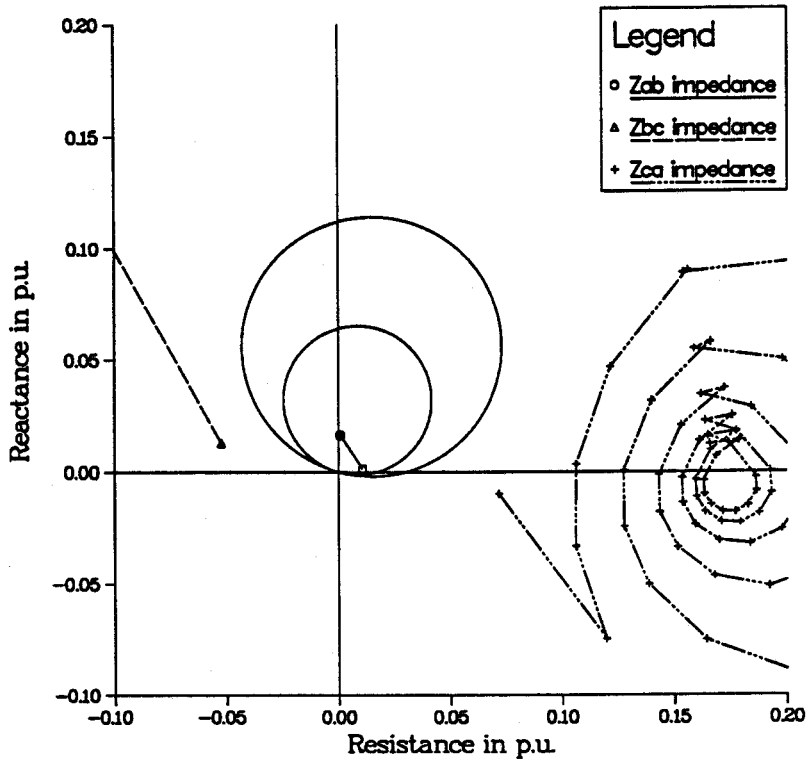

Figure 5.43: Trajectory of impedance estimates of the phase elements for a phase-phase fault using the R-L algorithm.

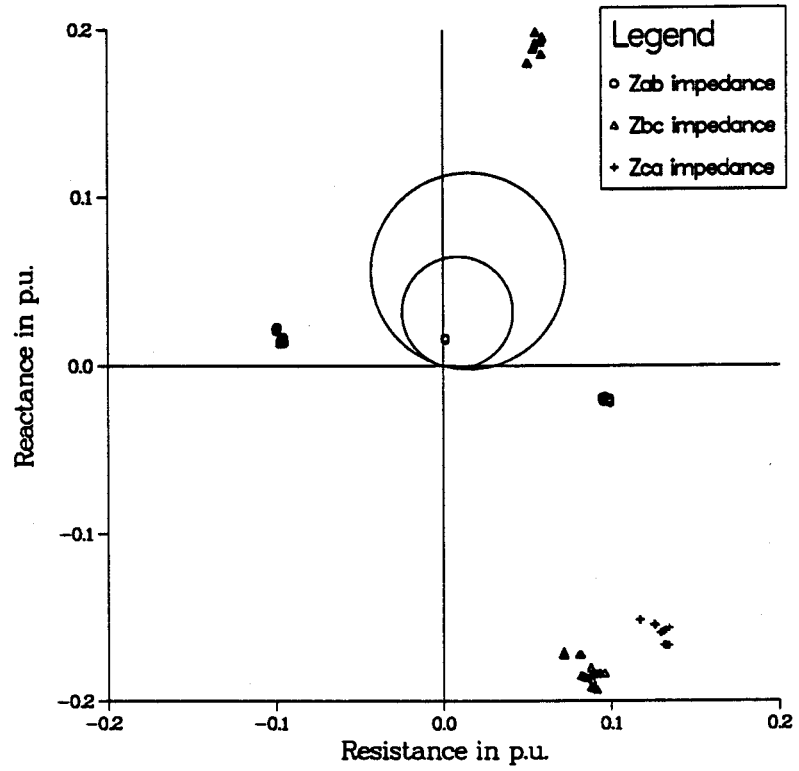

Figure 5.44: Trajectory of impedance estimates of the phase elements for a phase-phase fault using Mann and Morrison short window algorithm.

5.4. Summary

This chapter has described some test results from the studies for evaluating the performance of digital distance relay algorithms during the presence of inrush current and inrush current when a fault exists.

The distance digital relays did not issue a trip command in the presence of inrush current only. The presence of the decaying d.c. in the inrush current provoked rapid changes in the impedance estimates of the short window algorithms as well as the Fourier algorithm. The changes were, however, more pronounced in the short window algorithms. The ability of the Least Error Squares algorithm to suppress the decaying d.c. was demonstrated through the reduced movements of the impedance estimates. In all cases of inrush current in presence of a fault, the impedance estimates moved into the correct zone of the relay with the Least Error Squares algorithm settling down to the final value much faster than any of the other algorithms. Results of the healthy phase relays (unfaulted phases) were also shown because it is important to check that these relays do not operate incorrectly and give rise to unwanted trippings. Some of the results for faults at the midpoint of the transformer terminated line are presented in Appendix B.

6. FAULT DIRECTION DISCRIMINATING ALGORITHM

6.1. Introduction

Chapter 5 has described the evaluation of digital distance relay algorithms protecting a transformer terminated line. At times, the distance relay may lose its directional capabilities especially for faults on the secondary side of the transformer in the transformer terminated line [13]. To assure the direction of the faults for the relay, symmetrical components can be used. These furnish significant insight into the behaviour of three-phase power system operation during unbalanced conditions, such as, those caused by faults between phases and/or ground [11]. This chapter presents a fault direction discriminating algorithm which is based on the positive- and negative- sequence impedances calculated using the incremental voltages and currents. A similar approach is reported in the literature for generator protection [53] using the Least Error Squares algorithm.

6.2. Development of the Algorithm

Consider a transformer terminated line power system used for the studies reported in the previous chapter. If faults are created after the system has reached a steady state in front (forward fault) of the relay location, the resulting pre-fault and post-fault positive-sequence networks would be as shown in Figures 6.1 and 6.2 respectively. In both networks, the Thevenin's equivalent source is now represented by its positive-sequence impedance, Z_{g1}, and the positive-sequence internal voltage, E_{g1} [12]. The fault impedance, Z_f, shown in Figure 6.2, represents the fault resistance and, depending on the type of fault, the other sequence network(s). The pre-fault and post-fault negative-sequence networks are shown in Figures 6.3 and 6.4. For a fault behind (reverse fault) the relay location, the pre-fault and post-fault positive-sequence networks can be shown as in Figures 6.5 and 6.6 respectively. The pre-fault and post-fault negative-sequence networks are shown as in Figures 6.7 and 6.8.

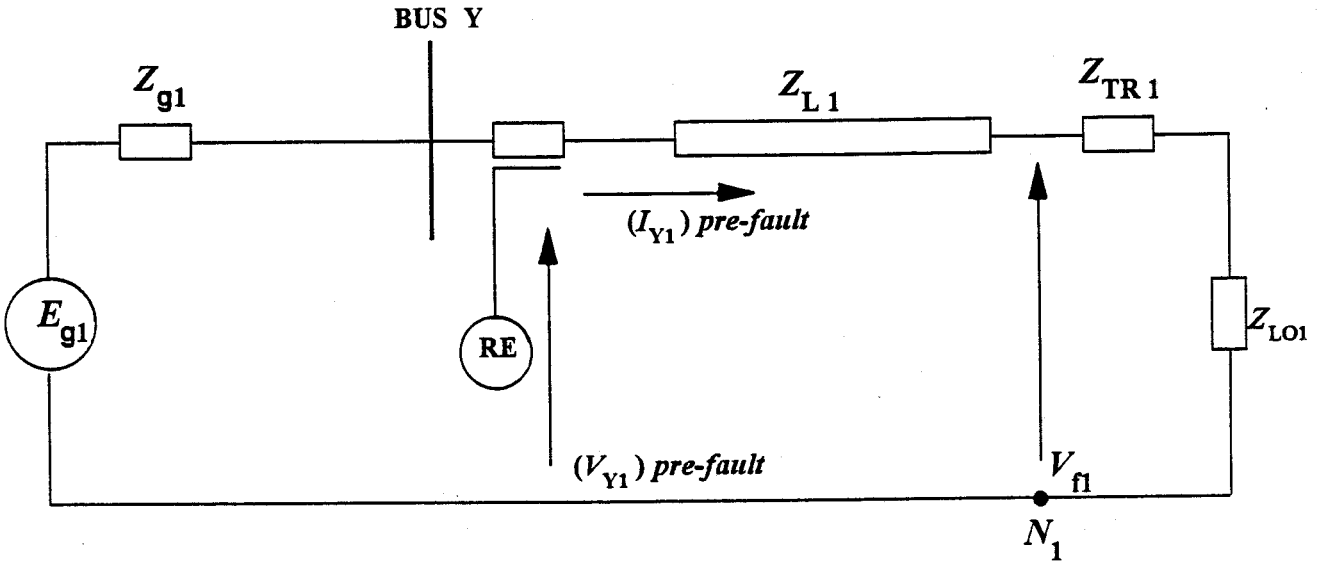

Figure 6.1: Pre-fault positive-sequence network of the transformer terminated line for a forward fault.

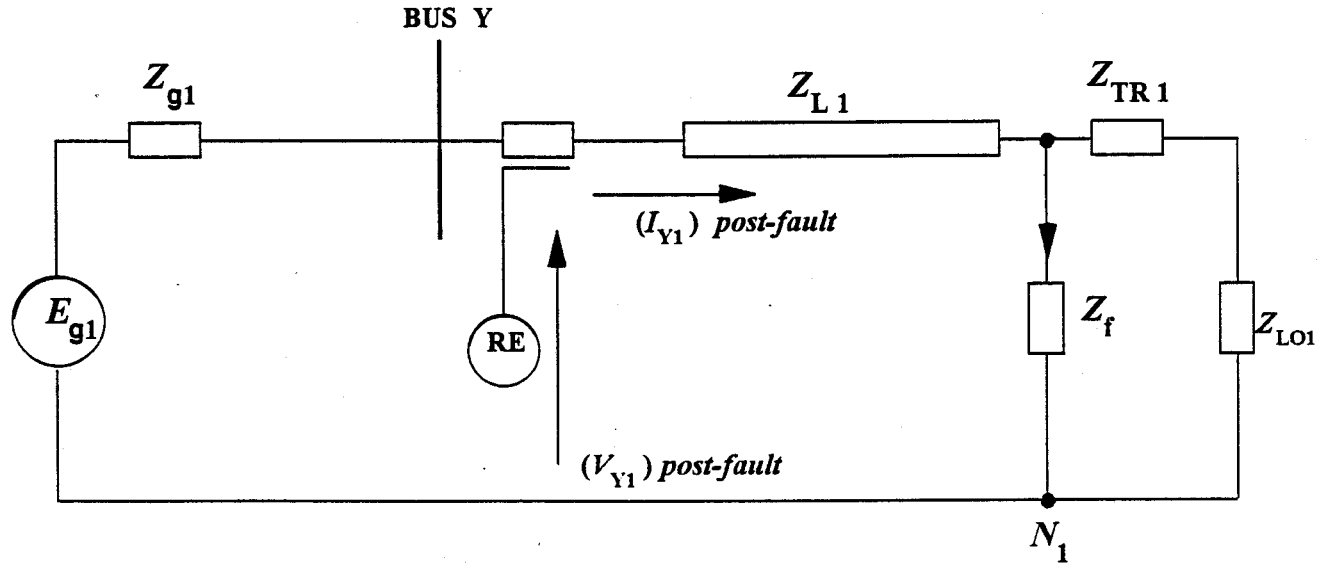

Figure 6.2: Post-fault positive-sequence network of the transformer terminated line for a forward fault.

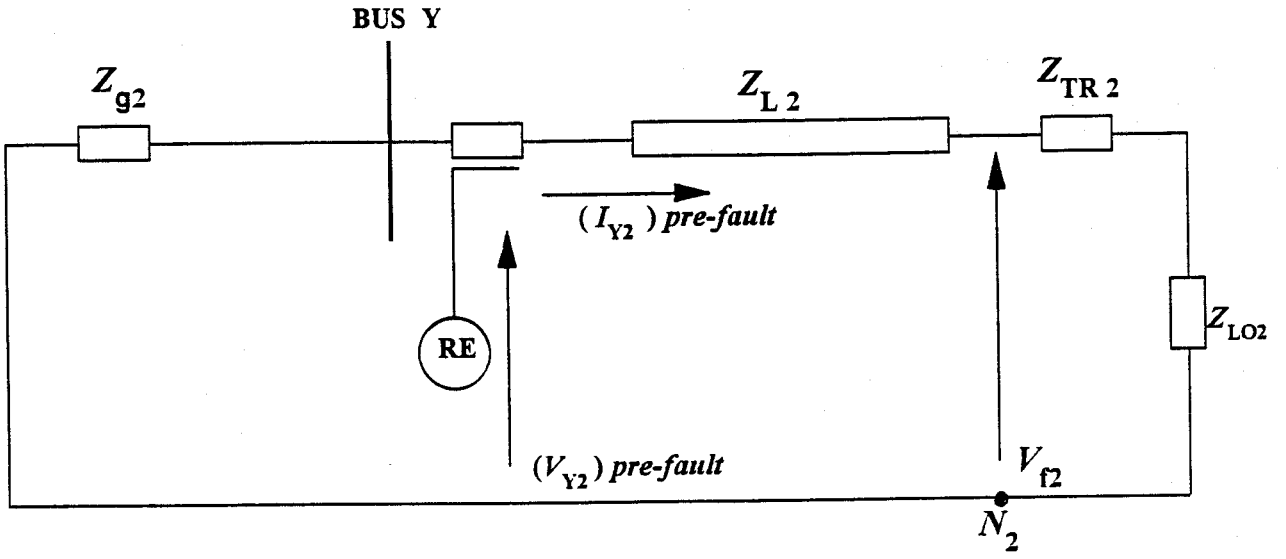

Figure 6.3: Pre-fault negative-sequence network of the transformer terminated line for a forward fault.

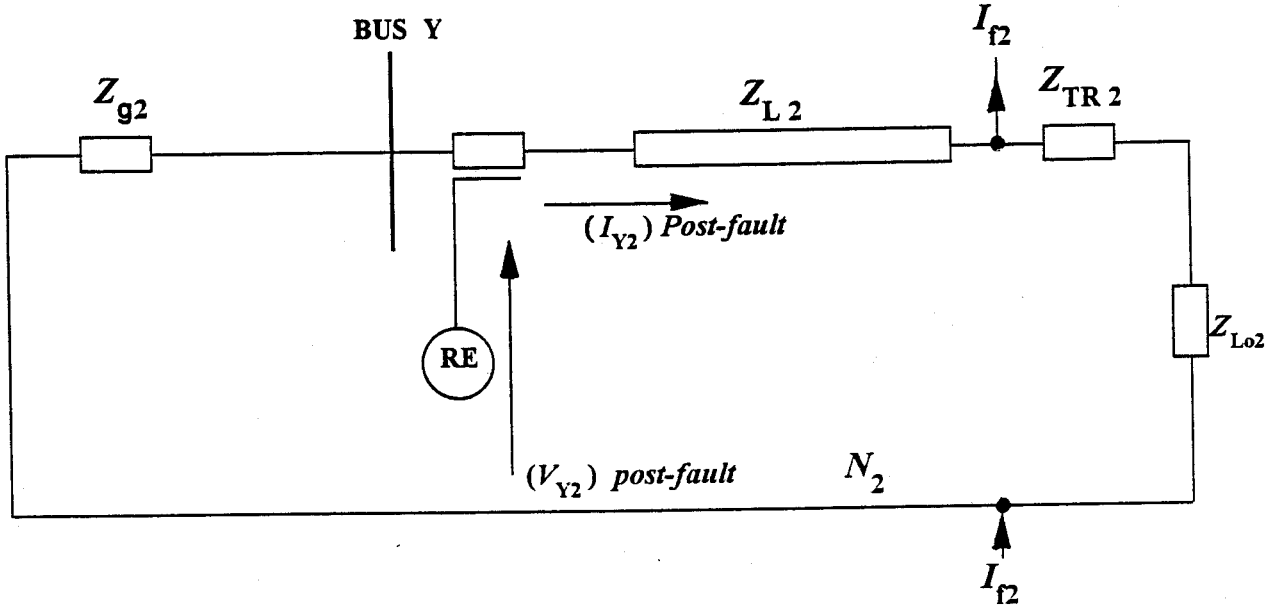

Figure 6.4: Post-fault negative-sequence network of the transformer terminated line for a forward fault.

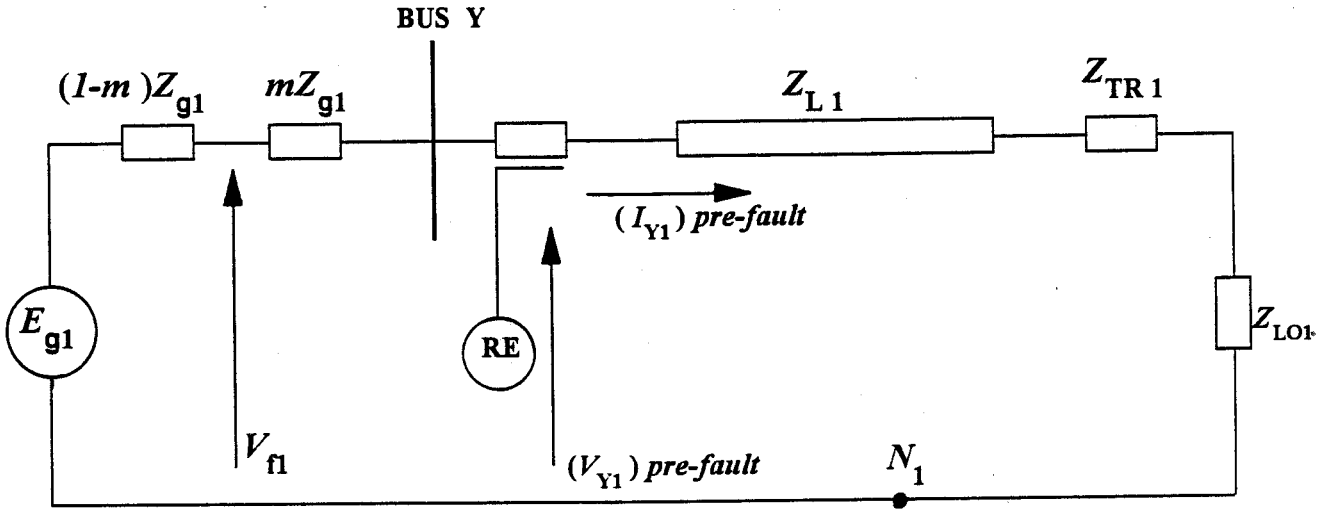

Figure 6.5: Pre-fault positive-sequence network of the transformer terminated line for a reverse fault.

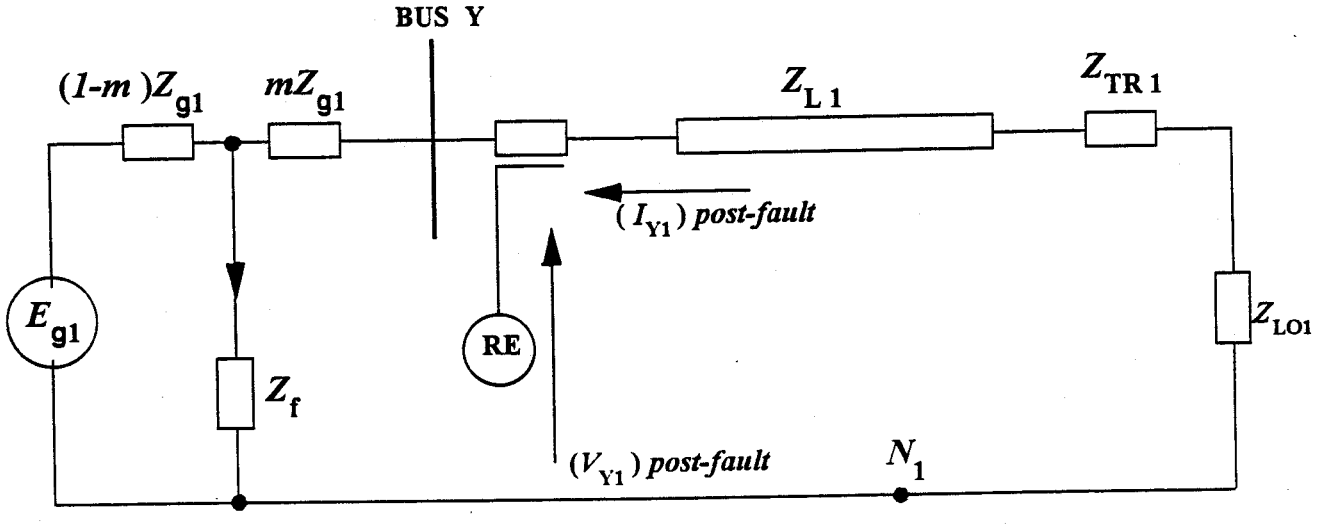

Figure 6.6: Post-fault positive-sequence network of the transformer terminated line for a reverse fault.

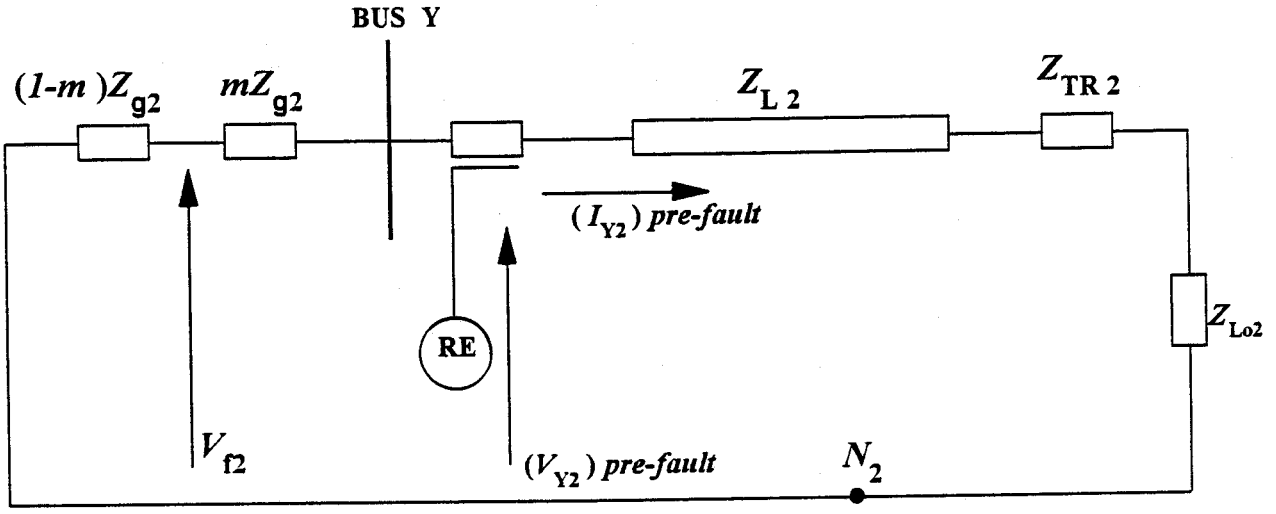

Figure 6.7: Pre-fault negative-sequence network of the transformer terminated line for a reverse fault.

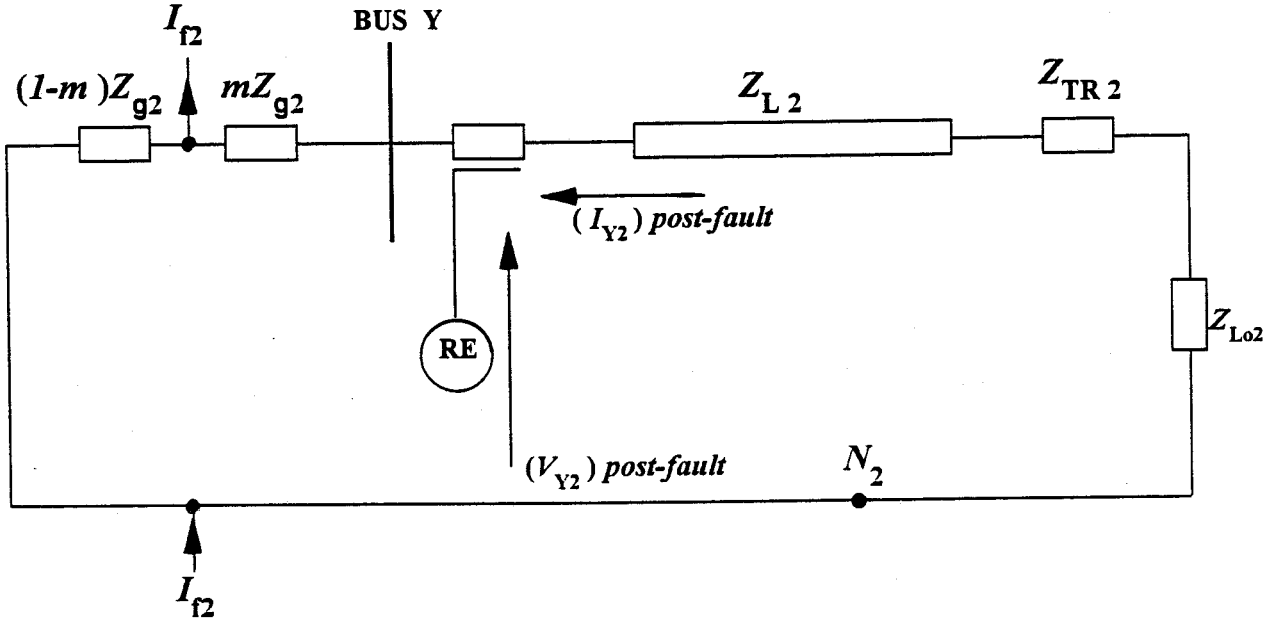

Figure 6.8: Post-fault negative-sequence network of the transformer terminated line for a reverse fault.

6.2.1. Forward Fault

Figure 6.9 shows the Thevenin's equivalent circuit of positive-sequence network of the power system as seen from Bus *Y*, for a forward fault. The Thevenin voltage is the pre-fault positive-sequence voltage at the fault point. The incremental voltage ΔV_{y1}, and the incremental current, ΔI_{y1}, can be expressed as follows:

$$\Delta V_{y1} = (V_{y1})post\text{–}fault - (V_{y1})pre\text{–}fault. \quad (6.1)$$
$$\Delta I_{y1} = (I_{y1})post\text{–}fault - (I_{y1})pre\text{–}fault. \quad (6.2)$$

where:

(V_{y1})*pre-fault* is the positive-sequence voltage at Bus *Y* prior to the occurrence of the fault,

(I_{y1})*pre-fault* is the positive-sequence current at Bus *Y* prior to the occurrence of the fault,

(V_{y1})*post-fault* is the positive-sequence voltage at Bus *Y* after the occurrence of the fault and

(I_{y1})*post-fault* is the positive-sequence current at Bus *Y* after the occurrence of the fault.

The relay uses the incremental positive-sequence voltage and current at relay location which can be expressed by Equations 6.3 and 6.4 respectively.

$$V_{relay}=\Delta V_{y1}=-Z_{g1}\Delta I_{y1} \quad (6.3)$$

$$I_{relay}=\Delta I_{y1} \quad (6.4)$$

where:

V_{relay} is the relay voltage and
I_{relay} is the relay current.

Substituting Equation (6.4) into Equation (6.3) gives:

$$V_{relay}=-Z_{g1}I_{relay} \quad (6.5)$$

From Equations (6.3) and (6.4) the positive-sequence impedance seen by the relay for a forward fault calculated using the incremental positive-sequence voltage and current will be:

$$\frac{V_{relay}}{I_{relay}} = -Z_{g1} \tag{6.6}$$

where:

Z_{g1} is the positive-sequence impedance of the Thevenin's equivalent source.

Using a similar approach, if the relay uses the incremental negative-sequence voltage and current, as shown in Figure 6.10, the negative-sequence impedance seen will be:

$$\frac{V_{relay}}{I_{relay}} = \frac{\Delta V_{y2}}{\Delta I_{y2}} = -Z_{g2} \tag{6.7}$$

where:

ΔV_{y2} is the incremental negative-sequence voltage at Bus Y,
ΔI_{y2} is the incremental negative-sequence current at Bus Y and
Z_{g2} is the negative-sequence impedance of the Thevenin's equivalent source.

6.2.2. Reverse Fault

For a reverse fault, the Thevenin's equivalent circuit of positive-sequence network of the power system can be as shown as in Figure 6.11. The incremental positive-sequence voltage and current at relay location are given by Equations 6.8 and 6.9 respectively.

$$V_{relay} = \Delta V_{y1} = -(Z_{L1} + Z_{TR1} + Z_{L01})\Delta I_{y1} \tag{6.8}$$

$$I_{relay} = -\Delta I_{y1} \tag{6.9}$$

From Equations (6.8) and (6.9) the positive-sequence impedance seen by the relay for this fault will be:

$$\frac{V_{relay}}{I_{relay}} = \frac{\Delta V_{y1}}{\Delta I_{y1}} = (Z_{L1} + Z_{TR1} + Z_{Lo1}) \tag{6.10}$$

where:
Z_{L1} is the positive-sequence impedance of the line,
Z_{TR1} is the positive-sequence impedance of transformer *TR* and
Z_{Lo1} is the positive-sequence impedance of the load.

Similarly, if the relay uses the incremental negative-sequence voltage and current as shown in Figure 6.12, the impedance seen will be:

$$\frac{V_{relay}}{I_{relay}} = \frac{\Delta V_{y2}}{\Delta I_{y2}} = (Z_{L2} + Z_{TR2} + Z_{Lo2}) \tag{6.11}$$

where:

Z_{L2} is the negative-sequence impedance of the line,
Z_{TR2} is the negative-sequence impedance of transformer *TR* and
Z_{Lo2} is the negative-sequence impedance of the load.

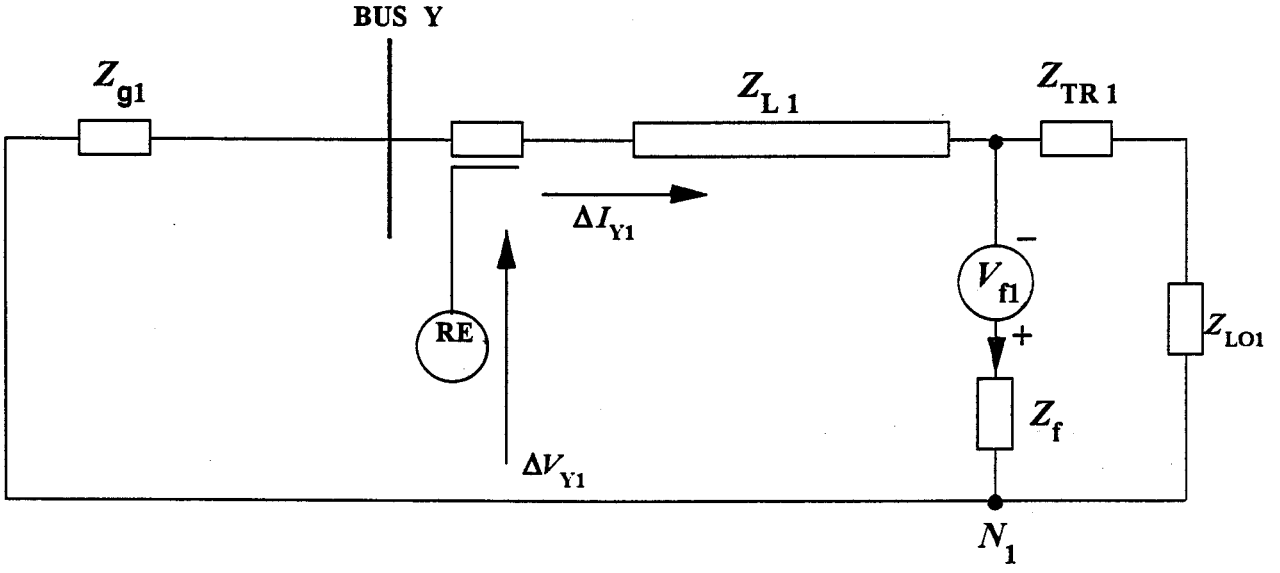

Figure 6.9: Thevenin's equivalent circuit for the postive-sequence network as seen from Bus *Y* in the transformer terminated line for a forward fault.

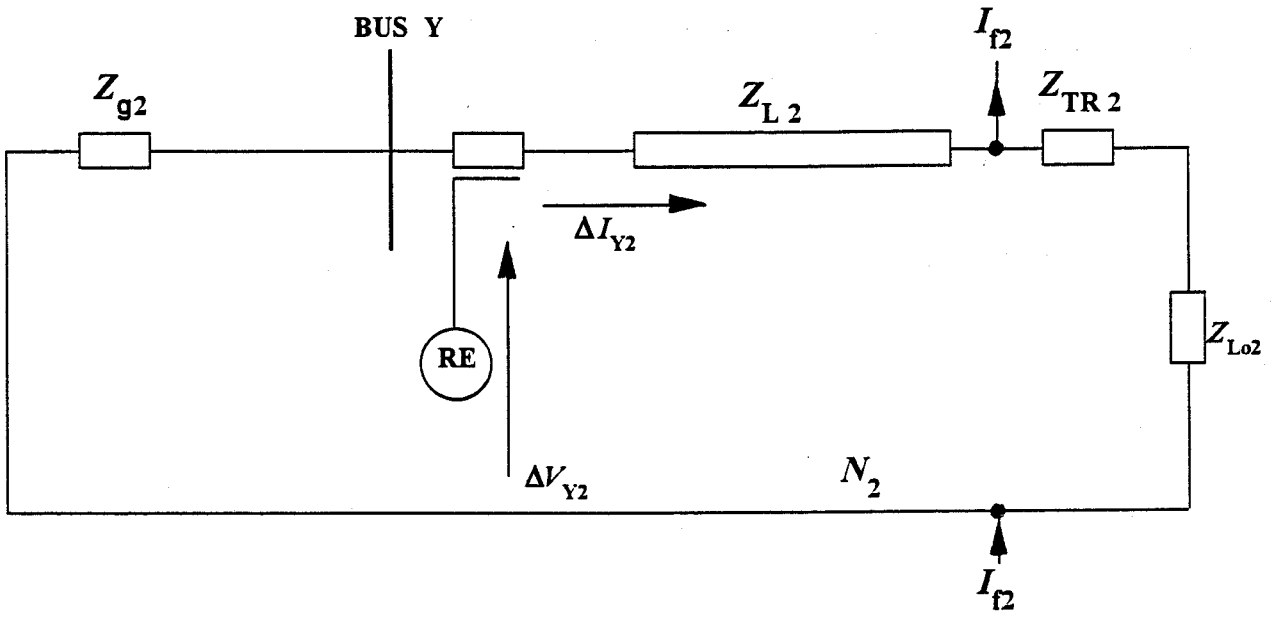

Figure 6.10: Thevenin's equivalent circuit for the negative-sequence network as seen from Bus *Y* in the transformer terminated line for a forward fault.

6.2.3. Direction Discrimination

From the equation for forward fault, it is clear that the positive-sequence impedance seen by the relay is the positive-sequence impedance behind the relay location with a negative sign. The negative-sequence impedance seen by the relay is also the negative-sequence impedance behind the relay location with a negative sign.

For reverse fault, the positive-sequence impedance seen by the relay is the total positive-sequence impedance in front of the relay location with a positive sign. The negative-sequence impedance seen by the relay in this case is also the total negative-sequence impedance in front of the relay with a positive sign.

The sign of the positive- and negative- sequence impedances seen by the relay can, therefore, be used to discriminate between internal and external faults for the protection of transformer terminated line.

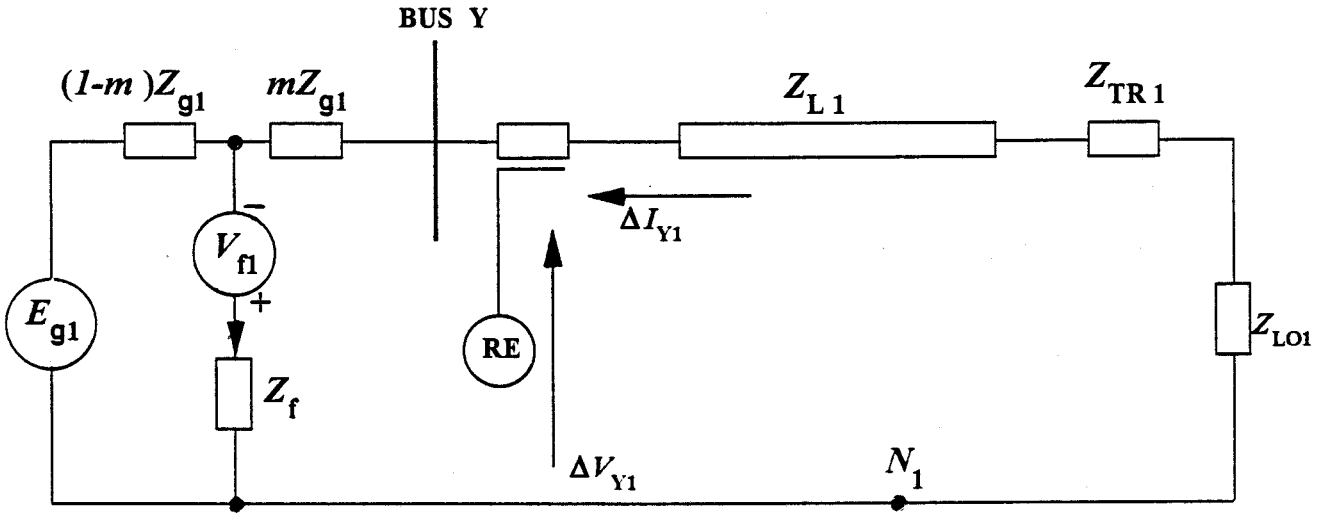

Figure 6.11: Thevenin's equivalent circuit for the postive-sequence network as seen from Bus *Y* in the transformer terminated line for a reverse fault.

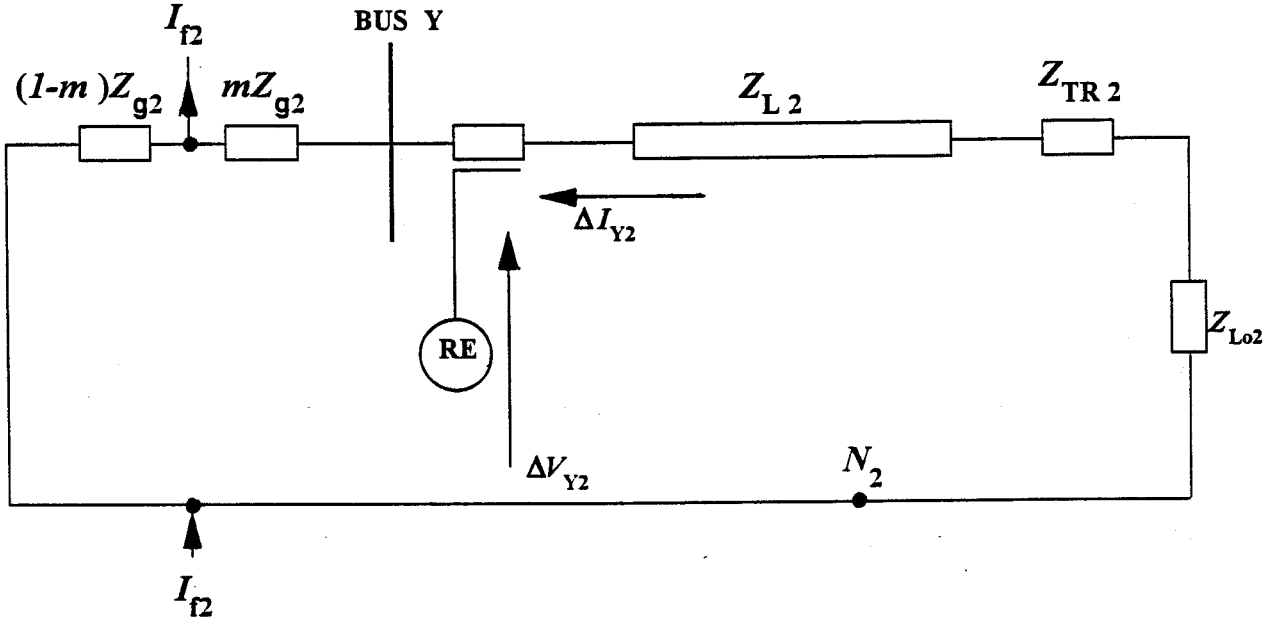

Figure 6.12: Thevenin's equivalent circuit for the negative-sequence network as seen from Bus *Y* in the transformer terminated line for a reverse fault.

6.3. Assessment of the Algorithm

A program was developed which compared filtered instantaneous voltage and current samples at the relay location with those from one cycle before. If the change is greater than a pre-defined threshold, then the most recent cycle of pre-fault phasors is used to calculate the corresponding incremental positive- and negative- sequence voltages and currents from the post-fault phasors. From these, impedance estimates were calculated using the Fourier algorithm. Figures 6.13 and 6.14 show the trajectories of the calculated positive- and negative- sequence impedances for the forward faults and Figures 6.15 and 6.16 for the reverse faults. The results show that for a forward fault, the positive-sequence impedance seen by the relay is the positive-sequence impedance of the network behind the relay with a negative sign. The negative-sequence impedance seen by the relay is the negative-sequence impedance behind the relay also with a negative sign. This means that the network in front of the relay is not verified for forward faults.

For the reverse faults, the positive-sequence impedance now seen by the relay is the total positive-sequence impedance in front of the relay with a positive sign. The negative-sequence impedance seen by the relay is the total negative-sequence impedance in front of the relay also with a positive sign. The network in front of the relay is verified in this case.

In the case of three-phase faults, the positive-sequence impedance alone is used in discriminating the faults since these are usually balanced faults and the negative-sequence impedance does not exist. Figures 6.17 and 6.18 show the trajectories of the positive-sequence impedances seen by the relay for a three-phase to ground fault in front and behind the relay location respectively. The results show that for the three-phase to ground fault in front of the relay, the impedance seen by the relay is the impedance behind the relay with a negative sign. For a three-phase to ground fault behind the relay, the impedance seen by the relay is the total impedance in front of the relay with a positive sign.

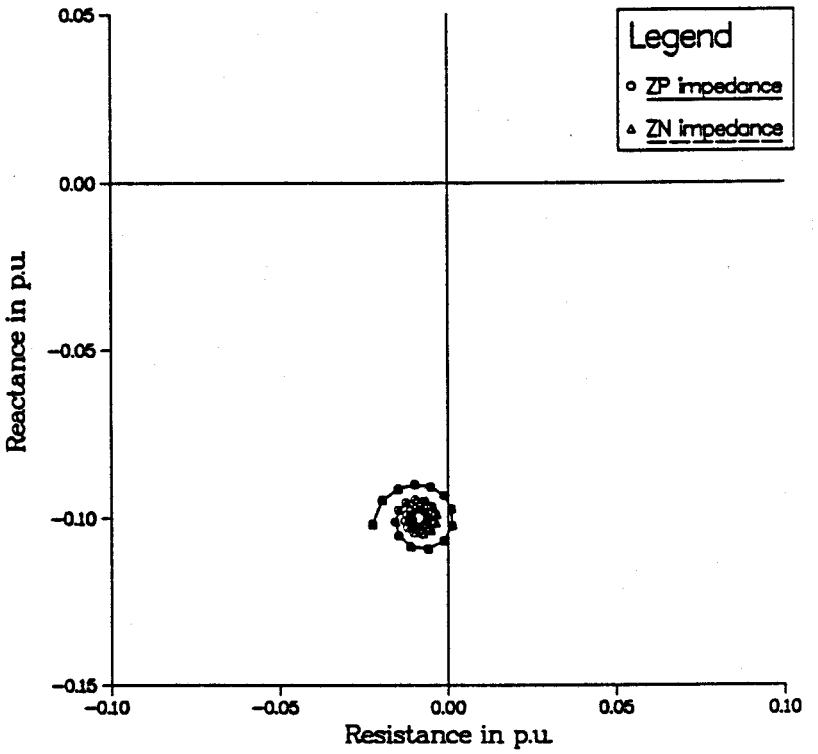

Figure 6.13: Trajectory of positive- and negative- sequence impedance estimates during a single-phase to ground fault in front of relay location.

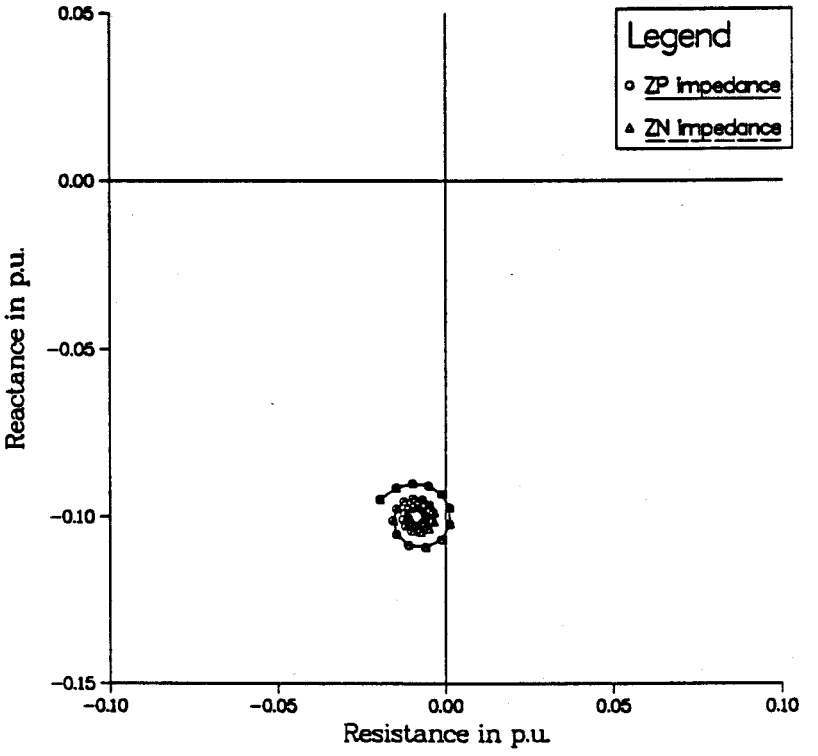

Figure 6.14: Trajectory of positive- and negative- sequence impedance estimates during a phase-phase fault in front of relay location.

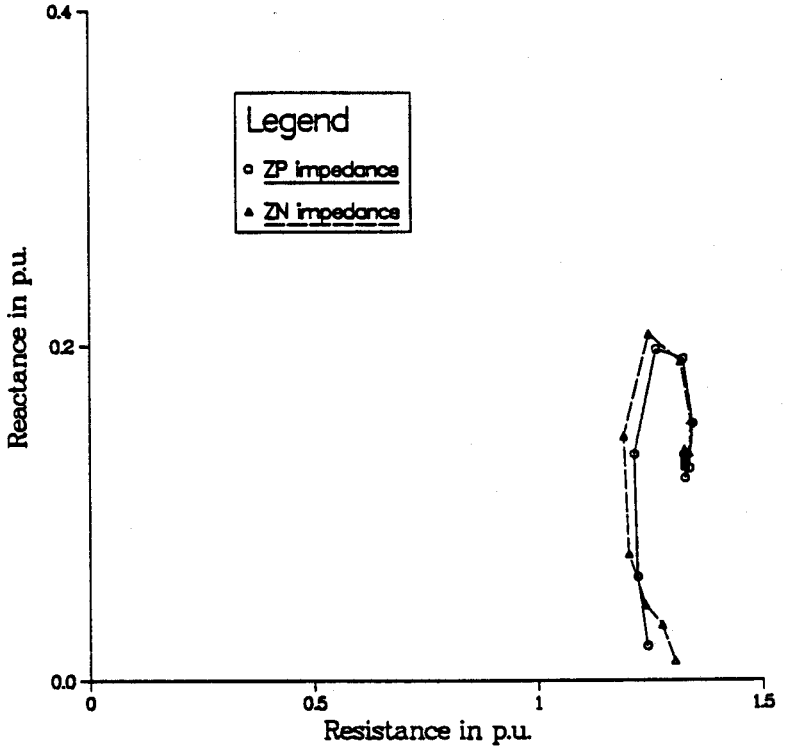

Figure 6.15: Trajectory of positive- and negative- sequence impedance estimates during a single-phase to ground fault behind the relay location.

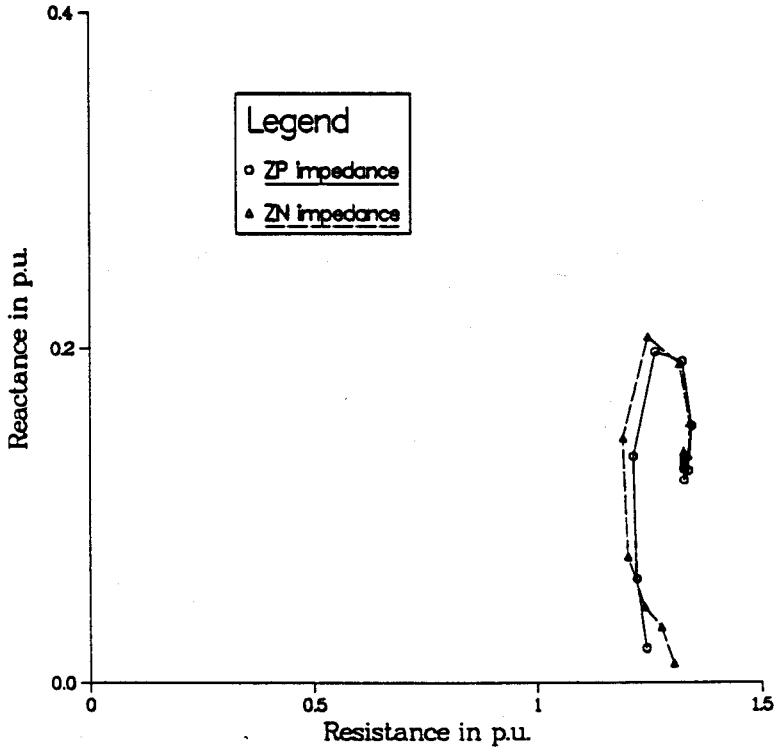

Figure 6.16: Trajectory of positive- and negative- sequence impedance estimates during a phase-phase fault behind the relay location.

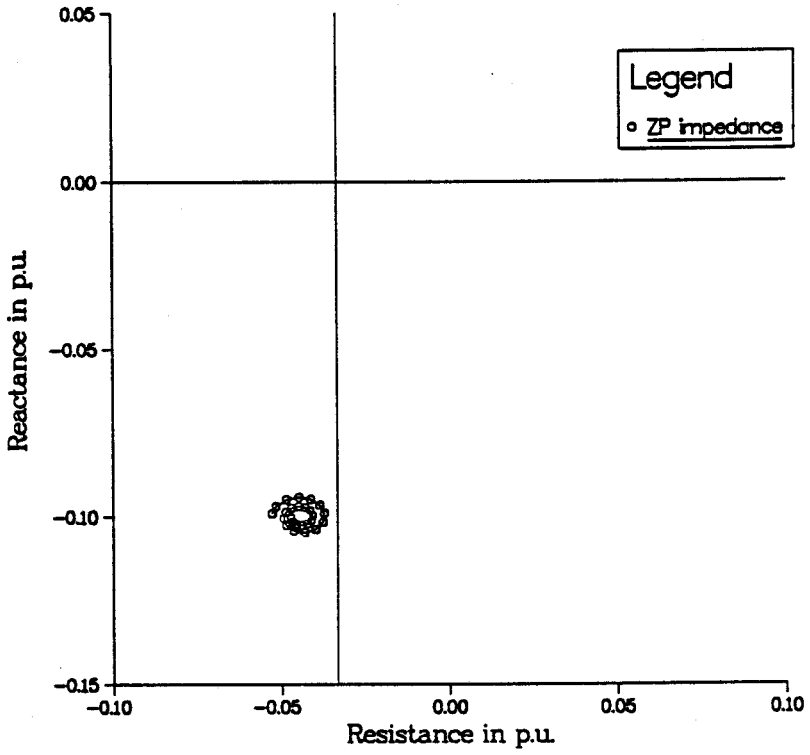

Figure 6.17: Trajectory of positive-sequence impedance estimate during a three-phase to ground fault in front of the relay location (forward fault).

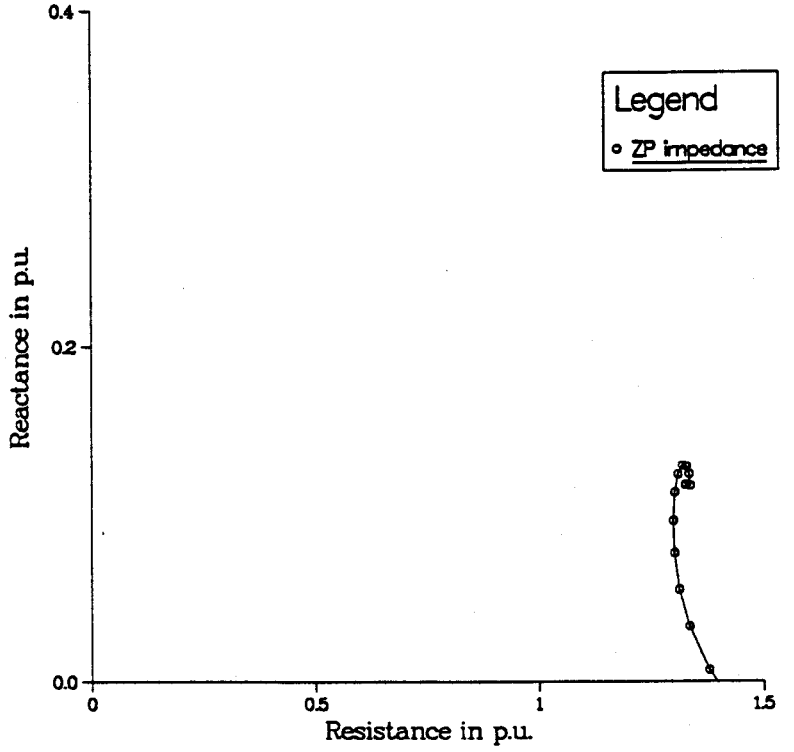

Figure 6.18: Trajectory of positive-sequence impedance estimate during a three-phase to ground fault behind the relay location (reverse fault).

6.4. Summary

This chapter has described a fault direction discriminating algorithm based on the positive- and negative- sequence impedances calculated using incremental voltages and currents. The advantage of using the incremental voltages and currents is that it eliminates the influence of the load.

The technique uses the sign of the positive- and negative- sequence impedances to give direction of the fault and the results presented demonstrate that this technique correctly discriminates the faults. However, the sign of the positive-sequence impedance is the only one used in the discrimination of three-phase faults since they are balanced and the negative-sequence impedance does not exist.

7. SUMMARY AND CONCLUSIONS

The main objectives of the research reported in this thesis were to develop a procedure for simulating magnetizing inrush current, to assess the performance of digital distance relaying algorithms during inrush current only, inrush current closed into fault, and to develop a fault direction discriminating algorithm.

Faults do occasionally occur in a power system. This can cause extensive damage to the equipment in the power system and can result in other problems, such as, system instability, severe drop in voltage and outages to customers. To limit these effects, the equipment of the power system must be sufficiently protected. A general introduction of protection of power systems and its developments has been presented in Chapter 1. The effects of transients on relays have also been discussed.

The types of faults that can be experienced by transmission lines have been described in Chapter 2. Various relays for protecting transmission lines have also been described including the protection of transformer terminated lines. Distance relays are the most commonly used relays for protecting transmission lines. The basic philosophy of distance protection schemes is to provide high speed protection for faults within the protected transmission line and provide time delayed protection for the adjacent sections of the power system. The impedance measuring element cannot however be set to accomplish high speed protection over 100% of line length. This limitation is due to transient errors, such as, their tendency to overreach when the fault current contains a d.c. offset.

Rapid advances in digital processor technology have prompted the application of microprocessors in protective relays. A number of digital algorithms for protection of transmission lines have been suggested in the past. These digital relay algorithms have

been presented in Chapter 3. Most of the existing algorithms proposed for use in digital relaying for transmission lines can be grouped into two categories. The first category is based on a model of the waveform itself i.e. the voltage and current. The second category involves a model of the system rather than the waveforms. The parameters of interest for relaying are the values of the apparent resistance, R and inductance, L of the line which must be estimated from the waveforms. The mathematical equations which form the basis of the various algorithms and the assumptions used for writing the equations have been given.

Modelling of transformers and the simulation of inrush current experienced during switching-on of transformers have been described in Chapter 4. Saturation in the transformers is modelled by current sources connected across the windings. It is assumed that there is no inter-phase magnetic coupling in the three-phase banks. Only the coupling between windings within the same phase is considered. Some simulated waveforms for inrush current have been presented. If the transformer could be switched in at that instant of voltage wave which normally corresponds to the actual magnetic density within the core at the moment, switching- in would be a smooth continuation of a previous operation without giving rise to a magnetic transient. But, in practice, there will be a random point-on-wave circuit closure, and, therefore, a magnetic transient is practically unavoidable. The worst condition of closure at or very near voltage zero will not always occur. Generally, if the residual magnetism is in the same direction as that flux set up by the applied voltage, then the excursion of flux is greater and the magnetizing current surge is also much increased.

The results from the evaluation of distance relaying algorithms in the presence of inrush current only and inrush current closed into a fault has been presented in Chapter 5. A distance relay should be able to protect a transmission line efficiently in the event of a fault at any location within its protective zone. The movement of the trajectories of the calculated impedances using different algorithms was used to assess the dynamic response of the relay. The results of the different algorithms in the presence of inrush current only, showed that there is no trip command which will be issued. In the case of inrush current closed into fault, the results showed inherent accuracy limitations of the

short window algorithms. The presence of one of the unmodelled signals, namely, decaying d.c. greatly affected the estimates of the impedance using the Mann and Morrison algorithm. The impedance estimates obtained using the Fourier algorithm are also affected, however, the effect is not as pronounced as for the Mann and Morrison algorithm. The Least Error Squares algorithm effectively suppressed the effects of the decaying d.c. and, therefore, this algorithm produces the least movements in the trajectories of the impedance estimates. In all cases of inrush current in the presence of fault, the trajectories of the impedances of the faulted phases entered the correct tripping zone. This shows that inrush current in the presence of a fault does not prevent correct tripping since the transformer terminal voltage will be considerably lower than the normal when a fault is present. The performance of the algorithms in terms of speed of settling down to the final values during fault detection were different, the 13-sample Least Error Squares algorithm showing the best performance.

Loss of directional capabilities can be experienced by distance relays particulary for faults on the secondary side of the transformer in transformer terminated lines. To secure this, a fault direction discriminating algorithm has been presented in Chapter 6. The algorithm uses the sign of the positive- and negative- sequence impedances to discriminate the faults. For three-phase faults, the positive-sequence impedance is the only one used in the discrimination since these faults are usually balanced and the negative-sequence impedance does not exist. The results presented show that the algorithm can effectively discriminate the faults. The advantage of using incremental voltages and currents in calculating the positive- and negative- sequence impedances is that it eliminates the influence of loads.

It can be concluded that, this research has demonstrated that the performance of digital relay algorithms can be evaluated off-line before on-line implementation and that inrush current is rich in harmonics. The ability of the digital distance relay to protect the transmission line during fault, even in the presence of inrush current has been shown. The results of the short window algorithms showed the accuracy limitations of these algorithms in the presence of harmonics. In addition, the decaying d.c. affected the Mann and Morrison short window algorithm. The Least Error Squares algorithm showed better

performance of the long window algorithms. The selected long window algorithms are however more suitable for protecting transformer terminated lines since they yield more accurate results than the short window algorithms. The fault direction algorithm, can supplement the directional capabilities of relays.

Future work could be to improve the transformer models so that there is magnetic coupling between windings of different phases in three-phase transformer models. In addition, the effect of using a Thevenin equivalent source instead of detailed representation of the power system can be assessed.

REFERENCES

1. K.K. Debnath, "Digital Computer Solution of Switching Transients in Transmission Line Models", Master's thesis, Department of Electrical Engineering Abstract 82A223, University of Saskatchewan, December 1982.

2. D. Ewart, "Digital Computer Simulation Model for Steel-Core Transformer", *IEEE Transactions on Power Delivery, Vol. 1, No. 3*, 1986, pp. 174-83.

3. E.B. Makram, R.L. Thompson and A.A. Girgis, "A New Laboratory Experiment for Transformer Modelling in the Presence of Harmonic Distortion using a Computer-Controlled Harmonic Generator", *IEEE Transactions on Power Systems*, 1988, pp. 1857-63.

4. J.R. Marti, "Accurate Modelling of Frequency-Dependent Transmission Lines in Electromagnetic Transient Calculations", *IEEE Transactions on Power Systems*, January 1982, pp. 147-157.

5. A.G. Phadke, "Digital Computer Simulation of Electrical Power Transients", *IEEE Tutorial Course Text, New York, N.Y.*, 1981.

6. L. Marti, "Low-order Approximation of Transmission Line Parameter for Frequency-Dependent Models", *IEEE Transactions on Power Apparatus and Systems*, November 1983, pp. 3584-3589.

7. H.W. Dommel, "Digital Computer Solution of Electromagnetic Transients in Single and Multiphase Networks", *IEEE Transactions on Power Apparatus and Systems, Vol. PAS-88*, April 1969, pp. 388-399.

8. A. Greenwood, *Electrical Transients in Power Systems*, John Wiley and Son Inc, New York, 1991.

9. J.P. Bickford and N. Mullineux, *Computation of Power-System Transients*, Peter Peregrinus Ltd, Southgate House, Herts. GG1 1 1HQ. England, 1976.

10. M.C. Russel, *The Art and Science of Protection Relaying*, John Wiley and Sons, Inc, 1956.

11. J.L. Blackburn, *Protective Relaying, Principles and Applications*, Marcel Dekker Inc., New York, 1987.

12. Jr. Stevenson and D. William, *Elements of Power Systems Analysis*, McGraw-Hill Book Co. Inc., 1975.

13. GEC Alsthom, *Protective Relay Application Guide*, GEC Alsthom, Measurements Ltd., U.K, 1990.

14. T.S. Madhava Rao, *Power System Protection- Static Relays,* McGraw-Hill Book Company, New York, 1981.

15. M.S. Sachdev, Coordinator, "Computer Relaying Tutorial Text", *IEEE Publication NO. 79 EH 0148 - 7 - PWR, New York,* 1979.

16. M.S. Sachdev, Coordinator, "Microprocessor Relays and Protection Systems", *IEEE Tutorial Course Text 88EH0269-1-PWR Piscataway, NJ 08854-1331,* 1988.

17. F.H. Last and A. Stalewsky, "Protective Gear as a Part of Automatic Power System Control", *Symposium on Automatic Control in Electricity Supply, IEE Conference Publication No. 16 Part 1, Manchester,* March 1966.

18. G.D. Rockfeller, "Fault Protection with a Digital Computer", *IEEE Transactions on Power Apparatus and Systems, Vol. PAS-88,* April 1969, pp. 438-464.

19. V. Cook, *Analysis of Distance Protection,* Research Studies Press, Letchworth and John Wiley and Son Inc, New York, 1985.

20. A.A. Girgis and J.W. Nims, "Effect of Voltage Harmonics on the Operation of Solid-State Relays in Industrial Applications", *IEEE Transactions on Power Delivery, Vol. 28, No. 5,* Sep/Oct 1992, pp. 1166-1173.

21. A.A. Girgis, "Measurement and Characteristic of Harmonic and High-Frequency Distortion for a Large Industrial Load", *IEEE Transactions on Power Delivery, Vol. 5, No. 1,* Jan 1990, pp. 427-434.

22. J.S. Thorp and A.G. Phadke, "A Microprocessor Based Three - Phase Transformer Differential Relay", *IEEE Transactions on Power Apparatus and Systems, Vol. PAS-101,* Feb 1982, pp. 426-432.

23. O.P. Malik, P.K. Dash and G.S. Hope, "Digital Protection of a Power Transformer", *IEEE PES Winter Meeting, New York,* January 1976, pp. 1-7.

24. B. Ravindranath and M. Chander, *Power System Protection and Switchgear,* Wiley Easten Limited, New Delhi, 1976.

25. W.A. Lewis and L.S. Tippett, "Fundamental Basis for Distance Relaying on Three Phase Systems", *AIEE Procceedings, Vol. 66,* 1947, pp. 694 - 708.

26. K. Ragallef, *Surges in High Voltage Networks,* Plenum Press, New York, 1980.

27. A.G. Phadke and T. Hlibka, "A Digital Computer System for E.H.V. Substations-Analysis and Field Tests", *IEEE Transactions on Power Apparatus and Systems, Vol. PAS-95, No. 1,* Jan/Feb 1976, pp. 291-301.

28. P.G. McLaren, G.W. Swift, A. Neufeld and Z. Zhang, "Open Systems Relaying", *IEEE/PES 1993 Summer Meeting, Vancouver, B.C.,* July 18-22 1993, pp. 1-7.

29. G.D. Rockfeller, C.L. Wagner and J.R. Linders, "Adaptive Transmission Relaying Concepts for Improved Performance", *IEEE/PES Summer Meeting (San Francisco),* July 1987, pp. 1446-1455.

30. B.J. Mann and I.F. Morrison, "Digital Calculation of Impedance for

Transmission Line Protection", *IEEE Transactions on Power Apparatus and Systems, Vol. PAS-90*, January/February 1971, pp. 270-276.

31. G.B. Gilcrest, G.D. Rockfeller and E.A. Udren, "High Speed Distance Relaying using a Digital Computer. Part-I-System Description", *IEEE Transactions on Power Apparatus and Systems, Vol. PAS-91. No. 3*, May/June 1972, pp. 1235-1243.

32. G.D. Rockfeller and E.A. Udren, "High Speed Distance Relaying using a Digital Computer. Part II", *IEEE Transactions on Power Apparatus and Systems, Vol. PAS-91. No. 3*, 1972, pp. 1244-1256.

33. J. Makino and Y. Miki, "Study of Operating Principals and Digital Filters for Protective Relays with Digital Computer", *IEEE PES Winter Power Meeting, New York*, January 1975, pp. 1-8.

34. R.G. Luckett, P.J. Munday and B.E. Murray, "A Substation Based Computer for Control and Protection", *IEE Conference Publication No. 125, London*, March 1975, pp. 252-260.

35. A.E. Brooks, "Distance Relaying using Least Squares Estimates of Voltage ,Current and Impedance", *Proceedings of 10th Power Industry Computer Application Conference*, May 1977, pp. 394-402.

36. M.S. Sachdev and M.A. Baribeau, "A New Algorithm for Digital Impedance Relays", *IEEE Transactions on Power Apparatus and Systems, Vol. PAS-98*, Nov/December 1979, pp. 2232-2237.

37. Computer Relaying, "Tutorial Text", *Publication No. 79 EH 0148-7-PWR, IEEE, New York, M.S. Sachdev Coordinator*, 1979.

38. A.D. McInnes and I.F. Morrison, "Real Time Calculation of Resistance and Reactance for Transmission Line Protection by Digital Computer", *Elect. Eng. Transactions, IE Australia, Vol. EE7, No. 1*, 1970, pp. 16-23.

39. W.D. Breingan and M.M. Chen, "The Laboratory Investigation of a Digital System for the Protection of Transmission Lines", *IEEE Transactions on Power Apparatus and Systems, Vol. PAS-98, No. 2*, March/April 1979, pp. 350-368.

40. A.D. McInnes and I.F. Morrison, "Real Time Calculation of Resistance and Reactance for Transmission Line Protection by Digital Computer", *Elec. Eng. Transactions, IE, Australia, Vol. EE7, No. 1*, 1970, pp. 16-23.

41. A.M. Ranjbar and B.J. Cory, "An Improved Method for the Digital Protection of High Voltage Transmission Lines", *IEEE Transactions on Power Apparatus and Systems. Vol. PAS-94, No.2*, March/April 1975, pp. 544-550.

42. Manitoba HVDC Research Centre, *EMTDC, Electromagnetic Transient DC Analysis Program*, Manitoba HVDC Research Centre, 1988.

43. E.E. Staff, *Principals of Electrical Engineering Series Magnetic Circuits and Transformers*, Members of the Staff-Department of Electrical Engineering M.I.T., 1965.

44. R.L. Bean, N. Chactan, *Transformers for the Electric Power Industry*, Westinghouse Electric Corporation, 1959.

45. L.F. Blume, A. Bojajian and T.C. Lennox, *Transformer Engineering. A Treatise on the Theory Operation and Application of Transformers,* John Wiley, New York, 1967.

46. A.C. Franklin and D.P. Franklin, *The J and P Transformer Book,* Butterworth and Co., Mid-County Press, London, SW15, 1983.

47. H.W. Dommel, A. Yan and S. Wei, "Harmonics From Transformer Saturation ", *IEEE Transactions on Power Delivery, Vol. 1, No. 2,* 1986, pp. 209-15.

48. A. Kusko and T. Wroblewski, *Computer-Aided Design of Magnetic Circuits,* The M.I.T. Press, Massachusetts, 1969.

49. S.A. Nasar, *Electric Machines and Transformers,* MacMillan and Collier MacMillan Publishing Co., 1984.

50. A.R. van C. Warrington, *Protective Relays: Their Theory and Practice,* London: Chapman and Hall, 1962.

51. P. Anderson, *Analysis of Faulted Power Systems,* The Iowa State University Press, Ames, Iowa, 1973.

52. R.E. Bogner, *Introduction to Digital Filtering,* John Wiley and Sons., London. New York. Sydney. Toronto, 1975.

53. T.S. Sidhu, B.R. Sunga and M.S. Sachdev, "A Digital Algorithm for Detecting Internal Faults in Synchronous Generators", *IEEE WESCANEX'93 (Saskatoon),* May 1993, pp. 1-16.

A. EMTDC Program

Digital computer programs for simulating electrical transients in systems have been developed and documented [42]. Most early programs were written for single-phase networks.

In recent programs, the single- phase simulation technique has been extended to handle multiphase networks by replacing the variables in single phase equations by matrix representations. The equations describe arbitrary interconnections of the elements of the power system. Algebraic, differential and integral equations are used to represent resistive, inductive and capacitive elements of the power system. The EMTDC is one such program and it uses the trapezoidal rule of integration to solve the equations. It simulates a transmission line shunt fault by closing time dependent switches at the fault location.

A.1. Scope of Simulation Studies

EMTDC was developed by Manitoba HVDC Research Centre and as a simulation tool can be used for simulation studies which include:

1. DC transmission configurations and control.
2. Synchronous and induction machines including torsional concerns and self excitation.
3. Static compensation.
4. Hydraulic and wind turbine and generation systems.
5. Non-linear control systems.
6. Transmission lines, cables and circuit analysis.
7. Transformer saturation studies such as ferroresonance and core saturation instability.
8. Development of digital control systems.

9. Steep front surge analysis.

Electric circuits including network elements, transmission lines, cables and transformers are entered in free format as a data file for the program to read at the start of the simulation. Voltages at nodes and currents in branches are easily accessible. The user can assemble or build models making user written FORTRAN statements. This flexibility provides great power to the user so that any power system problem, if appropriate models can be conceived, can be examined using your own subroutines.

A.1.1. Limitations

Some of the limitations of the EMTDC program include:

1. Not in real time.
2. The user must have considerable expertise in the system being studied for EMTDC to be used effectively.
3. Initialization of complex systems must be run upto steady- state at which point dynamic parameters can be stored for successive starts.

B. Results on Dynamic Response of the Digital Relay

The ability of the digital distance relay to detect faults at the midpoint of the transformer terminated line discussed in Chapter 5 in the presence of inrush current, is examined in this appendix. The transformer was switched in with the faults at the midpoint. Only the Fourier and Least Error Squares algorithms were used to obtain the impedance estimates since these two algorithms showed more accurate results than the short window algorithms for the case studies presented in Chapter 5.

B.1. Inrush Current with a Single-Phase to Ground Fault

Figures B.1 and B.2 show the ground elements of the Fourier and Least Error Squares algorithms respectively. The phase A impedance moves into the correct operating zone of the relay with the impedance estimate of the Least Error Squares algorithm settling much faster.

Figures B.3 and B.4 show the impedance estimates of the phase elements. None of the estimates moves into the operating zones of the relay. In both cases, the relays operated correctly.

B.2. Inrush Current with a Phase to Phase Fault

The phases A and B are the phases involved in the fault. Figures B.5 and B.6 show the impedance estimates of the ground elements. It is clear from Figure B.6 that the impedance estimate of the Fourier algorithm moves across the operating zones of the relay just like when the fault was created at the far end of the line. This might result in tripping as pointed out in Chapter 5. Figures B.7 and B.8 show the impedance estimates of the phase elements. The A-B impedance estimates for both algorithms move into the correct tripping zone of the relay. The Least Error Squares algorithm, overall, still shows better performance than the Fourier algorithm.

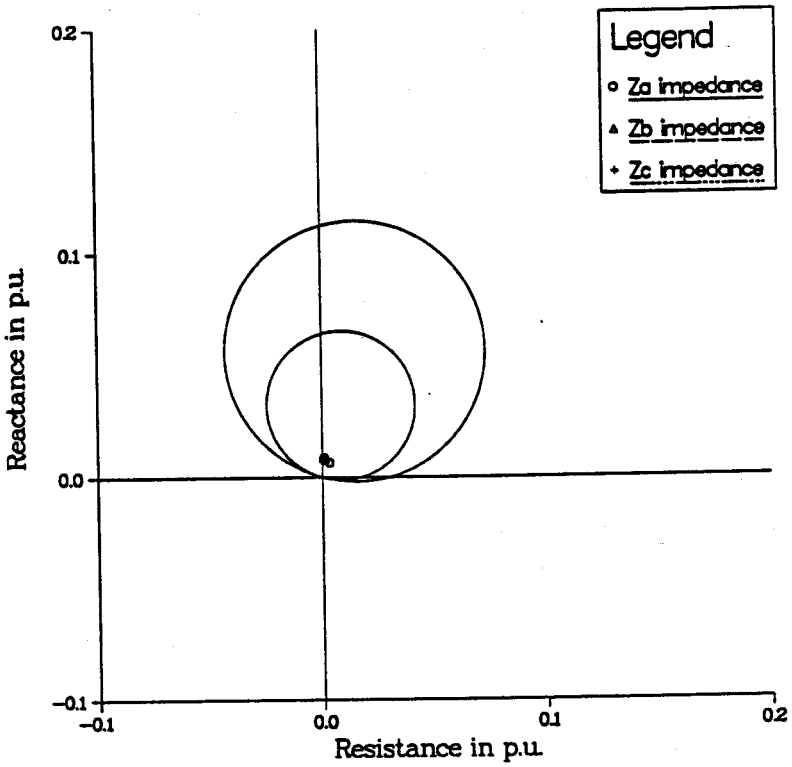

Figure B.1: Trajectory of impedance estimates of the ground elements for a single- phase to ground fault at the mid-point of the line using the Least Error Squares algorithm.

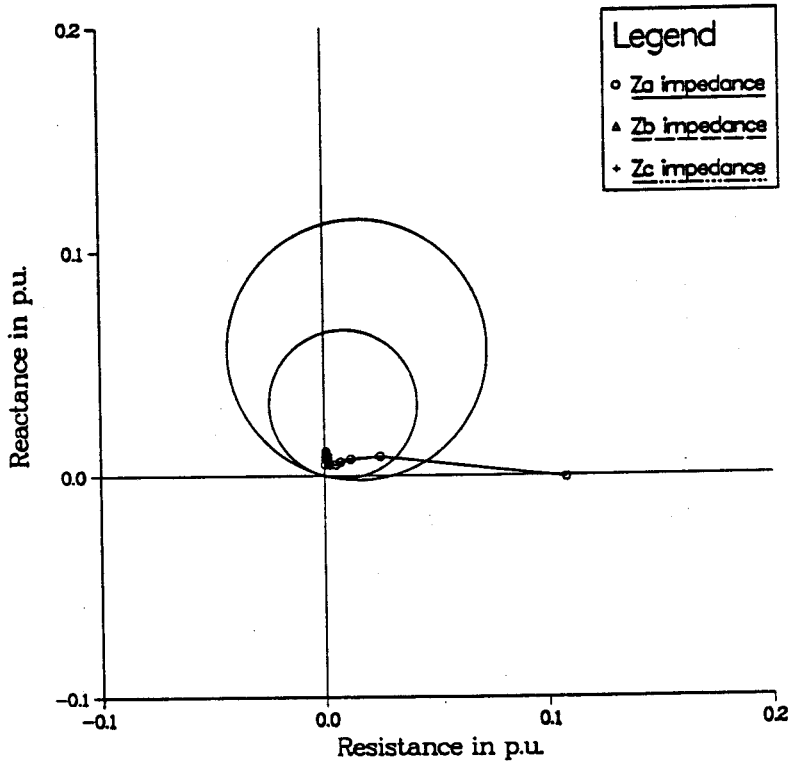

Figure B.2: Trajectory of impedance estimates of the ground elements for a single-phase to ground fault at the mid-pont of the line using the Fourier algorithm.

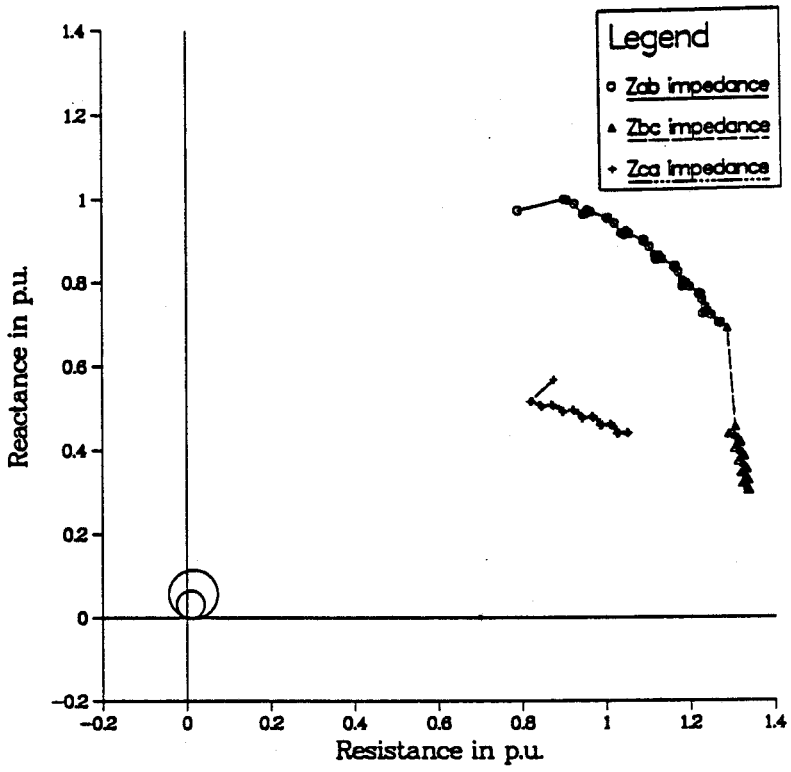

Figure B.3: Trajectory of impedance estimates of the phase elements for a single-phase to ground fault at the mid-point of the line using the Least Error Squares algorithm.

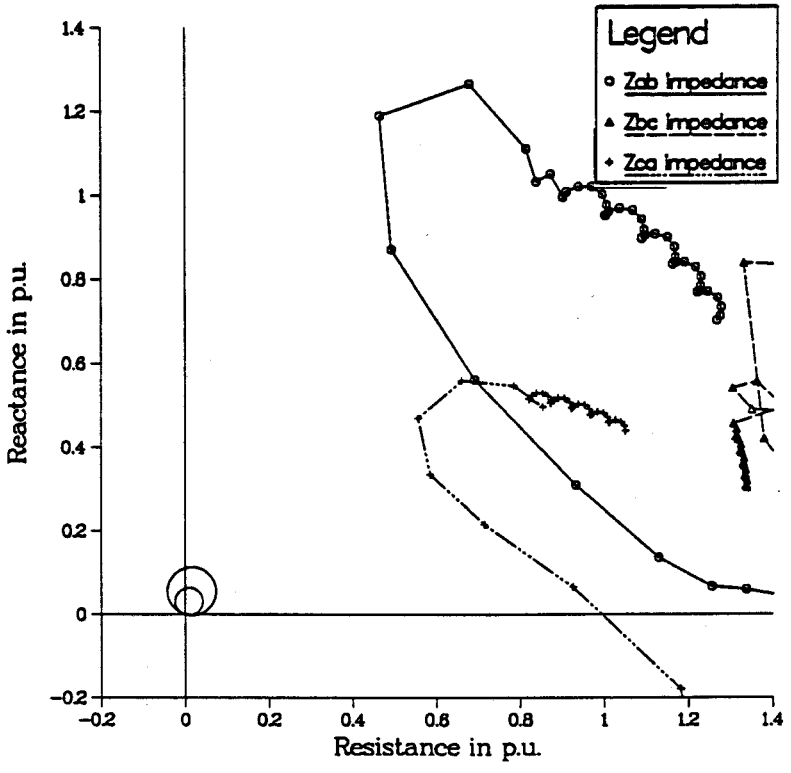

Figure B.4: Trajectory of impedance estimates of the phase elements for a single-phase to ground fault at the mid-point of the line using the Fourier algorithm.

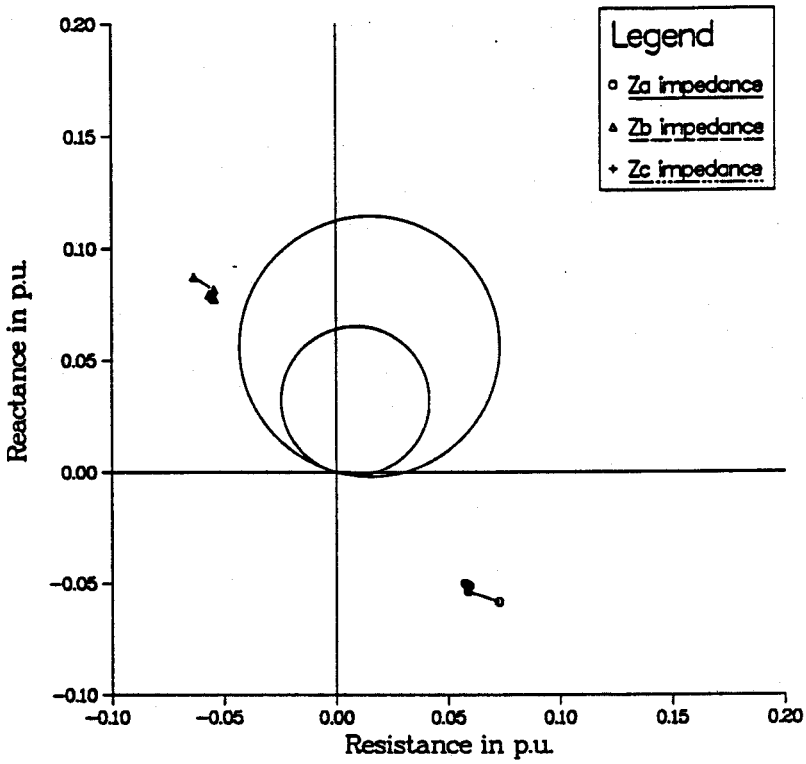

Figure B.5: Trajectory of impedance estimates of the ground elements for a phase-phase fault at the mid-point of the line using the Least Error Squares algorithm.

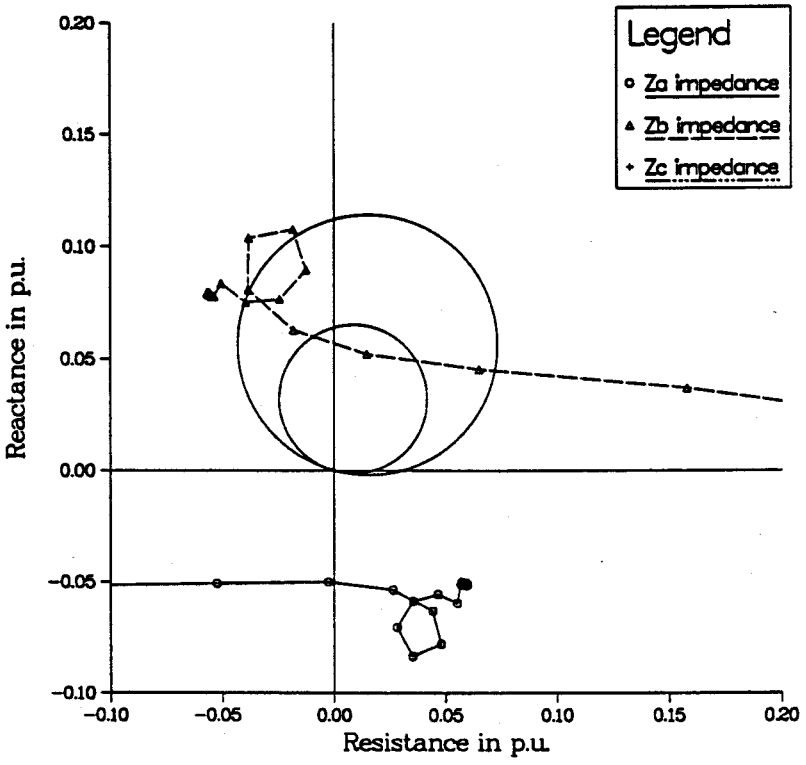

Figure B.6: Trajectory of impedance estimates of the ground elements for a phase-phase fault at the mid-point of the line using the Fourier algorithm.

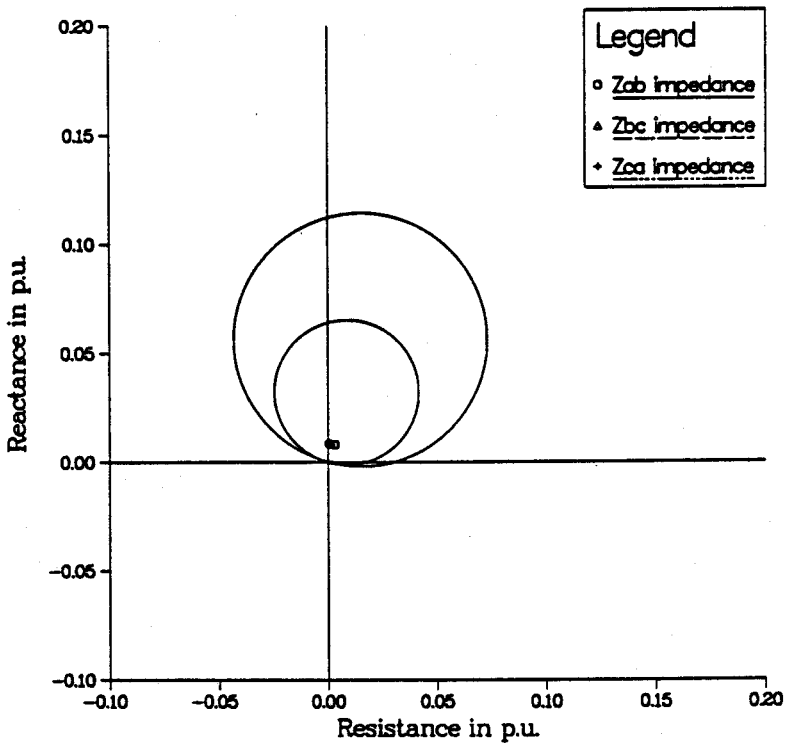

Figure B.7: Trajectory of impedance estimates of the phase elements for a phase-phase fault at the mid-point of the line using the Least Error Squares algorithm.

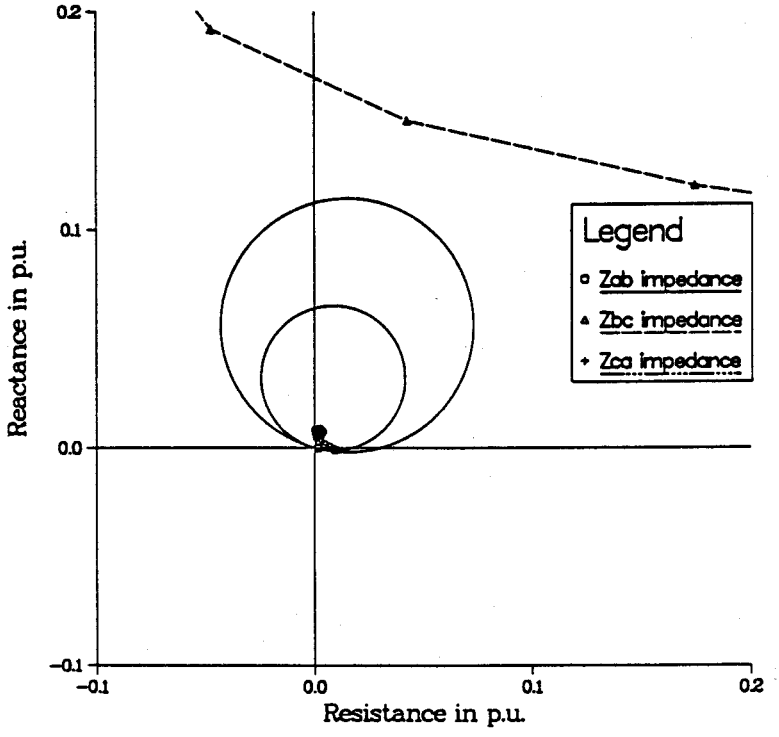

Figure B.8: Trajectory of impedance estimates of the phase elements for a phase-phase fault at the mid-point of the line using the Fourier algorithm.